SAND80-2380
Unlimited Release
UC-13

Prediction of Forces and Moments on Finned Bodies at High Angle of Attack in Transonic Flow

William L. Oberkampf

Prepared by Sandia National Laboratories, Albuquerque, New Mexico 87185
and Livermore, California 94550 for the United States Department
of Energy under Contract DE-AC04-76DP00789

Printed April 1981

Sandia National Laboratories

SF 2900-Q(3-80)

DISCLAIMER

Issued by Sandia National Laboratories, operated for the United States Department of Energy by Sandia Corporation.

Printed in the United States of America

Available from
National Technical Information Service
U. S. Department of Commerce
5285 Port Royal Road
Springfield, VA 22161

NTIS price codes
Printed copy: $7.00
Microfiche copy: A01

SAND80-2380
Unlimited Release
Printed April 1981

Distribution
Category UC-13

Prediction of Forces and Moments on Finned Bodies at High Angle of Attack in Transonic Flow

William L. Oberkampf*
Aeroballistics Division 5631
Sandia National Laboratories
Albuquerque, NM 87185

Abstract

This report describes a theoretical method for the prediction of fin forces and moments on bodies at high angle of attack in subsonic and transonic flow. The body is assumed to be a circular cylinder with cruciform fins (or wings) of arbitrary planform. The body can have an arbitrary roll (or bank) angle, and each fin can have individual control deflection. The method combines a body vortex flow model and lifting surface theory to predict the normal force distribution over each fin surface. Extensive comparisons are made between theory and experiment for various planform fins. A description of the use of the computer program that implements the method is given.

*This work was sponsored in part by the Air Force Armament Laboratory (AFATL/DLJ), Eglin AFB, FL, under Air Force Contract No. F08635-77-C-0049. The contract was in support of research done while the author was on the faculty of the Department of Mechanical Engineering, University of Texas at Austin. The contract monitor for AFATL was D. C. Daniel (DLJ).

Acknowledgment

The author thanks D. C. Daniel, Aerodynamics Research Manager of the Air Force Armament Laboratory, Eglin AFB, FL for his comments and suggestions during the investigation.

Contents

Illustrations

Figure

Illustrations (Cont)

Illustrations (Cont)

Nomenclature

a	Body radius
A_e	Aspect ratio of fins based on exposed planform area, Eq (19c)
A_p	Planform aspect ratio of fins based on extension through the body b^2/S_{f_p}
b	Fin span
b_o	Fin semispan
B	Root bending moment (Figure 29)
C_ℓ	Roll moment coefficient ($\ell/q_\infty S_b d$)
$C_{\ell p}$	Roll damping moment coefficient derivative $(\partial C_\ell/\partial p)_{p\to o}$
C_m	Pitch moment coefficient ($m/q_\infty S_b d$)
C_n	Yaw moment coefficient ($n/q_\infty S_b d$)
C_n	Local normal force coefficient of fin, Eq (14)
C_N	Local normal force coefficient of fin due to angle of attack, Eq (33)
C_{N_α}	Normal force coefficient derivative of fin $(\partial C_N/\partial\alpha)_{\alpha\to o}$
C_b	Panel root bending moment coefficient $[B/q_\infty(b_o - a) S_f]$
C_h	Panel hinge moment coefficient ($H/q_\infty c_r S_f$)
C_p	Panel normal force coefficient ($N/q_\infty S_f$)
c_r	Root chord of fin
C_y	Side force coefficient ($F_y/q_\infty S_b$)
C_z	Normal force coefficient ($F_z/q_\infty S_b$)
d	Body diameter
F_x, F_y, F_z	Forces in the x,y,z directions, respectively (Figure 1)
H	Panel hinge moment (Figure 29)
$\vec{i}, \vec{j}, \vec{k}$	Unit vectors in the x,y,z directions, respectively
I_d	Fin deflection interference coefficient, Eq (39)
I_p	Rolling-motion interference coefficient, Eq (44)
k_B	Interference lift ratio (Figure 51)
K_p	Potential flow lift coefficient, Eq (34h)
K_v	Vortex flow lift coefficient, Eq (34i)
L_s	Length of the vortex sheet, Eq (6a)
ℓ, m, n	Roll, pitch, and yaw moments, respectively (Figure 1)
M	Mach number
$\vec{n}$	Unit normal vector for fin surface
N	Normal force
N_v	Total number of vortices in cross-flow plane
p	Dimensionless roll speed ($\dot{\phi}\, b_o/U_\infty$)
q	Dynamic pressure ($1/2\ \rho U^2$)
r_c	Radius of vortex core
r, ϕ	Polar coordinates in cross-flow plane
r_1, ϕ_1	Coordinates of primary body vortex
s	Complex position in the cross-flow plane ($y + i z$)
S_b	Frontal area of missile body (πa^2)
S_f	Exposed planform area of fin, Eq (19d)
S_{f_p}	Planform area of two fins including extension through the body, Eq (40b)
u,v,w	Velocities in the x,y,z directions, respectively (Figure 1)
U	Magnitude of velocity
U_c	Freestream cross-flow velocity, $U_\infty \sin\alpha_b$
v_c, w_c	Cross-flow velocities in the y,z directions, respectively, Eq (2)
$\vec{V}$	Flow field velocity ($u\vec{i} + v\vec{j} + w\vec{k}$)
x,y,z	Body Cartesian coordinates (Figure 1)
y_v, z_v	Location of primary body vortex in cross-flow plane
α	Angle of attack
α_ℓ	Local angle of attack
α_s	Stall angle of attack of the fin, Eq (35b)
Γ_p	Strength of the primary body vortex
Γ_s	Stength of vortex sheet
δ_j	Control deflection of the j'th fin (Figure 10)
σ	Geometric scaling factor for fin, Eq (20a)
Λ	Sweep angle of fin
ξ,η	Fin-oriented surface coordinates, Eq (18)
ρ	Fluid density
ϕ	Roll angle (Figure 10)
$\dot{\phi}$	Roll rate (rad/s)

Subscripts:

b	Missile body
e	"Effective" value of argument
ℓe	Leading edge
te	Trailing edge
∞	Freestream conditions

Superscripts:

$\dot{}$	Derivative with respect to time
$\hat{}$	"Effective" value of argument

Summary

The present investigation is concerned with the theoretical prediction of fin forces and moments on bodies at high angle of attack in subsonic and transonic flow. The body is assumed to be a circular cylinder with a streamlined nose and only cruciform fins (or wings) as attached lifting surfaces. The fins are assumed to be planar and have straight leading, trailing and tip chord edges. The leading edge can have arbitrary sweep back and the trailing edge can be swept back or forward. The body can have an arbitrary roll (or bank) angle and each fin can have arbitrary control deflection. The vortices shed from the body are assumed to be symmetrically located with respect to the angle of attack plane and of equal strength but opposite rotational sense. The highest angle of attack of the body for which the body vortices remain symmetric depends on the nose fineness ratio, body fineness ratio, and Mach number; normally this angle is near 25°. The body flow field model and lifting theory use some empirical data, but the user of the method need not provide any additional data. A description of the construction and use of the program FINLOAD, which implements the method, is given.

Extensive comparisons are made between predicted results and experimental measurements. Included in the comparisons are: panel normal force, root bending moment, induced roll moment, nonlinear roll damping moment, pitch (or yaw) control forces, and roll control moment. The force and moment predictions are compared with experimental data for six different fin geometies; these include delta, clipped delta, and rectangular planforms. Predictions for wing alone normal force characteristics are compared with data for rectangular, delta, clipped delta, diamond, arrow, clipped arrow, and trapezoidal planforms. Extensive discussions are given that explain the underlying aerodynamic causes of fin force and moment nonlinearities and how these are related to fin geometry. Good agreement between the present method and experiment is obtained, except for control force and moment where the agreement could be characterized as "fair."

Prediction of Forces and Moments on Finned Bodies at High Angle of Attack in Transonic Flow

Introduction

The aerodynamics of missiles and bombs at high angle of attack has become increasingly important for modern design requirements. Examples of this are high maneuverability of air-to-air-missiles and tolerance of large disturbances at store separation. At high angle of attack, a body of revolution sheds two symmetric vortices from the leeside of the body, and these grow in strength along the length of the body. The body's attached lifting surfaces are immersed in this vortex wake flow and, consequently, the surface pressure distributions are significantly changed from the potential flow case. This, in turn, causes nonlinearities in the forces and moments produced by the lifting surfaces. These nonlinearities have been known to cause serious flight stability and controllability problems in vehicle flight dynamics.

Attempts at predicting the forces and moments produced by lifting surfaces in a symmetric body-vortex wake have met with moderate success. Very early work was done by Mello and Sivier[1] for a cruciform-fin missile in supersonic flow. References 2 and 3 report reasonably successful work for incompressible and supersonic flow, respectively, but only rectangular fin planforms were considered. The approach taken was to calculate the body-flow field using a vortex-modeling technique and then use this as input to a lifting theory.[2,3] The most extensive work on the subject has been achieved by Nielson and his associates.[4-7] They have attacked the very difficult problem of a general canard-fin-body configuration in transonic and supersonic flow with both symmetric and asymmetic body vortices and canard vortices. Their approach is a combination of slender-body theory, Deffenbaugh's[8,9] method for the impulse flow analogy, and data base experimental input for fin (or wing) alone characteristics.

The present approach uses the body flow field model developed in Reference 10 and combines it with an approximate lifting surface theory to predict fin forces and moments. The lifting surface theory and the equations for fin forces and moments are developed in detail. The applicability and accuracy of the present method is evaluated by extensive comparisons of theory and experiment. The purpose of the present work is to develop a force and moment predictive method that is applicable to a wide variety of fin planforms over the subsonic and transonic speed range.

Aerodynamic Analysis

The general approach to the aerodynamics of the problem is to calculate the body flow field and then calculate the forces and moments of attached lifting surfaces exposed to this flow field. This approach is clearly based on the assumption that the body flow field is not significantly affected by the flow induced by lifting surfaces. This assumption implies that the present analysis is not appropriate for missile configurations in which the fin-root chord is a large portion of the length of the missile body (e.g., the Phoenix air-to-air missile (AIM-54A)). The present analysis also assumes that there is only one set of lifting surfaces (wings or fins) and that it is arranged in a cruciform configuration. The present approach could be applied to a two- or three-fin configuration by making appropriate modifications to the lifting theory.

This present approach naturally divides the analysis into two areas: the body flow field and the prediction of lifting surface forces and moments. The model of the body flow field was developed previously in References 2 and 10. For completeness, however, the model and the associated computational procedures are described in this report. The prediction of lifting surface forces and moments is described in two phases. First, the lifting theory for calculating the normal force distribution and the

total normal force of the lifting surface in uniform approach flow is described. Second, the model of the body flow field and the lifting theory are combined to yield a method for predicting forces and moments of attached lifting surfaces.

Body Flow Field

The flow field of a circular cylindrical body at high angle of attack is dominated by the presence of body vortices and their associated feeding sheets. Figure 1 shows the coordinate system and a schematic of the body vortex wake flow. These vortices increase in strength as the angle of attack or body length increases. To model this complex separated flow, the flow is divided into the cross-flow components (v_c and w_c) and the axial flow component, $U_\infty \cos \alpha_b$. The local flow velocity can then be expressed as:

$$\bar{V} = U_\infty \cos \alpha_b \bar{i} + v_c \bar{j} + w_c \bar{k} . \qquad (1)$$

It is assumed that the steady, three-dimensional, body flow field can be divided into (1) constant axial-flow component and (2) the two-dimensional, potential, flow about a circular cylinder with vortices in the wake and their associated image vortices inside the cylinder. Essentially all of the vorticity is located inside the vortex cores of the primary body vortices and the vortex feeding sheets connecting the body boundary layer separation points and the primary body vortices. Figure 2 shows the primary and sheet vortices in the cross-flow plane. Using this model, the cross-flow velocity components can be written as

$$v_c = \left[\frac{-2U_c a^2 yz}{(y^2 + z^2)^2} + \frac{\Gamma_p}{2\pi} \sum_{j=1}^{4} (-1)^j \frac{z - z_j}{(y - y_j)^2 + (z - z_j)^2} + \frac{2\Gamma_s}{\pi(N_v - 4)} \sum_{j=5}^{N_v} (-1)^j \frac{z - z_j}{(y - y_j)^2 + (z - z_j)^2} \right] [1 - e^{-C}] \qquad (2a)$$

$$w_c = \left\{ U_c \left[1 + \frac{a^2(y^2 - z^2)}{(y^2 + z^2)^2} \right] - \frac{\Gamma_p}{2\pi} \sum_{j=1}^{4} (-1)^j \cdot \frac{y - y_j}{(y - y_j)^2 + (z - z_j)^2} - \frac{2\Gamma_s}{\pi(N_v - 4)} \sum_{j=5}^{N_v} (-1)^j \cdot \frac{y - y_j}{(y - y_j)^2 + (z - z_j)^2} \right\} \{1 - e^{-C}\} \qquad (2b)$$

where

$$C = 1.254 [(y - y_v)^2 + (z - z_v)^2] / r_c^2$$

$$y_v, z_v = \begin{cases} y_1, z_1 & y \geq 0 \\ y_4, z_4 & y < 0 \end{cases}$$

U_c = $U_\infty \sin \alpha_b$ is the free-stream cross-flow velocity
a = body radius
Γ_p = strength of a primary body vortex
Γ_s = strength of a vortex sheet
y_j, z_j = location of the j'th vortex
N_v = total number of vortices in the cross-flow plane
r_c = vortex core radius

The dependence of Γ_p, Γ_s, y_1, z_1, and r_c on angle of attack and body length is taken from experimental measurements.

The exponential term in Eqs (2a) and (2b) was included to model the solid body type rotation in the cores of the primary body vortices. This method of approximating the vortex cores yields a cross-flow velocity field that is continuous, whereas simply imposing a solid body rotation onto a potential flow field does not.

Using the assumption of a symmetric vortex wake, the relationship between the locations of all of the vortices in the cross-flow plane becomes

$$\left. \begin{aligned} y_j = -y_{j+1} &= a^2 y_{j+1} / (y_{j+1}^2 + z_{j+1}^2) \\ z_j = z_{j+1} &= a^2 z_{j+1} / (y_{j+1}^2 + z_{j+1}^2) \end{aligned} \right\} \text{ for } j = 2,6,10,\ldots N_v\text{-}2 \qquad (3a)$$

$$y_j = -y_{j-3} \text{ and } z_j = z_{j-3} \quad \text{for } j = 4,8,12,\ldots N_v . \qquad (3b)$$

With these equations the location of all of the vortices can be related to the location of the vortices external to the body in the positive (y,z) quadrant; i.e., $j = 1,5,9,\ldots N_v\text{-}3$.

The location of the right-handed vortex sheet, $s_s = r_s e^{i\phi}$, is given as

$$s_s = [a \cos(\pi \phi / 2\phi_1) + (r_1 + r_c) \sin^2(\pi \phi / 2\phi_1) / \{1 + (r_1 + r_c)(\phi_1 - \phi)/a\}] e^{i\phi} \quad \phi_{ss} \leq \phi \leq \phi_1 \qquad (4)$$

where r_1 and ϕ_1 are the radial and angular locations, respectively, of primary vortex number 1, and ϕ_{ss} is the angle at which the sheet separates from the body. The vortex sheet location as given by Eq (4) yields a slight improvement in comparison with experimental data of Reference 11 as compared with that used in References 2 and 10. Equation (4) requires that the vortex sheet terminates at the core radius of the primary vortex, whereas the equations used in References 2 and 10 terminated the sheet at the center of the primary vortex.

ϕ_{ss} is defined as the angle at which the radial location of the sheet achieves a value of 1.01a; therefore, ϕ_{ss} is defined by the equation

$$\cos(\pi\,\phi_{ss}/2\,\phi_1) + (r_1 + r_c)\,\sin^2(\pi\,\phi_{ss}/2\,\phi_1)/$$
$$[a + (r_1 + r_c)(\phi_1 - \phi_{ss})] = 1.01 . \qquad (5)$$

The low-strength vortices which represent the vortex sheet are equally spaced in the arc length along the sheet. The arc length of the vortex sheet is

$$L_s = \int_{\phi_{ss}}^{\phi_1} \left[r_s^2 + \left(\frac{dr_s}{d\phi} \right)^2 \right]^{1/2} d\phi \qquad (6a)$$

where r_s is the magnitude of s_s, from Eq (4), and

$$\frac{dr_s}{d\phi} = -(a\,\pi/2\,\phi_1)\sin(\pi\,\phi/2\,\phi_1) + [\{(r_1 + r_c)\pi/\phi_1\}$$
$$\sin(\pi\,\phi/2\,\phi_1)\cos(\pi\,\phi/2\,\phi_1)\{1 + (r_1 + r_c) \cdot$$
$$(\phi_1 - \phi)/a\} + \{(r_1 + r_c)^2/a\}\sin^2(\pi\,\phi/2\,\phi_1)]/$$
$$\{1 + (r_1 + r_c)(\phi_1 - \phi)/a\}^2 . \qquad (6b)$$

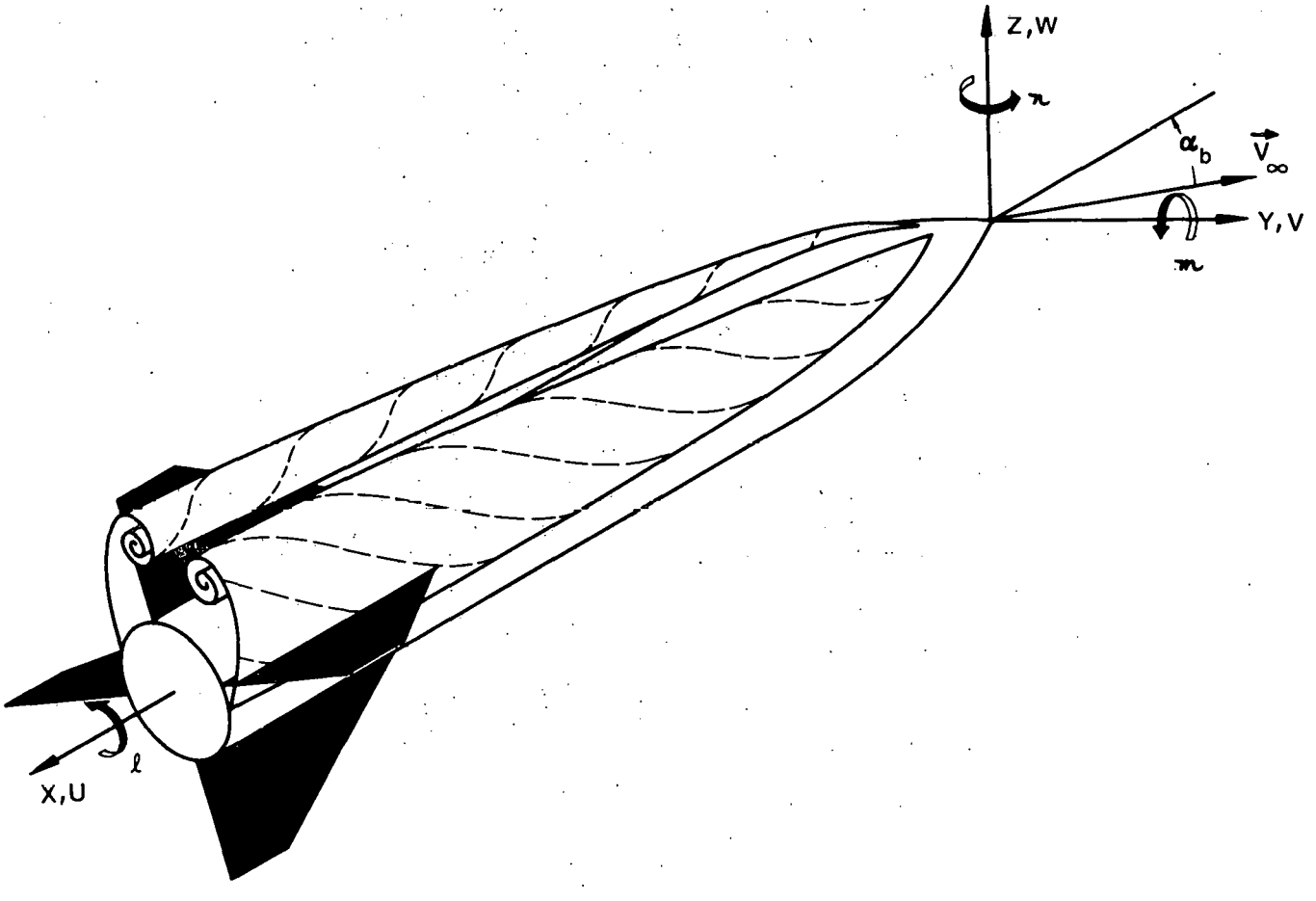

Figure 1. Coordinate System and Schematic of Body Vortices

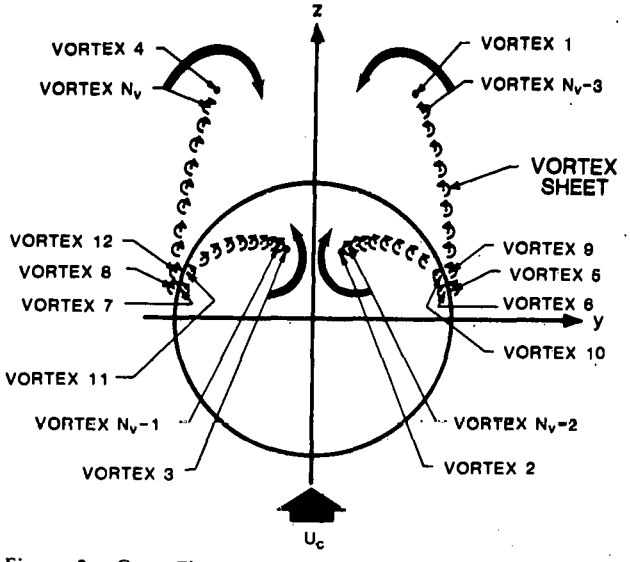

Figure 2. Cross-Flow Plane Flow Model

The first vortex in the sheet (vortex 5) is located at the point where the sheet leaves the body so that $r_5 = 1.01a$ and $\phi_5 = \phi_{ss}$. The angular position for vortices 5,9,13,...N_v-3 is found from

$$\left(\frac{j - 5}{N_v - 4}\right) L_s = \int_{\phi_{ss}}^{\phi_j} \left[r_s^2 + \left(\frac{dr_s}{d\phi}\right)^2 \right]^{1/2} d\phi \quad . \qquad (7)$$

Once the angular position is known from Eq (7), then from Eq (4) one obtains the radial location:

$$r_j = a\cos(\pi\,\phi_j/2\,\phi_1) + (r_1 + r_c)\sin^2(\pi\,\phi_j/2\,\phi_1)/$$

$$\{1 + (r_1 + r_c)\,(\phi_1 - \phi_j)/a\} \quad . \qquad (8)$$

The experimental inputs required by the theory will now be discussed. The total strength of all the vorticity, Γ_t (primary vortex and feeding sheet), in each half-plane of the wake is taken from the experimental data of Grosche[12]

$$\Gamma_t/(\pi\, d\, U_\infty) = 0.35(x/a - 6)\,\alpha_b^2 \quad \text{for } x/a > 6 \quad . \qquad (9)$$

This equation represents the data of Grosche for $7° \le \alpha_b \le 20°$ and $5 \le x/d \le 13$ for incompressible flow. No extensive body-vortex wake surveys have been conducted in compressible subsonic flow.

The division of vorticity between the primary vortex and the feeding sheet is taken from a correlation of data given in Reference 11. This correlation is represented by

$$\frac{\Gamma_p}{\Gamma_t} = 1 - 0.15\,(x/a)\,\alpha_b + 0.008\,(x/a)^2\,\alpha_b^2 \qquad (10)$$

where $\Gamma_t = \Gamma_p + \Gamma_s$. Although the data from Reference 11 are for supersonic flow, it is reasonable to assume that the ratio of primary vortex strength to total vorticity is the same in subsonic and supersonic flow.

The location of the primary vortex is taken from the experimental data of Grosche,[12] Tinling and Allen,[13] and Fidler, Nielsen, and Schwind.[14] The experimental data for the location of the right-hand primary vortex (vortex 1) in polar coordinates are approximated by

$$\phi_1 = 74° \qquad (11)$$

$$r_1/a = 0.70 + 0.06\sqrt{M_\infty + 1}\,(x/a + 6)\sqrt{\alpha_b} \quad .$$

These equations incorporate the moderate increase in radial location of the vortex center with Mach number measured by Tinling and Allen.

The radius of the vortex core is taken from the data of Reference 11. A fit of the data for angles of attack of 10° and 15° and body lengths from 7 to 14 calibers is given by

$$r_c/a = 0.030\,(x/a)\sqrt{\alpha_b} \quad . \qquad (12)$$

The computational procedure for the body flow field model will now be discussed. The order of calculation is as follows:

(a) α_b and x are set.
(b) Γ_t is calculated from Eq (9).
(c) Γ_p and Γ_s are calculated from Eq (10).
(d) ϕ_1 and r_1 are calculated from Eq (11).
(e) r_c is calculated from Eq (12).
(f) ϕ_{ss} is computed from Eq (5) by increasing ϕ_{ss} from 0° in increments of $0.01\phi_1$ until Eq (5) is satisfied. Recall that $\phi_{ss} = \phi_5$ and $r_5 = 1.01a$.
(g) L_s is calculated from Eq (6) by Simpson's Rule of numerical integration.
(h) ϕ_j for j = 9,13,...N_v-3 is calculated by increasing ϕ_j from ϕ_{j-4} in increments of $0.01\,\phi_1$ until the integral equation is satisfied. The integral is evaluated by Simpson's Rule. In the present work, N_v is set at 44; that is, 10 vortices in each sheet.
(i) r_j for j = 9,13...N_v-3 is calculated from Eq (8).
(j) y_j, z_j for j = 1,5,9,...N_v-3 are calculated from ϕ_j, r_j using the polar to Cartesian transformation.
(k) y_j, z_j for all remaining vortices are calculated from Eq (3).
(l) v_c, w_c are calculated from Eq (2).

Lifting Theory

Various lifting theories were considered for use with the present flow model for the prediction of forces and moments produced by fins. The criteria by which a lifting theory was chosen was that the theory must be able to consider very nonuniform, rotational, approach flow and it must include fin stall and poststall characteristics. These criteria quickly limited the possible theories to strip theory. In strip theory it is assumed that the normal force on a chordwise strip of fin can be calculated by using the local dynamic pressure and angle of attack of the strip, independent of adjacent chordwise strips. Significant elements included in the present lifting theory are the following: normal force distribution over the lifting surface depends upon fin aspect ratio and leading and trailing edge sweep; individual control deflection of each fin is allowed; fin-fin interference due to both control deflection and rolling rate is included; normal force depends upon free-steam Mach number; and nonuniform approach flow alters the effective leading edge sweep.

a. Local Normal Force

The local normal force on a differential element of the fin surface is written as (see Figure 3)

$$dN = C_n \, q \, dx \, dr \tag{13}$$

where C_n is the local normal-force coefficient and q is the local dynamic pressure (including that due to missile rolling speed). The local normal force coefficient C_n is composed of three separate functions: (1) the normal force due to the local angle of attack of the differential element, (2) the local chordwise distribution, and (3) the local spanwise distribution. Assuming a product form of the function, one has

$$C_N = \sigma \, C_n(\alpha_\ell) \, C(x,r) \, S(r) \tag{14}$$

where σ is a geometric scaling factor, $C_N(\alpha_\ell)$ is the local normal force coefficient due to local angle of attack, and C(x,r) and S(r) are the chordwise and spanwise normal force distributions, respectively, for uniform approach flow.

For arbitrary planform fins, it greatly simplifies matters if C and S are written in terms of appropriate fin-oriented coordinates. To determine the appropriate fin-oriented variables, the x coordinate of the leading and trailing edges of the fin is written as

$$x_{\ell e} = x_1 + (x_2 - x_1)(r - a)/(b_o - a)$$

$$x_{te} = x_3 + (x_4 - x_3)(r - a)/(b_o - a) \tag{15}$$

where x_1, x_2, x_3, and x_4 are defined in Figure 3, and b_o is the semispan of the fin. x_2, x_3, and x_4 can be related to the leading edge sweep $\Lambda_{\ell e}$, and the root chord of the fin c_r as

$$x_2 = x_1 + (b_o - a) \tan \Lambda_{\ell e}$$

$$x_3 = x_1 + c_r$$

$$x_4 = x_3 + (b_o - a) \tan \Lambda_{\ell e} \, . \tag{16}$$

Substituting these equations into Eq (15), one obtains

$$x_{\ell e} = x_1 + (r - a)\tan \Lambda_{\ell e}$$

$$x_{te} = x_1 + c_r + (r - a)\tan \Lambda_{te} \, . \tag{17}$$

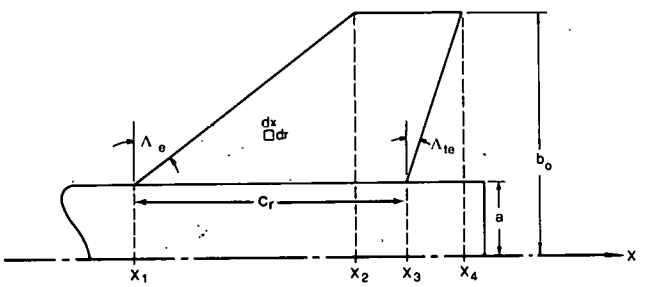

Figure 3. General Planform Fin

Using the boundaries of the fin planform (i.e., $x_{\ell e}$, x_{te}, a, and b_o) as scaling variables, a convenient set of fin-oriented coordinates are

$$\xi = (x - x_{te})/(x_{\ell e} - x_{te})$$

$$\eta = (r - a)/(b_o - a) \tag{18}$$

where ξ is the chordwise variable and η is the spanwise variable (Figure 4).

b. Normal-Force Distribution

Experimental data[15-19] for normal-force distribution over the surface of a number of fin planforms was studied in order to arrive at general expressions for $C(\xi)$ and $S(\eta)$. After devising and testing a considerable number of expressions for the chordwise and spanwise distributions, the following equations were adopted

$$C(\xi) = \sqrt{\xi} \, \exp\left[\xi^2/\sqrt{\cos \Lambda_{\ell e}}\right] \tag{19a}$$

$$S(\eta) = (1 + \eta^{2A_e}) \sqrt{1 - \eta^2} \tag{19b}$$

where

$$A_e = 2\,(b_o - a)^2/S_f \tag{19c}$$

$$S_f = \frac{1}{2}(b_o - a)\,[2\,c_r/(b_o - a) - \tan\Lambda_{\ell e} + \tan\Lambda_{te}]\ . \tag{19d}$$

A_e is the exposed aspect ratio; that is, the aspect ratio of the lifting surface formed by eliminating the body and placing the root chords of two adjacent fins together. S_f is the planform area of a single fin. Equations (19a) and (19b) have been shown to give valid results for exposed aspect ratios from 0.5 to 5, leading edge sweep from 0° to 80°, and trailing edge sweep from -60° to 80°.

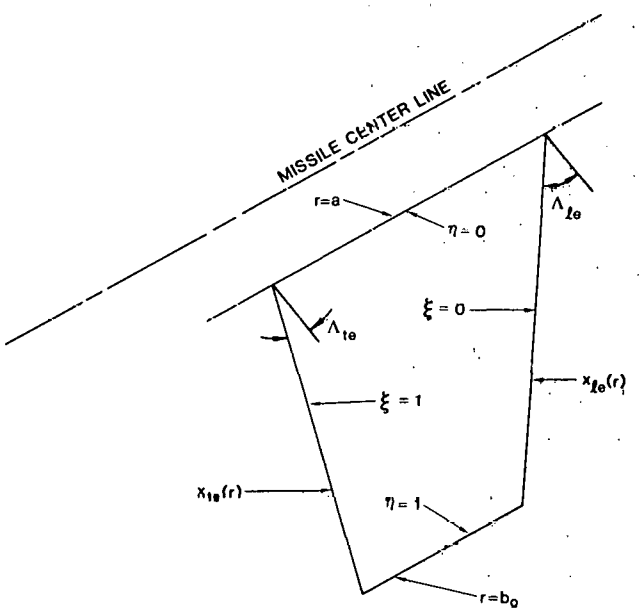

Figure 4. Fin-Oriented Coodinates ξ, η

The normal force distribution over the surface of the fin for uniform approach flow is then provided by the product of Eqs (19a) and (19b). This expression was compared qualitatively with experimental data by means of a three-dimensional computer graphics routine, DISSPLA.* This routine provided a means of visualizing the normal force distribution over the surface of the fin. Shown in Figures 5 through 9 are sets of three-dimensional perspective plots of typical planforms that were examined. Figure 5 shows a sequence of untappered fins with $\Lambda_{\ell e} = \Lambda_{te} = 60°$ for $A_e = 0.5$, 1, and 3. The view in the perspective plot is from behind and above the fin surface, looking upstream and slightly inboard. The graphics routine uses a rectangular area over which the surface function is defined. Consequently, the regions that show a surface value of zero are not part of the fin planform. For example, on Figure 5 the trailing edge of the fin is located at the junction of the nonzero and zero surface values. Another point to note on the perspective plots is a "spike" character at the leading edge of the planform. This characteristic is not inherent in the equations but simply is a result of the mesh size on the surface and the zero value of the surface just ahead of the leading edge.

Figure 6 shows a sequence of fins with $\Lambda_{\ell e} = 60°$, $\Lambda_{te} = 20°$ for $A_e = 0.5$, 1, and 2.92. In Figure 6 the taper ratio decreases until in Figure 6c an arrow wing is achieved. Note in this sequence of figures that as the leading edge becomes longer the normal force loading reflects the very high loading near the leading edge caused by the increasing strength of the leading edge vortex.

Figure 7 shows a rectangular planform for $A_e = 0.5$, 1., and 3. For the low aspect ratio planform (Figure 7a), note the increase in normal force near the tip chord due to the tip vortex increasing in strength along the tip chord. For the high aspect ratio planform (Figure 7c), it can be seen that the spanwise load distribution nears the classical elliptic loading.

Figure 8 presents the loading for $\Lambda_{\ell e} = 60°$, $\Lambda_{te} = 0°$, and $A_e = 0.5$, 1., and 2.31. Figures 8a and 8b show clipped deltas, and Figure 8c shows a delta planform. When the distribution for the delta planform is compared with experimental data,[18] it is seen that the empirical equation models the data except near the leading edge.

Figure 9 shows a trapezoid planform with decreasing taper ratio, $\Lambda_{\ell e} = -\Lambda_{te} = 40°$ and $A_e = 0.5$, 1., and 2.38. The planform with $A_e = 2.38$ (Figure 8c) has a taper ratio of zero and is, therefore, a diamond planform.

The geometric scaling factor in Eq (14) can now be determined. σ is evaluated by the requirement that the integrated average of the assumed normal force distribution over the surface of the fin must be unity; i.e., the assumed normal force loading must be normalized. Therefore, one may write

$$q_\infty \int_{fin}\int C_n\ dA = q_\infty\ C_N\ S_f\ .$$

*DISSPLA is a graphics of software package available from Integrated Software Systems Corporation, San Diego, CA.

Substituting C_n from Eq (14), one has

$$\sigma = \int_a^{b_o} \int_{x_{\ell e}}^{x_{te}} C(x,r)\ S(r)\, dx\, dr = S_f \ .$$

Transforming to the fin coordinates ξ,η (Eq 18) and solving for σ, one obtains

$$\sigma = \frac{S_f}{(b_o - a) \int_o^1 \int_o^1 \Omega(\eta)\, C(\xi)\, S(\eta)\, d\xi\, d\eta} \qquad (20a)$$

where

$$\Omega(\eta) = c_r - (b_o - a)(\tan \Lambda_{\ell e} - \tan \Lambda_{te})\, \eta \qquad (20b)$$

and $C(\xi)$ and $S(\eta)$ are given by Eq (19).

c. Local Angle of Attack

Referring back to Eq (14), C_N depends on the local angle of attack of the chordwise strip. The local angle of attack is calculated by using the unit normal vector of the fin surface, $\vec{n}$, and the total velocity, $\vec{V}$ (Figure 10). The geometric local angle of attack can be shown to be

$$\alpha_\ell = \sin^{-1} [\vec{n} \cdot \vec{V}/(|\vec{n}|\ |\vec{V}|)] \ . \qquad (21)$$

The surface normal vector of the fin depends on the roll angle ϕ and the control deflection of each fin δ_j, j = 1, 2, 3, 4. Let the sign convention of the control deflection of each fin be as follows: positive control deflection of Fins 1 and 3 produces a positive normal force, i.e., a pitch down maneuver; positive control deflection of Fins 2 and 4 produces a positive side force, i.e., a yaw left maneuver (see Figure 10). The sign convention for the surface normal vector, however, is such that the vector always points in the counterclockwise direction. Referring to Figure 10, the surface-normal vector is

$$\vec{n} = \sin(\Delta\, \delta_j)\, \vec{i} - \cos(\delta_j) \sin \phi\, \vec{j} + \cos(\delta_j) \cos \phi\, \vec{k} \qquad (22)$$

where

$$\Delta = \cos \phi / |\cos \phi| \ ;$$

Δ simply provides the sign of δ_j which is consistent with the above-mentioned sign convention.

The local total velocity (i.e., the velocity of the fluid relative to the chordwise strip) is composed of two types of terms: the fluid velocity relative to the fixed coordinate system and the velocity of the fixed coordinate system relative to the spinning chordwise strip. Therefore, using Eq (1) it can be written

$$\vec{V} = U_\infty \cos \alpha_b\, \vec{i} + (v_c + \dot{\phi} r \sin \phi)\, \vec{j} + (w_c - \dot{\phi} r \cos \phi)\, \vec{k} \qquad (23)$$

where v_c and w_c are given by Eq (2) and $\dot{\phi}$ is the roll rate of the missile.

The axial location at which the flow model is evaluated is calculated from the pin planform characteristics. The axial location is chosen as the average quarter chord location of the root and tip chords; i.e.,

$$x_v = (x_1 + 0.25\, c_r + x_2 + 0.25\, c_t)/2$$

where x_v is the axial location of the vortex model and c_t is the length of the tip chord. Rewriting this equation, one has

$$x_v = x_1 + (0.25\, c_r + 0.25\, c_t + (b_o - a)\tan \Lambda_e)/2 \ .$$

This axial location is used in Eqs (9) through (12).

The geometric local angle of attack can now be calculated by substituting Eqs (22) and (23) into Eq (21). Interference between fins, however, will alter α_ℓ for control deflection and a rolling missile. These interference effects are considered in the paragraph entitled Roll Moment.

d. Effective Aspect Ratio

Consider an aerodynamic effect that occurs when the lifting surface is attached to the missile body. If the body is at high angle of attack, the angle in the plane of the fin between the approach flow and the fin leading edge can vary significantly, depending on the roll angle of the body; that is, the fin is yawed with respect to the approach flow for various roll angles around the body. This yaw angle results in an effective change in the leading and trailing edge sweep and effective aspect ratio of the fin. A simple example of this is to consider Fin 4 at a roll angle of 0° with the body at angle of attack α_b (see Figure 10). The effective leading edge sweep of Fin 4 at $\phi = 0°$ then is approximately $\Lambda_{\ell e} - \alpha_b$. If $\Lambda_{\ell e} = 0°$, then the fin at this roll angle would actually be swept forward.

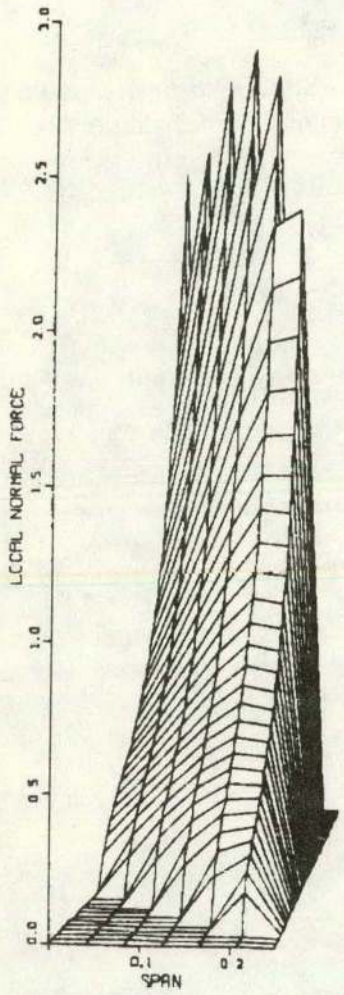

a) $A_e = .5$

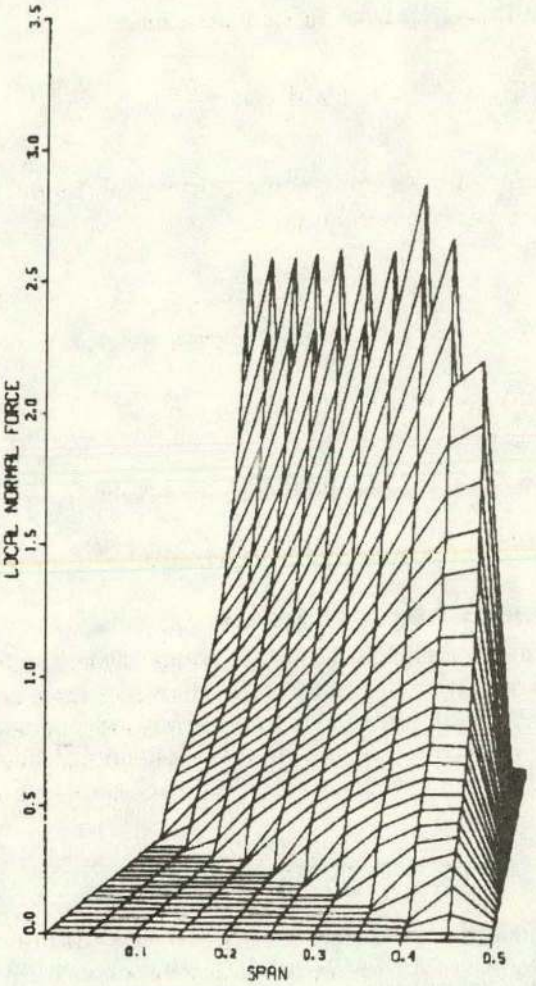

b) $A_e = 1.$

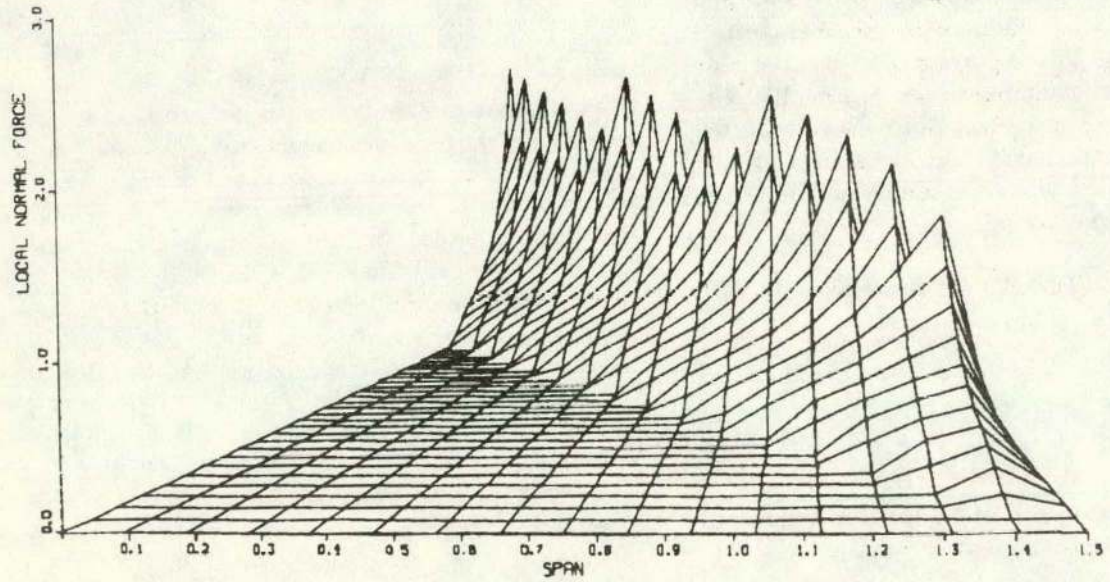

c) $A_e = 3.$

Figure 5. Normal Force Distribution Over Fin Surface for $\Lambda_{\ell e} = \Lambda_{te} = 60°$

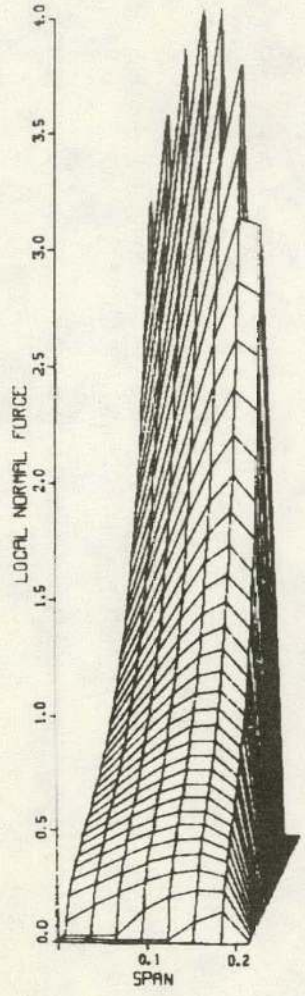

a) $A_e = .5$

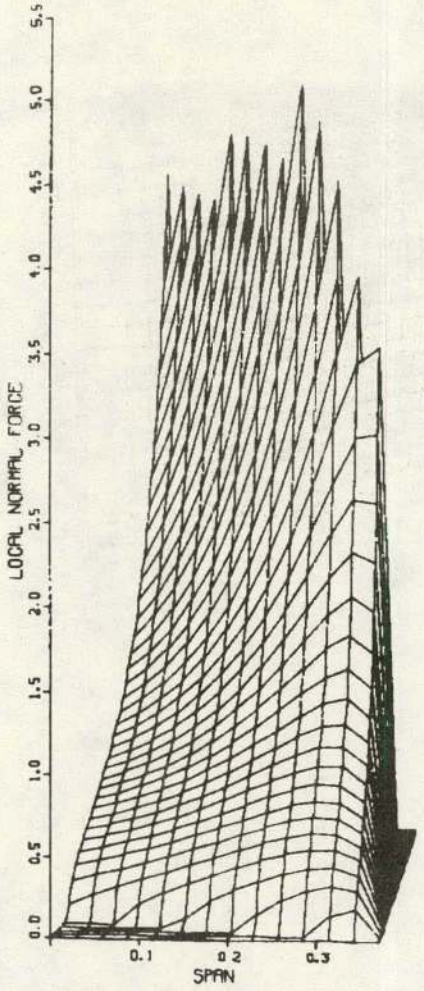

b) $A_e = 1.$

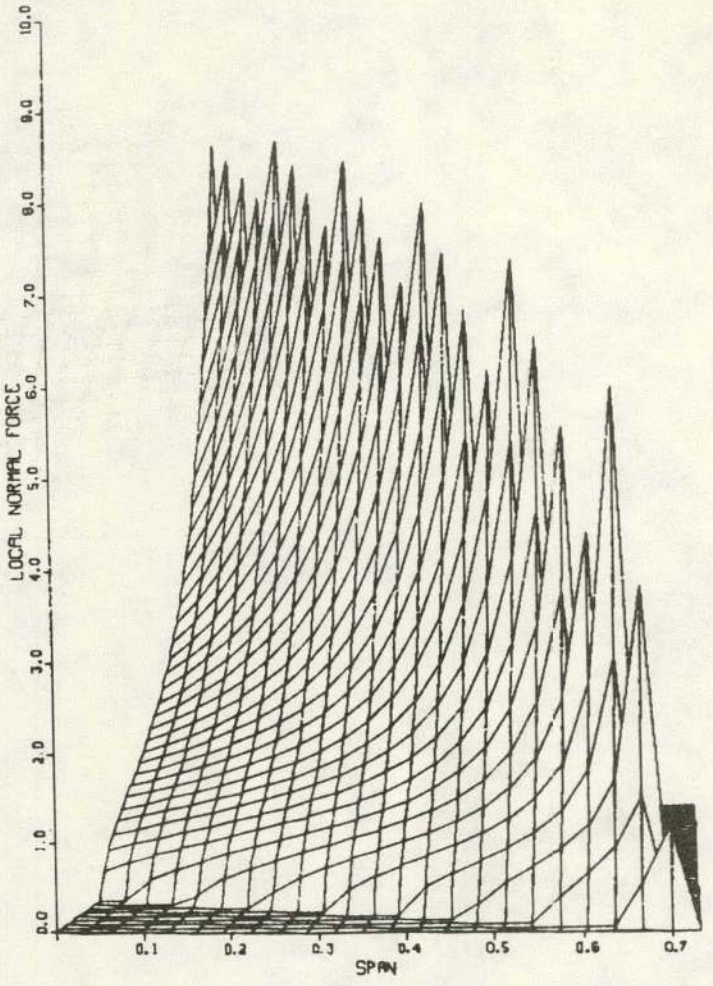

c) $A_e = 2.92$

Figure 6. Normal Force Distribution Over Fin Surface for $\Lambda_{\ell e} = 60°$ and $\Lambda_{te} = 20°$

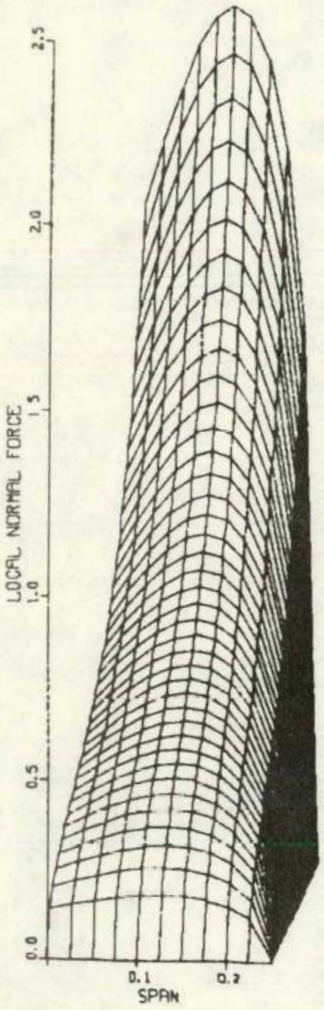

a) $A_e = .5$

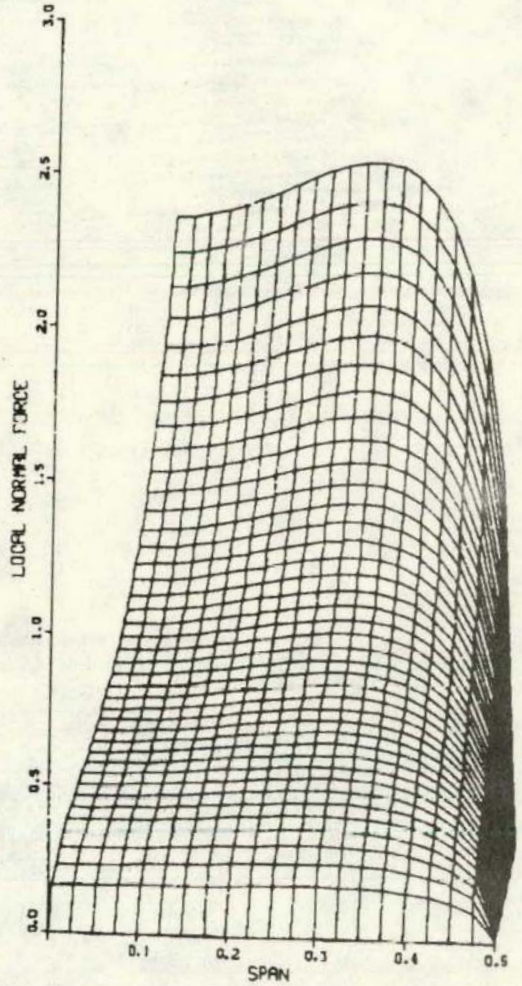

b) $A_c = 1$

Figure 7. Normal Force Distribution Over Fin Surface for $\Lambda_{\ell e} = \Lambda_{te} = 0°$

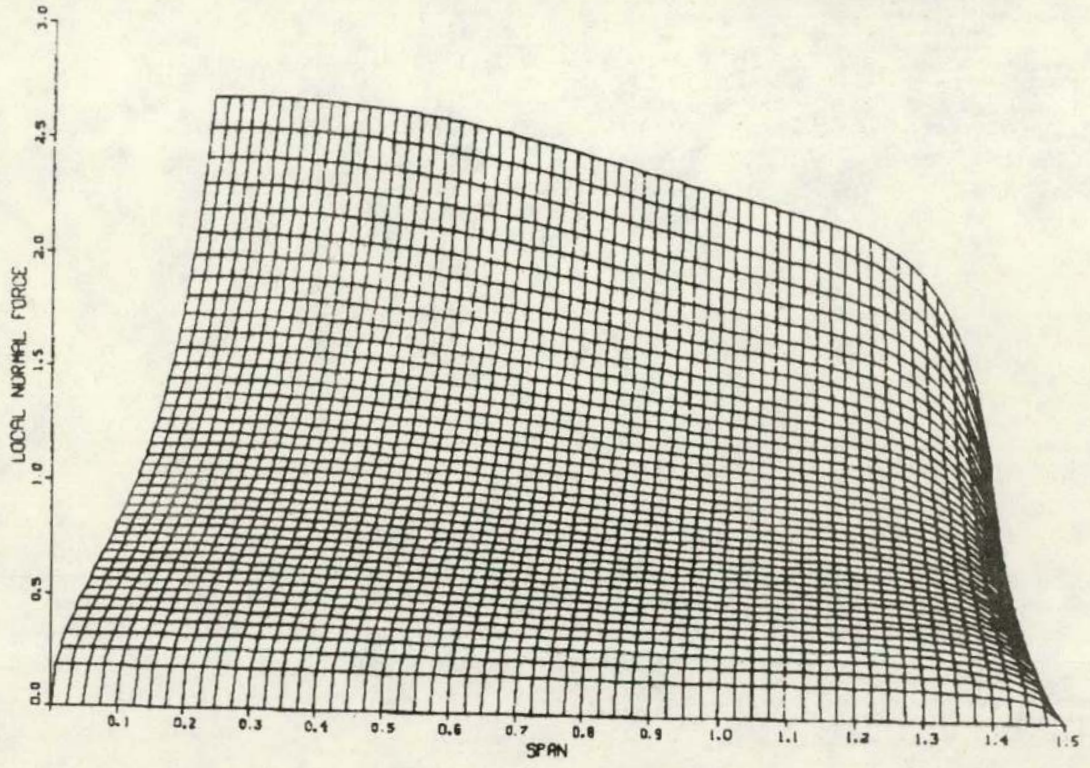

c) $A_e = 3.$

Figure 7. (Concluded)

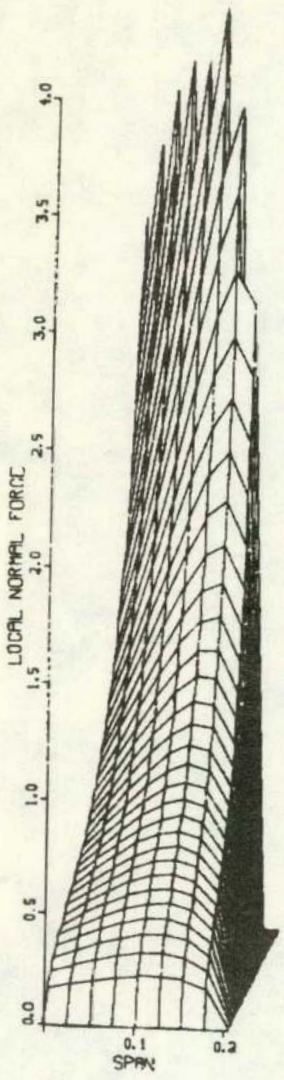

a) A_e = .5

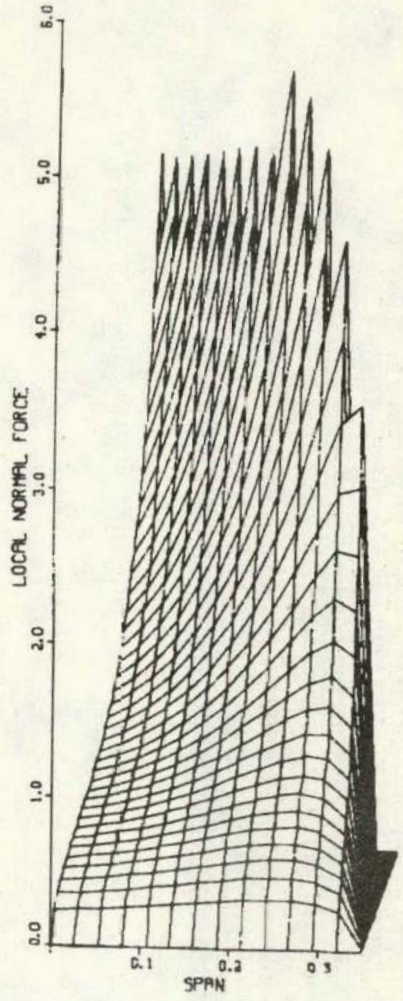

b) A_e = 1.

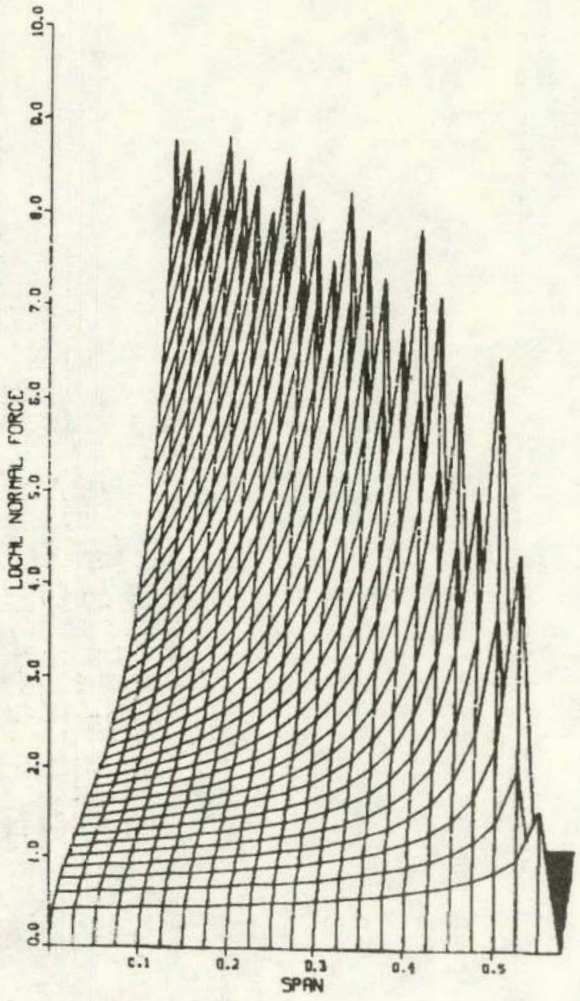

c) A_e = 2.31

Figure 8. Normal Force Distribution Over Fin Surface for $\Lambda_{\ell e} = 60°$ and $\Lambda_{te} = 0°$

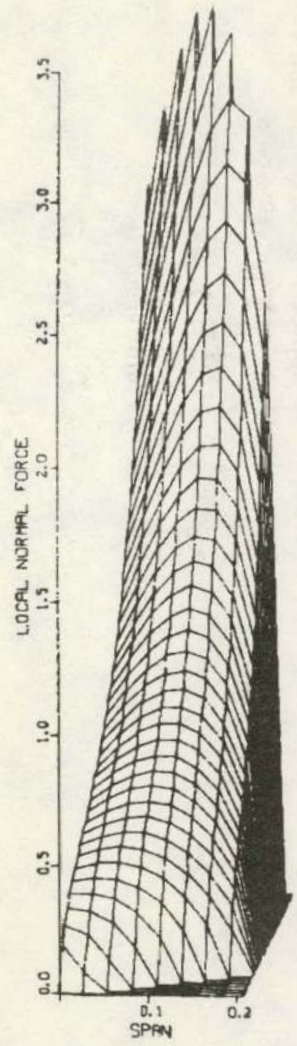

a) A_e = .5

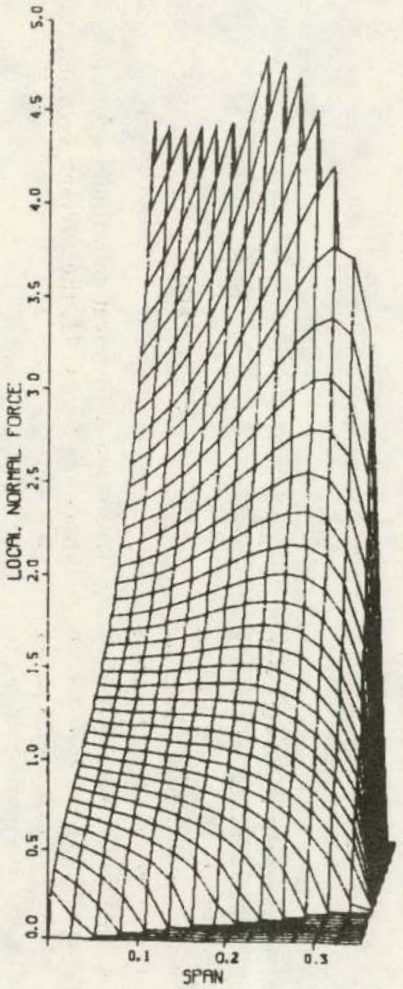

b) A_e = 1.

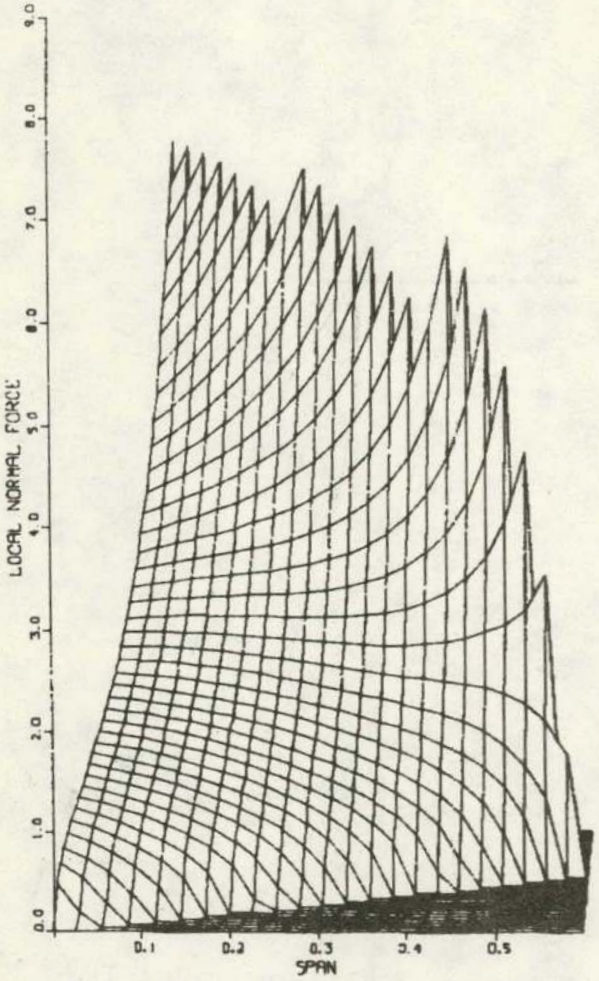

c) A_e = 2.38

Figure 9. Normal Force Distribution Over Fin Surface for $\Lambda_{\ell e}$ = 40° and Λ_{te} = -40°

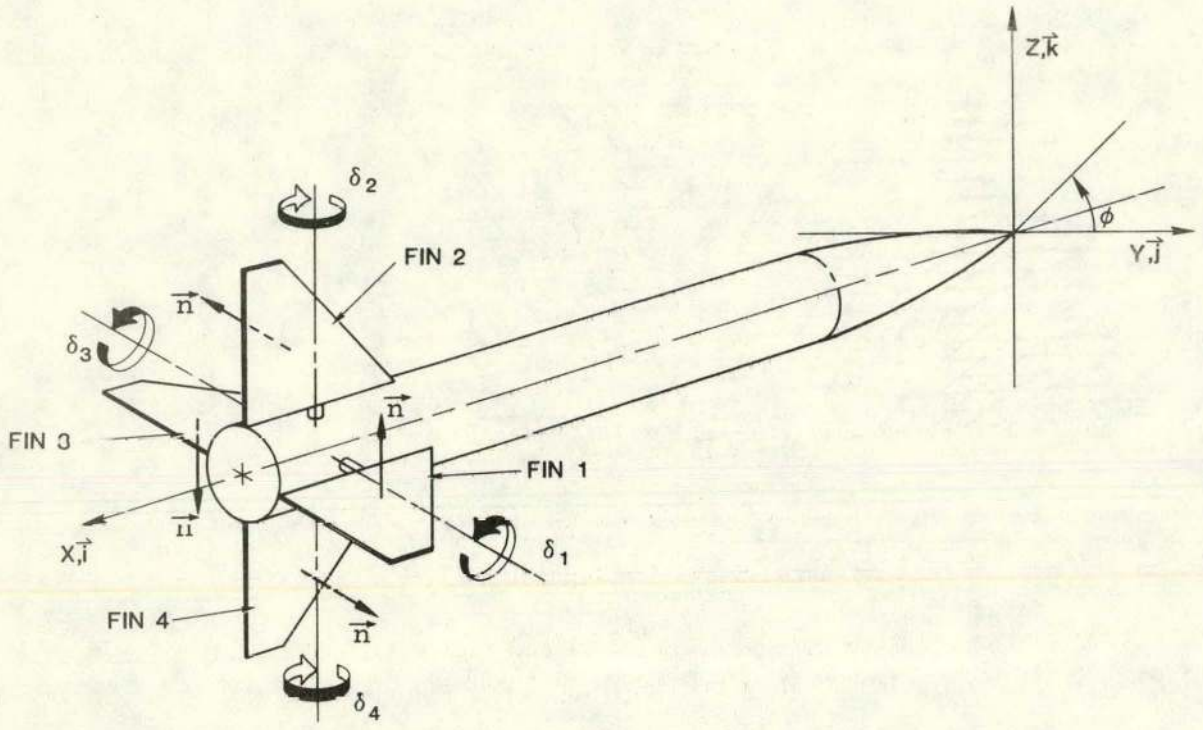

Figure 10. Surface Normal Vector and Sign Convention for Fin Control Deflection

The effective leading edge sweep, $\hat{\Lambda}_{\ell e}$, and effective trailing edge sweep $\hat{\Lambda}_{te}$, are derived by relating the average flow velocity along the fin to the leading and trailing edge unit vectors, respectively. The most convenient coordinate system to use is cylindrical coordinates with the orthogonal unit vectors located in the plane of the fin (see Figure 11). Let $\bar{v}_c$ and $\bar{w}_c$ be the average cross-flow velocity components along the exposed semispan of the fin at a given roll angle; then,

$$\bar{v}_c = \frac{1}{b_o - a} \int_a^{b_o} v_c(r, \phi)\, dr$$

and

$$\bar{w}_c = \frac{1}{b_0 - a} \int_a^{b_o} w_c(r, \phi)\, dr$$

where v_c and w_c are given by Eq (2). Rewriting these equations in terms of fin-oriented coordinates, one has

$$\bar{v}_c = \int_o^1 v_c(\eta, \phi)\, d\eta \qquad (24a)$$

and

$$\bar{w}_c = \int_o^1 w_c(\eta, \phi)\, d\eta \,. \qquad (24b)$$

Using the cylindrical coordinate unit vectors $\vec{e}_x$, $\vec{e}_r$, shown in Figure 11, the average velocity along the leading edge is

$$\vec{V} = \bar{u}\vec{e}_x + \bar{v}_r\vec{e}_r$$

where

$$\bar{u} = U_\infty \cos \alpha_b$$

$$\bar{v}_r = \bar{v}_c \cos \phi \mid \bar{w}_c \sin \phi \,.$$

Since the sweep angle is measured from a line perpendicular to the approach velocity, the unit vector perpendicular to the average velocity is

$$\vec{V}_\perp = \bar{v}_r/\sqrt{\bar{u}^2 + \bar{v}_r^2}\,\vec{e}_x + \bar{u}/\sqrt{\bar{u}^2 + \bar{v}_r^2}\,\vec{e}_r \,. \qquad (25)$$

The leading edge unit vector is

$$\vec{e}_{\ell e} = \sin \Lambda_{\ell e}\vec{e}_x + \cos \Lambda_{\ell e}\vec{e}_r \,. \qquad (26)$$

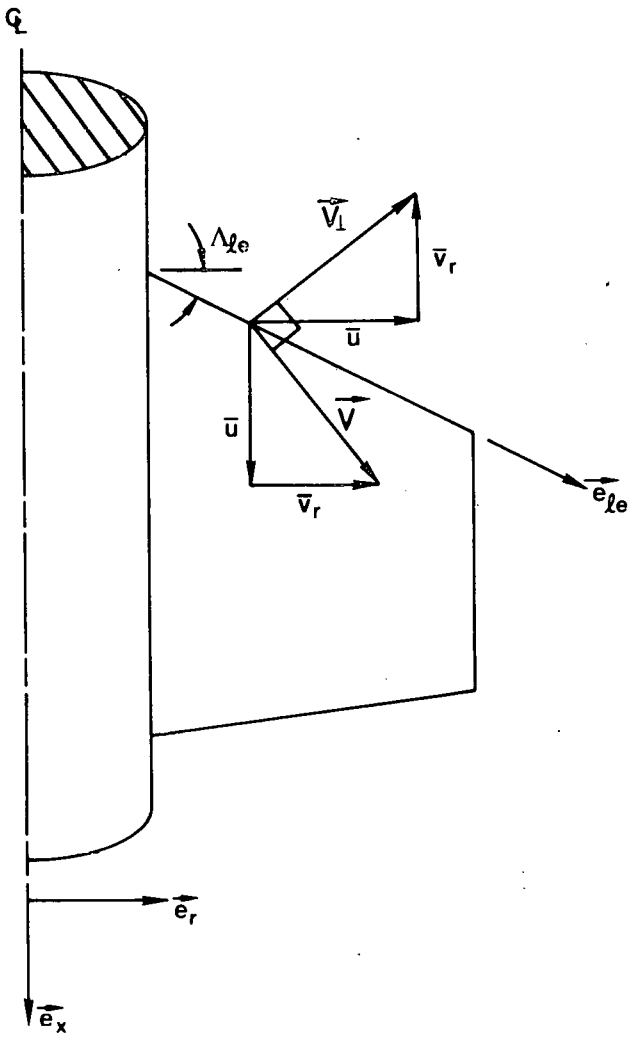

Figure 11. Fin Surface Cylindrical Coordinates

The effective leading edge sweep angle is the angle between $\vec{V}_\perp$ and $\vec{e}_{\ell e}$. Using the scalar product, one obtains

$$\hat{\Lambda}_{\ell e} = \cos^{-1}(\vec{V}_\perp \cdot \vec{e}_{\ell e}) \ .$$

Substituting in Eqs (25) and (26),

$$\hat{\Lambda}_{\ell e} = \cos^{-1}\left[(\bar{u}\cos\Lambda_{\ell e} - \bar{v}_r \sin\Lambda_{\ell e})/\sqrt{\bar{u}^2 + \bar{v}_r^2}\right] \ . \quad (27)$$

This expression presents difficulties in evaluation because the arc cosine function is double valued. This problem can be nicely circumvented by noting that the argument of the arc cosine function suggests $\hat{\Lambda}_{\ell e}$ might be split into two angles. Let

$$\hat{\Lambda}_{\ell e} = \Lambda_{\ell e} + \epsilon_{\ell e} \quad (28)$$

where $\epsilon_{\ell e}$ is the deviation of the effective leading edge sweep from the geometric leading edge sweep. Now Eq (27) can be written as

$$\cos(\Lambda_{\ell e} + \epsilon_{\ell e}) = \frac{\bar{u}}{\sqrt{\bar{u}^2 + \bar{v}_r^2}}\cos\Lambda_{\ell e} - \frac{\bar{v}_r}{\sqrt{\bar{u}^2 + \bar{v}_r^2}}\sin\Lambda_{\ell e} \ .$$

Using the trigonometric identity for the cosine of a sum, one has

$$\cos\epsilon_{\ell e}\cos\Lambda_{\ell e} - \sin\epsilon_{\ell e}\sin\Lambda_{\ell e} = \frac{\bar{u}}{\sqrt{\bar{u}^2 + \bar{v}_r^2}}\cos\Lambda_{\ell e} - \frac{\bar{v}_r}{\sqrt{\bar{u}^2 + \bar{v}_r^2}}\sin\Lambda_{\ell e} \ .$$

In matching terms, one notes that two mathematically equivalent expressions can be written for $\epsilon_{\ell e}$. The one involving the cosine function, however, suffers from the same difficulty mentioned above; therefore use

$$\sin\epsilon_{\ell e} = \bar{v}_r/\sqrt{\bar{u}^2 + \bar{v}_r^2} \ .$$

Substituting this into Eq (28), one finally obtains

$$\hat{\Lambda}_{\ell e} = \Lambda_{\ell e} + \sin^{-1}\left(\bar{v}_r/\sqrt{\bar{u}^2 + \bar{v}_r^2}\right) \ . \quad (29a)$$

Using exactly the same procedure, the effective trailing edge sweep is given by

$$\hat{\Lambda}_{te} = \Lambda_{te} + \sin^{-1}\left(\bar{v}_r/\sqrt{\bar{u}^2 + \bar{v}_r^2}\right) \ . \quad (29b)$$

The effective leading and trailing edge sweep caused by high angle of attack results in an effective aspect ratio of the fin. This is significant since the local normal force coefficient due to angle of attack, $C_N(\alpha_\ell)$, will now reflect effective changes in fin geometry due to apparent yaw of the fin. To derive an expression for $\hat{A}_e$, begin with the definition of A_e

$$A_e = 2(b_o - a)^2/S_f$$

where S_f is the exposed planform area of a fin. Writing this in terms of fin semispan, root chord, and leading and trailing edge sweep, one has

$$A_e = 4/[2c_r/(b_o - a) - \tan\Lambda_{\ell e} + \tan\Lambda_{te}] \ . \quad (30)$$

Referring to Figure 12, it can be seen that the exposed fin semispan and root chord also effectively change. It can be shown that

$$\widehat{b_o - a} = (b_o - a)\cos\hat{\Lambda}_{\ell e}/\cos\Lambda_{\ell e}\ ; \qquad (31a)$$

$$\hat{c}_r = c_r \cos\Lambda_{te}/\cos(\hat{\Lambda}_{\ell e} - \Lambda_{\ell e} + \Lambda_{te})\ . \qquad (31b)$$

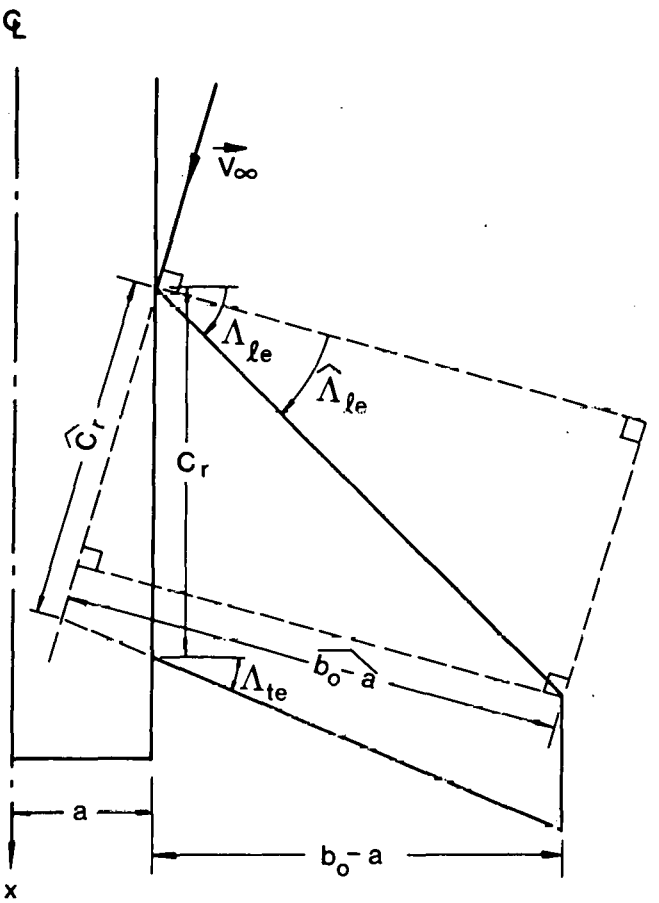

Figure 12. Geometry for Determining Effective Aspect Ratio

Using Eqs (30) and (31), the effective aspect ratio is written as

$$\hat{A}_e = \frac{4}{\dfrac{2c_r\cos\Lambda_{\ell e}\cos\Lambda_{te}}{(b_o-a)\cos\hat{\Lambda}_{\ell e}\cos(\hat{\Lambda}_{\ell e} - \Lambda_{\ell e} + \Lambda_{te})} - \tan\hat{\Lambda}_{\ell e} + \tan\hat{\Lambda}_{te}} \qquad (32)$$

e. Expression for C_N (α_ℓ)

The functional dependence of C_N on the local angle of attack is given by an empirical expression based on lifting surfaces in uniform approach flow. Other investigators (for example, Reference 6) have used experimental data for C_N (α_ℓ) directly in their analysis. This is rarely an appealing approach because it requires vast amounts of data to construct a data base sufficiently general to address general planforms over a large range of Mach numbers. Also, this is not possible in the present approach because the effective geometry of the fin (discussed earlier) changes with the character of the nonuniform approach flow.

As the local angle of attack on a missile fin can be approximately 40° to 50° when the angle of attack of the body is 25°, the expression for C_N (α_ℓ) must include prestall, stall, and poststall characteristics. The prestall expression for C_N (α_ℓ) is taken from the work of Lecat and Rietschlin.[20] Their analysis is based on Polhamus suction analogy.[21] They extended the original work of Polhamus on delta wings to include arbitrary planforms and transonic flow. Their analysis is not repeated here, but their equations are given in the present nomenclature.

Their expression for C_N (α) is

$$C_N(\alpha) = K_p \sin\alpha\cos\alpha + K_v \sin^2\alpha\ . \qquad (33)$$

Note that this equation shows C_N continually increasing with α and, as a result, is not appropriate for angles near or greater than the stall angle. Although Lecat and Reitschlin state their method is applicable to subsonic and supersonic flow, the present analysis is considered appropriate for subsonic flow and only supersonic flow with subsonic leading edges.

The calculation procedure for K_p and K_v is as follows:

(1) Calculate $\widehat{b_o - a}$, $\hat{c}_r$, and $\hat{A}_e$ from Eqs (31) and (32).

(2) Calculate the distance from x_1 to the aftmost point of maximum span, c_r^*

$$c_r^* = \hat{c}_r + (\widehat{b_o - a})\tan\hat{\Lambda}_{te} \qquad (34a)$$

(3) Calculate the sweep of the semispan diagonal, γ.

$$\gamma = \tan^{-1}[\hat{c}_r/(\widehat{b_o - a}) + \tan\hat{\Lambda}_{te}] \qquad (34b)$$

(4) Calculate the ratio of planform area to rectangular reference area, S_f/S_f^*

$$S_f/S_f^* = 2/[\hat{A}_e \tan\gamma] \qquad (34c)$$

(5) If $M_\infty > 1$, calculate the complement of the Mach angle, γ_M.

$$\gamma_M = \cos^{-1}(1/M_\infty) \qquad (34d)$$

(6) Calculate the planform parameter, p^*.

$$p^* = \begin{cases} S_f/S_f^* & \text{for } M_\infty \le 1 \\ \dfrac{S_f/S_f^*}{1 - [\tan\gamma_M/(2\tan\gamma)]} & \text{for } M_\infty > 1 \end{cases} \tag{34e}$$

(7) Calculate the planform angle, ψ.

$$\psi = \begin{cases} \tan^{-1}(2p^*\tan\gamma) & M_\infty \le 1 \\ \tan^{-1}[2p^*(\tan\gamma - \tan\gamma_M)] & M_\infty > 1 \end{cases} \tag{34f}$$

(8) Calculate the compressibility factor, β.

$$B = \begin{cases} \sqrt{1 - M_\infty^2} & M_\infty \le 1 \\ \sqrt{M_\infty^2 - 1} & M_\infty > 1 \end{cases} \tag{34g}$$

(9) Calculate the potential flow lift coefficient, K_p.

$$K_p = \frac{4\pi}{\tan\psi + \sqrt{\tan^2\psi + (\sin^2\psi/p^{*2}) + 4\beta^2}} \tag{34h}$$

(10) Calculate the vortex flow lift coefficient, K_v.

$$K_v = [K_p - (K_p^2\tan\psi)/4\pi]\sqrt{1 + \tan^2\psi} \tag{34i}$$

An empirical expression was devised for the normal force coefficient, $C_N(\alpha_\ell)$, based on the expression of Lecat and Rietschlin, Eq (33). The new expression is more general since it applies both at stall and beyond stall. This expression was constructed after examining and comparing a large number of trial expressions with experimental data[10,15-23] for a wide variety of planforms. This expression is

$$C_N(\alpha_\ell) = \begin{cases} (K_p\sin\alpha_\ell\cos\alpha_\ell + K_v\sin^2\alpha_\ell)\,[1 - (1-\mu)(\alpha_\ell/\alpha_s)^3] & 0 \le \alpha_\ell \le \alpha_s \\ f<A_e, \Lambda_{\ell e}> C_N<\alpha_s> + [A_e\cos\Lambda_{\ell e} C_N<\alpha_\ell - \alpha_s>]/10 & \alpha_s < \alpha_\ell \le 2\alpha_s \\ f<A_e, \Lambda_{\ell e}> C_N<\alpha_s> + [A_e\cos\Lambda_{\ell e} C_N<\alpha_s>]/10 & 2\alpha_s < \alpha_\ell \end{cases} \tag{35a}$$

where the symbol $< >$ is used to denote functional dependence in situations where the standard symbol, which is a set of parentheses, would be confusing. Also,

$$\mu = 0.9 - 0.2\,A_e\sin 2\Lambda_{\ell e}$$

$$\alpha_s = 38[1 + 0.02\,(A_e - 2)^4][1 + 1.1\,(A_e - 1)^{2.5}\cos^2\Lambda_{\ell e}] \cdot \{1 + [6(A_e - 1)^2\sin^4\Lambda_{\ell e}]/e^{A_e}\}/[\cos\Lambda_{\ell e} + 1]^{2(A_e - 1)} \tag{35b}$$

$$f(A_e, \Lambda_{\ell e}) = 1 - 0.35\left\{1 + \frac{1}{8}e^{A_e}\sin^{\frac{1}{A_e}}\Lambda_{\ell e} \cdot \sin[(A_e - 2.1)\Lambda_{\ell e}]\right\}/[1 + 0.5(A_e - 1)^3] \tag{35c}$$

and K_p and K_v are given by Eq (33).

As can be seen, $C_N(\alpha_\ell)$ is composed of three angle of attack ranges: zero angle up to the stall angle, stall up to twice the stall angle, and angles larger than twice the stall angle. For angles less than α_s, the expression of Lecat and Reitschlin[20] (Eq (33)) has been modified for α_ℓ near α_s. Equation (35a) for $\alpha_\ell < \alpha_s$ shows that as α_ℓ approaches α_s the normal force coefficient increases more slowly. This characteristic is consistent with experimental measurements. The parameter μ represents the portion of C_N predicted by Lecat and Reitschlin which remains at $\alpha_\ell = \alpha_s^-$. The expression for α_s, although rather lengthy, gives a good estimate of the stall angle (in degrees) for planforms with aspect ratios from 1 to 5 and leading edge sweep from 0° to 70°.

$f(A_e, \Lambda_{\ell e})$ represents the portion of $C_N(\alpha_s)$ existing for $\alpha_\ell = \alpha_s^+$. Note that μ, α_s, and $f(A_e, \Lambda_{\ell e})$ show no dependence on free-stream Mach number. This is not necessarily a reflection of the physics, but simply an admission of lack of data.

$C_N(\alpha_\ell)$ as predicted by Eq (35) was compared with data for a very wide variety of planform geometries in order to determine its range of applicability. Figures 13 through 22 show typical comparisons of Eq (35) with experimental data for incompressible flow. The figures are placed in order of increasing aspect ratio from 1 to 4. The leading edge sweep angle varies from 0° to 70°; planform geometries include: rectangular, diamond, clipped delta, delta, arrow, clipped arrow, and trapezoidal. The comparisons are good for all planforms except that for the aspect ratio 3 trapezoid (Figure 21) and rectangular planforms of $A_e \ge 3$ (comparisons not shown). For these types of planforms (i.e., high aspect ratio with small leading edge sweep), the normal force past stall is significantly overestimated by the present expression.

f. Fin - Fin Interference

Two types of fin - fin interference are included in the present lifting theory. The first type is caused by control deflection of the fins, and the second type by the rolling motion of the missile. When a control deflection is input to a fin, the lifting flow field of that fin induces an angle of attack on the adjacent fins. This induced angle of attack causes the adjacent fins to generate forces and moments which depend

on the magnitude and direction of the control input. Rolling motion interference occurs for a similar reason except that the angle of attack of a fin is generated by the angular velocity of the fin relative to the oncoming stream. Control deflection interference will be considered first and then rolling motion interference will be analyzed. Results of slender-body theory are used to evaluate both types of interference considered here.

Figure 23 (taken from Reference 24) shows the interference flow fields and pressures induced on adjacent fins for two types of control input: positive pitch control and positive roll control with horizontal fins. For the pitch control, it is seen that a negative pressure coefficient is produced on both sides of the top fin and a positive pressure coefficient is generated on both sides of the bottom fin. For roll contol (i.e., differential deflection), a negative pressure is generated on the top right and bottom left sides of the vertical fins, and a positive pressure is generated on the top left and bottom right sides of the vertical fins. In the present analysis these induced pressures are included by considering the adjacent fins to be at an effective deflection angle.

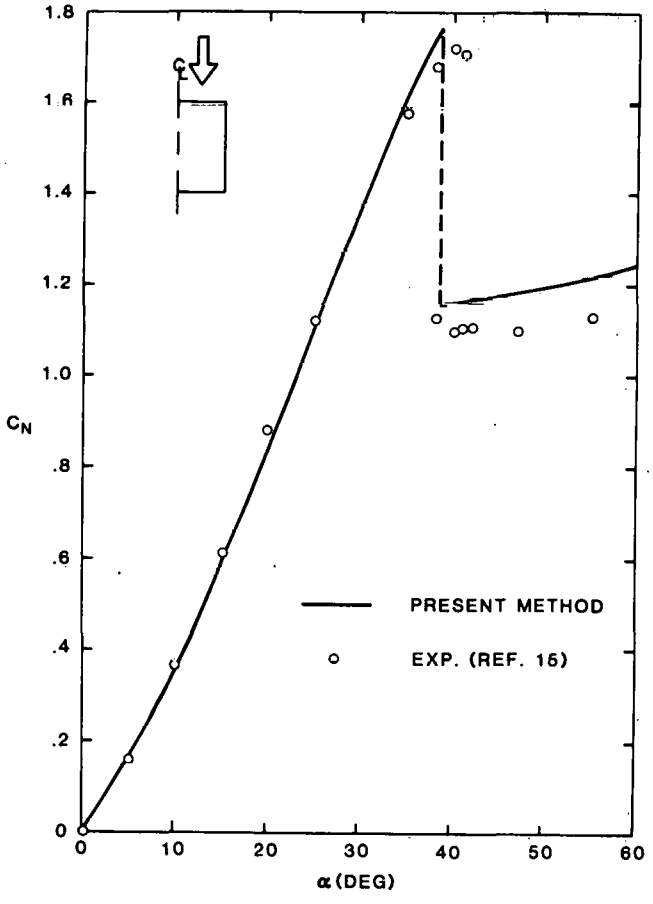

Figure 13. Normal Force Coefficient vs α for Rectangular Planform ($A_e = 1$)

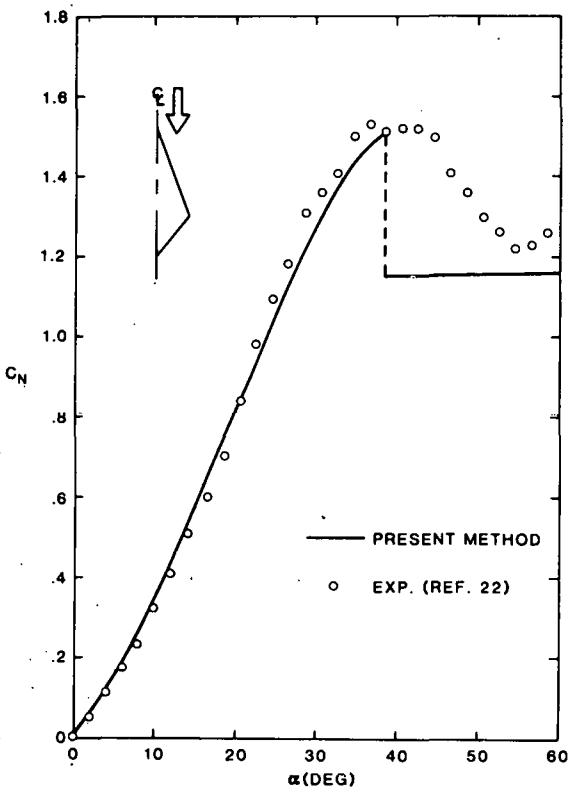

Figure 14. Normal Force Coefficient vs α for Diamond Planform ($A_e = 1$)

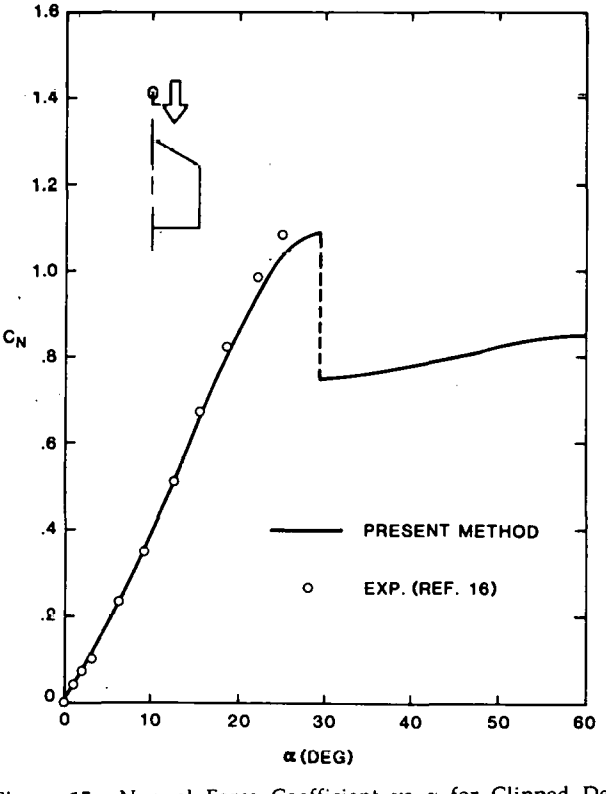

Figure 15. Normal Force Coefficient vs α for Clipped Delta Planform ($A_e = 1.23$)

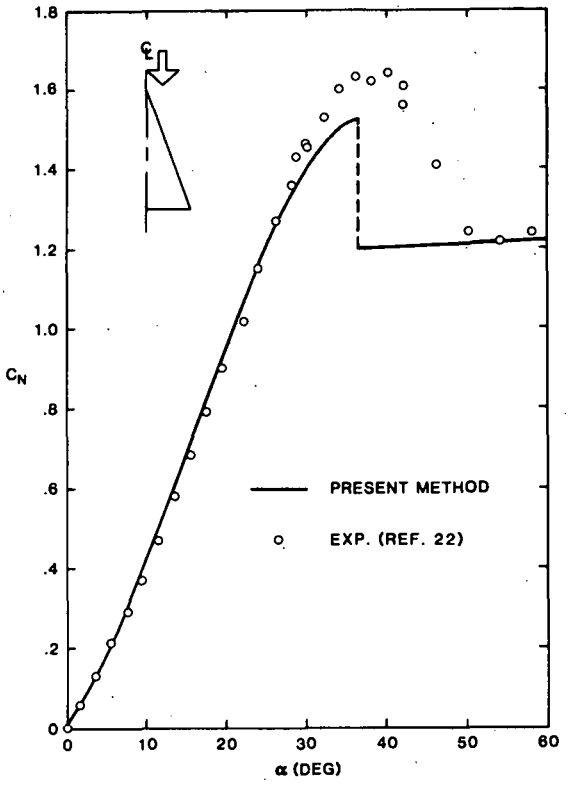

Figure 16. Normal Force Coefficient vs α for Delta Planform (A_e = 1.46)

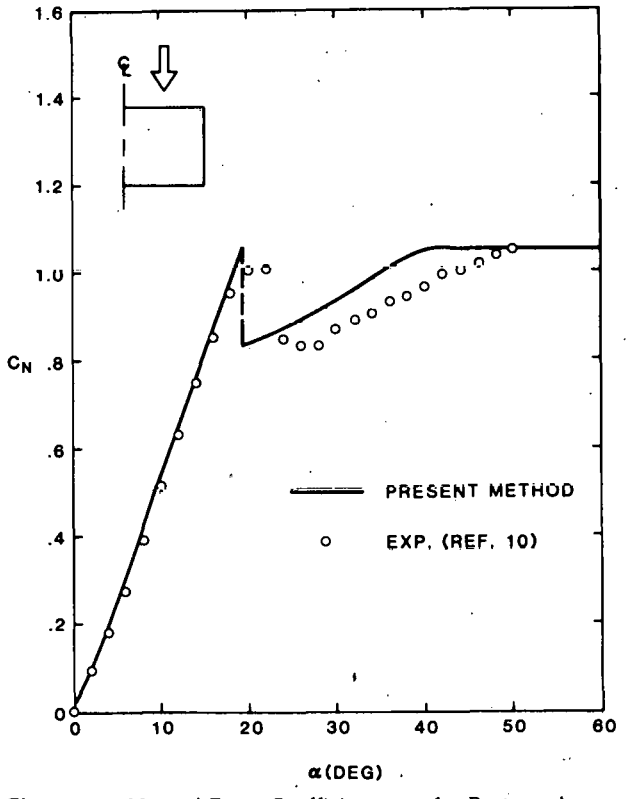

Figure 17. Normal Force Coefficient vs α for Rectangular Planform (A_e = 2)

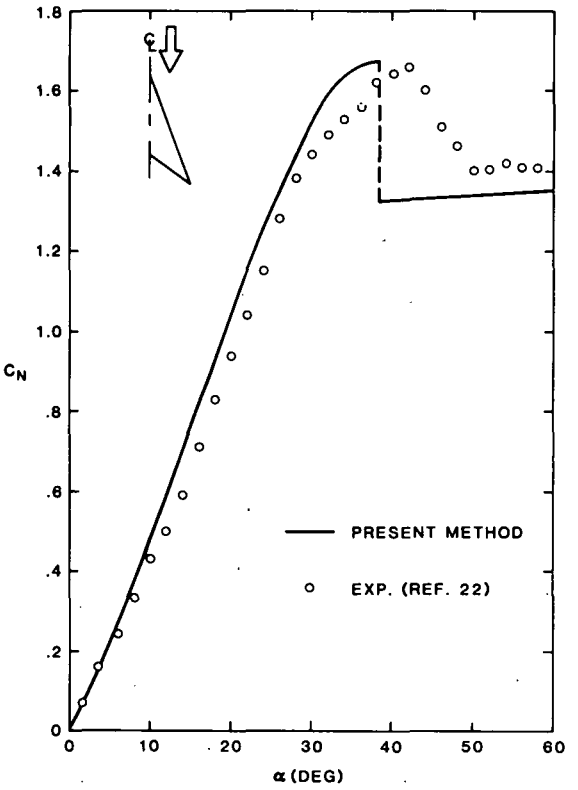

Figure 18. Normal Force Coefficient vs α for Arrow Planform (A_e = 2)

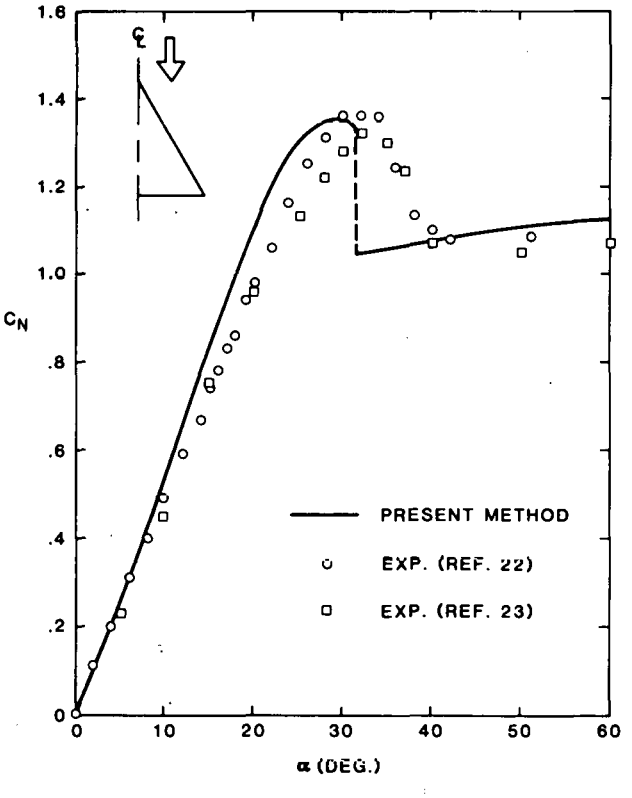

Figure 19. Normal Force Coefficient vs α for Delta Planform (A_e = 2.31).

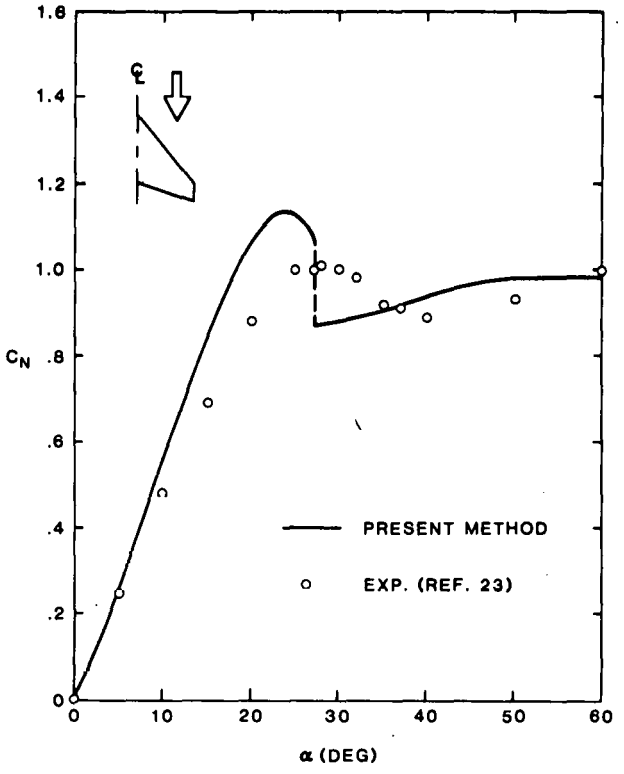

Figure 20. Normal Force Coefficient vs α for Clipped Arrow Planform (A_e = 2.61)

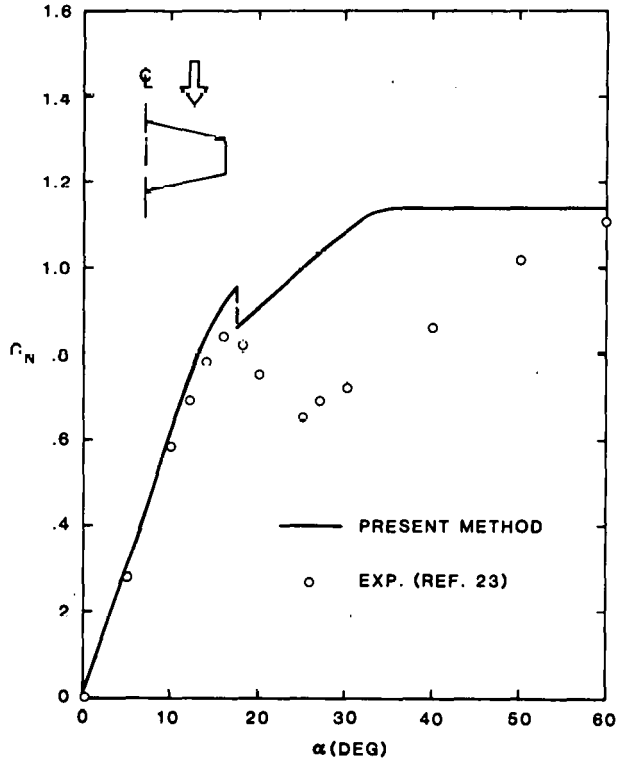

Figure 21. Normal Force Coefficient vs α for Trapezoidal Planform (A_e = 3.)

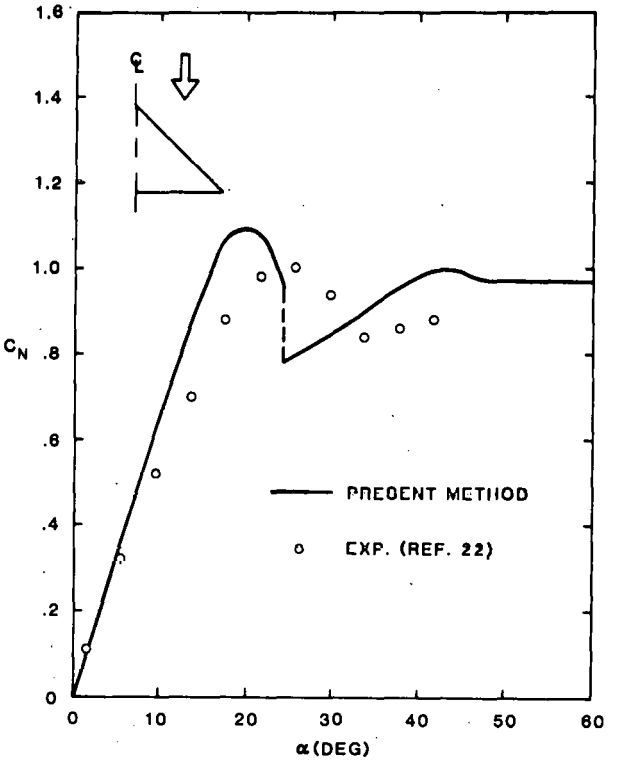

Figure 22. Normal Force Coefficient vs α for Delta Planform (A_e = 4.)

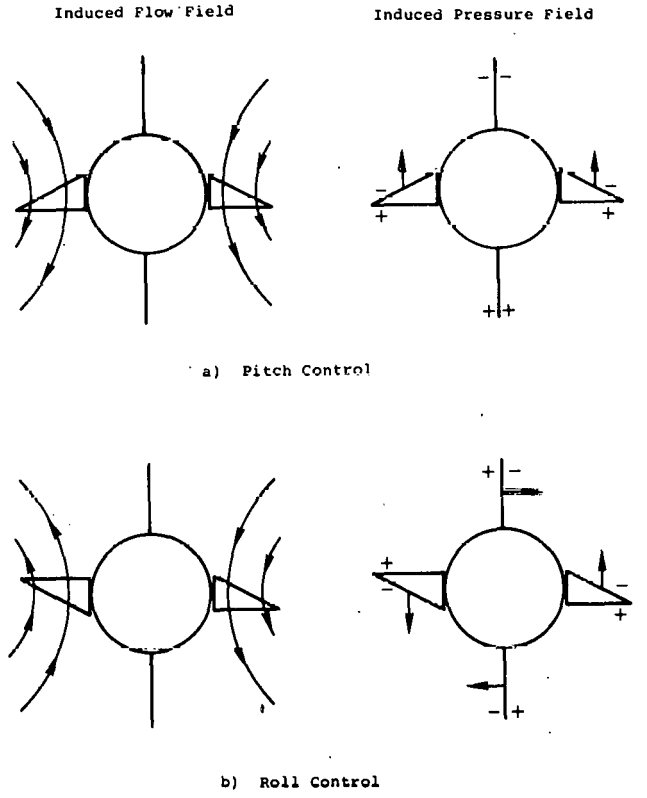

Figure 23. Control Interference for Pitch and Roll Control (from Ref. 24)

Consider the induced pressures on adjacent fins for individual deflection of each fin. Shown in Figure 24 is the induced pressure and effective deflection force for positive deflection of each fin. If we let I_d be the deflection interference coefficient, the following equations describe the interference depicted in Figure 24.

$$\text{for } \delta_1 > 0 \begin{cases} \delta_{e_2} = I_d\delta_1 \\ \delta_{e_3} = 0 \\ \delta_{e_4} = -I_d\delta_1 \end{cases} \qquad \text{for } \delta_2 > 0 \begin{cases} \delta_{e_1} = I_d\delta_2 \\ \delta_{e_3} = -I_d\delta_2 \\ \delta_{e_4} = 0 \end{cases}$$

$$\text{for } \delta_3 > 0 \begin{cases} \delta_{e_1} = 0 \\ \delta_{e_2} = -I_d\delta_3 \\ \delta_{e_4} = I_d\delta_3 \end{cases} \qquad \text{for } \delta_4 > 0 \begin{cases} \delta_{e_1} = -I_d\delta_4 \\ \delta_{e_2} = 0 \\ \delta_{e_3} = I_d\delta_4 \end{cases} \tag{36}$$

Summing all of the effective control deflections given in Eq (36) and including the actual control deflection, one obtains

$$\begin{aligned} \delta_{e_1} &= \delta_1 + I_d(\delta_2 - \delta_4) \\ \delta_{e_2} &= \delta_2 + I_d(\delta_1 - \delta_3) \\ \delta_{e_3} &= \delta_3 + I_d(\delta_4 - \delta_2) \\ \delta_{e_4} &= \delta_4 + I_d(\delta_3 - \delta_1) . \end{aligned} \tag{37}$$

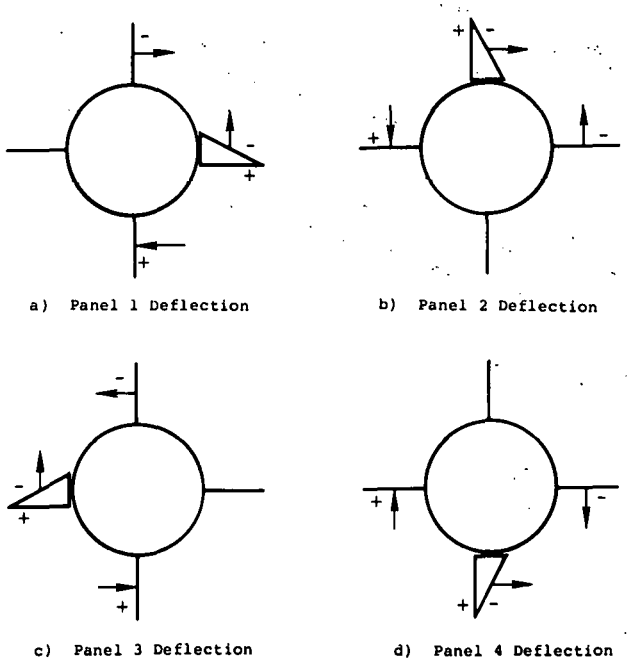

Figure 24. Control Interference for Individual Panel Deflection

I_d is evaluated by using the slender body theory results of Adams and Dugan.[25] They derived results from the roll moment coefficient derivative, C_{ℓ_δ}, vs a/b_o for differential deflection of two fins. They further showed results for the roll moment coefficient induced on the vertical fins because of differential deflection of the horizontal fins. Assuming the induced angle of attack of the upwash and downwash of the deflected fin on the undeflected fin is constant along the span, one can write

$$\frac{[C_{\ell_\delta}]_{\text{induced}}}{[C_{\ell_\delta}]_{\text{deflected}}} = \frac{\delta_e}{\delta} \tag{38}$$

This equation can be proven, given the stated assumption, by writing the roll moment of the induced and deflected fin in double integral form. Noting that the ratio shown in Eq (38) is for differential deflection of two fins, one has

$$I_d = \frac{1}{2}\frac{[C_{\ell_\delta}]_{\text{induced}}}{[C_{\ell_\delta}]_{\text{deflected}}} . \tag{39}$$

Figure 25 plots I_d vs a/b_o, using the results of Adams and Dugan for $[C_{\ell_\delta}]_{\text{induced}}$ and $[C_{\ell_\delta}]_{\text{deflected}}$; it should be noted that they use the planform aspect ratio of the fins, A_p. In the present nomenclature

$$A_p = b^2/S_{f_p} \tag{40a}$$

where S_{f_p} is the planform area of two fins, including their imaginary extension through the body. It can be shown that

$$S_{f_p} = 2S_f + a[2c_r + a(\tan\Lambda_{\ell e} - \tan\Lambda_{te})] . \tag{40b}$$

I_d, as given in Figure 25, is used in Eq (37) to calculate the effective control deflection of each fin.

Now consider the case of fin - fin interference due to rolling motion. The strategy of this derivation is to determine the interference coefficient by matching the present roll moment formulation for zero angle of attack of the body to that obtained by slender body theory. Assuming $\alpha_b = 0$ and the rolling speed is $\dot{\phi}$, the differential roll moment can be written (Figure 26)

$$d\ell = 4\,r\,C_n\frac{1}{2}\rho_\infty[U_\infty + (\dot{\phi}r)]^2 dx\,dr .$$

Assuming the rolling speed is small compared to U_∞ and substituting in C_n from Eq (14), one has

$$d\ell = 4\, q_\infty r\, \sigma\, C_n(\alpha_e)\, C(x, r)\, S(r)\, dx\, dr \qquad (41a)$$

where α_e is the effective local angle of attack along the span. Adams and Dugan[25] showed that the spanwise loading induced on one fin by the other fins was roughly quadratic along the span. In the present analysis, this induced loading will be simply approximated by a linear spanwise function; therefore,

$$\alpha_e = -\frac{\dot{\phi} r}{U_\omega} + I_p \frac{\dot{\phi} r}{U_\infty} \qquad (41b)$$

where I_p is the rolling motion interference coefficient. The first term in Eq (41b) is the local angle of attack caused by rolling speed and the second is the reduction in local angle of attack caused by fin - fin interference.

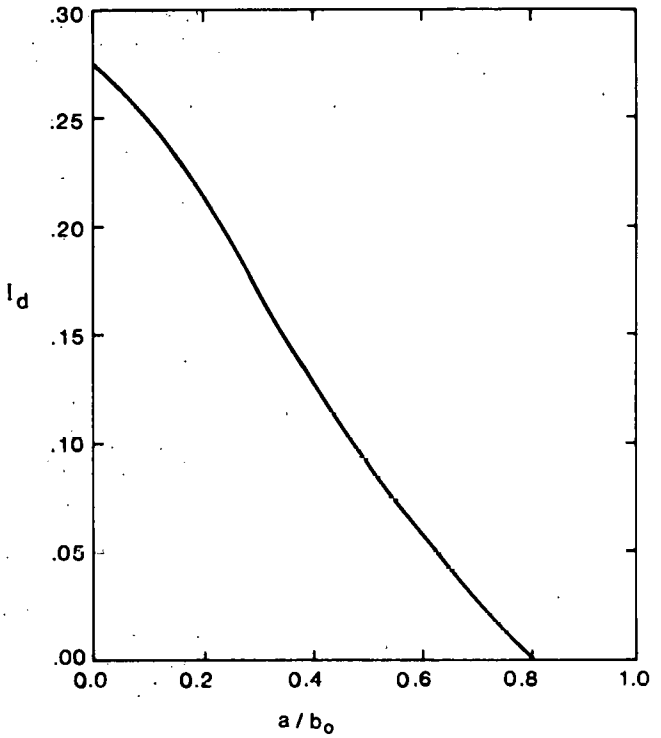

Figure 25. Deflection Interference Coefficient vs a/b_o

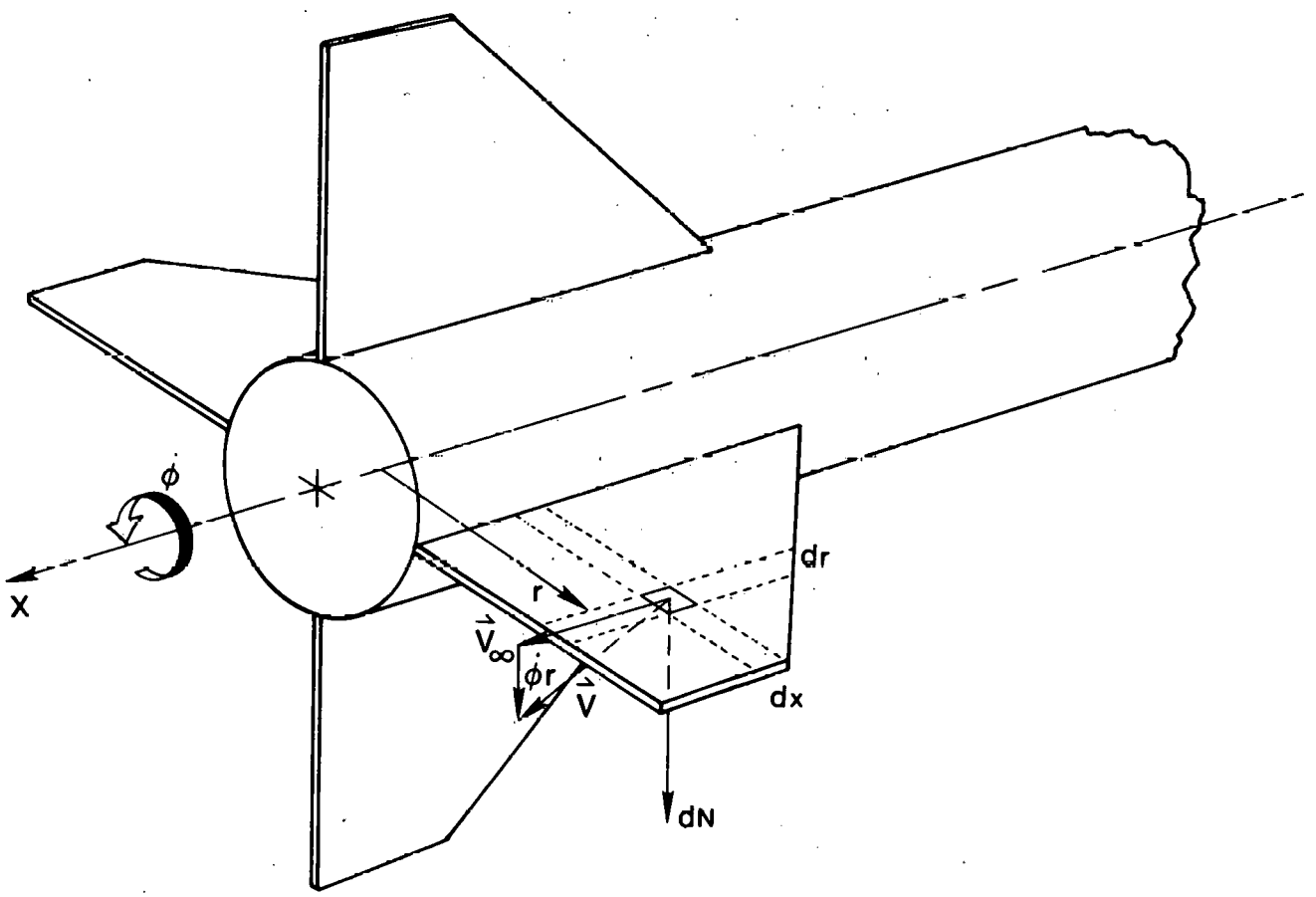

Figure 26. Induced Angle of Attack Due to Rolling Speed

Integrating over the surface of the fin, Eq (41a) becomes

$$\ell = 4\sigma q_\infty \int_a^{b_o}\int_{x_{\ell e}}^{x_{te}} r\, C_N(\alpha_e)\, C(x,r)\, S(r)\, dr\, dx. \quad (42)$$

Assuming α_e is small and using Eq (41b), Eq (42) can be written

$$\ell = -4\sigma q_\infty C_{N_\alpha}(1 - I_p)\frac{\dot\phi}{U_\infty}\int_a^{b_o}\int_{x_{\ell e}}^{x_{te}} r^2 C(x, r)\, S(r)\, dx\, dr.$$

Transforming coordinates (x,r) to fin coordinates (ξ,η) and nondimensionalizing with respect to $q_\infty S_b d$, one obtains

$$C_\ell = -\frac{2}{\pi}\sigma\, C_{N_\alpha}\frac{(b_o - a)}{a^3 b_o}(1 - I_p)\frac{\dot\phi b_o}{U_\infty} \cdot \int_0^1\int_0^1 \Re^2(\eta)\, \Omega(\eta)\, C(\xi)\, S(\eta)\, d\xi\, d\eta \quad (43a)$$

where

$$\Re(\eta) = a + (b_o - a)\eta. \quad (43b)$$

Taking the partial derivative of Eq (43) with respect to p, where $p = \dot\phi b_o/U_\infty$, and solving for I_p, one finally obtains

$$I_p = 1 + \frac{C_{\ell_p}}{\frac{2}{\pi}\sigma\frac{(b_o - a)}{a^3 b_o}C_{N_\alpha}\int_0^1\int_0^1 \Re^2(\eta)\, \Omega(\eta)\, C(\xi)\, S(\eta)\, d\xi\, d\eta}. \quad (44)$$

C_{ℓ_p} is computed from the results of Adams and Dugan (see Figure 27). C_{N_α} is obtained by numerically differencing Eq (35) for $\alpha_\ell \to 0$.

Roll Moment

The above described body flow field and lifting theory will now be applied to the prediction of the roll moment produced by cruciform fins. If one desired, the present analysis could be applied in a straightforward manner to two or three fin configurations. Consider the missile at angle of attack α_b, roll angle ϕ, and roll rate $\dot\phi$. The roll moment produced by a differential surface element on each of the four fins is

$$d\ell = q_\infty r \sum_{j=1}^{4} C_{n_j}(U_j/U_\infty)^2\, dx\, dr$$

where j refers to the j'th fin and U_j is the magnitude of the velocity on the j'th fin. Substituting C_n from Eq (14) and integrating over the fin surfaces, one has

$$\ell = \sigma q_\infty \int_a^{b_o}\int_{x_{\ell e}}^{x_{te}} r\, C(x, r)\, S(r) \sum_{j=1}^{4} C_{N_j}(U_j/U_\infty)^2\, dx\, dr.$$

Transforming to fin coordinates (ξ,η) and nondimensionalizing by $q_\infty S_b d$, one obtains the roll moment coefficient

$$C_\ell = \frac{\sigma(b_o - a)}{2\pi a^3}\int_0^1\int_0^1 \Re(\eta)\, \Omega(\eta)\, C(\xi)\, S(\eta) \cdot \sum_{j=1}^{4} C_{N_j}(U_j/U_\infty)^2 d\xi\, d\eta \quad (45)$$

where $\Re(\eta)$ is given by Eq (43b), $\Omega(\eta)$ is given by Eq (20b), $C(\xi)$ is given by Eq (19a), and $S(\eta)$ is given by Eq (19b).

U_j is found by taking the magnitude of the local velocity given in Eq (23):

$$U_j = \sqrt{U_\infty^2 \cos^2\alpha_b + (v_{q_j} + \dot\phi\, r \sin\phi)^2 + (w_{q_j} - \dot\phi\, r \cos\phi)^2}. \quad (46)$$

Note that if ϕ appears without the subscript j (as in the above equation), the angle ϕ is measured from the y axis for the particular fin under consideration.

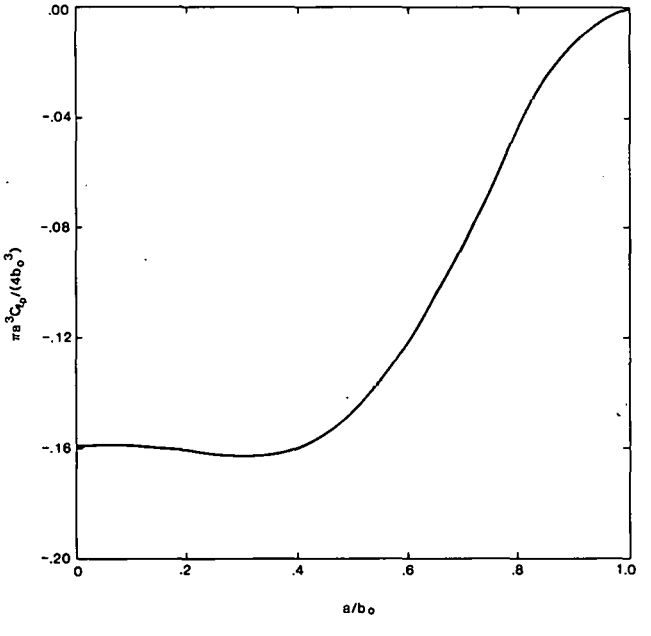

Figure 27. Roll Damping Moment Coefficient vs a/b_o

C_{N_j} depends upon the local effective angle of attack α_{e_j}. To determine this angle, the effective surface normal vector must be found taking into account control deflection and rolling motion interference. Using $\vec{n}$ from Eq (22), the effective fin deflection angle δ_{e_j} from Eq (37), and noting that the rolling motion interference affects the $\vec{i}$ component of the normal vector, one can write*

$$\vec{n}_{e_j} = [\sin(\Delta\delta_{e_j}) + I_p\dot{\phi}\, r/U_\infty]\vec{i} - \cos(\delta_{e_j})\sin\phi\,\vec{j} + \cos(\delta_{e_j})\cos\phi\,\vec{k}.$$

Substituting $\vec{n}_e$ and $\vec{V}$ into the equation for α_ℓ, Eq (21), one obtains the local effective angle of attack.

$$\alpha_{e_j} = \sin^{-1}[\{U_\infty\cos\alpha_b[\sin(\Delta\delta_{e_j}) + I_p\dot{\phi}\, r/U_\infty] - (v_{c_j} + \dot{\phi}\, r\sin\phi)\cos(\delta_{e_j})\sin\phi + (w_{c_j} - \dot{\phi}\, r\cos\phi)\cos(\delta_{e_j})\cos\phi\}/(|\vec{n}_{e_j}|U_j)] \quad (47)$$

where

$$|\vec{n}_{e_j}| = 1 + 2\sin(\Delta\delta_{e_j})I_p\dot{\phi}r/U_\infty + (I_p\dot{\phi}\, r/U_\infty)^2.$$

Normal Force and Pitch Moment

The equations for the normal force and pitch moment produced by the fins will now be considered. The differential fin force in the z direction produced by the four fins is (see Figure 28)**

$$dF_z = dN_1\cos\delta_1\cos\phi_1 - dN_2\cos\delta_2\sin\delta_2 - dN_3\cos\delta_3\cos\phi_3 + dN_4\cos\delta_4\sin\phi_4.$$

Writing the right side of this equation as a summation and substituting dN_j from Eq (13), one obtains

$$dF_z = q_\infty\sum_{j=1}^{4} C_{n_j}(U_j/U_\infty)^2\cos\delta_j\cos\phi\, dx\, dr.$$

Substituting in C_n from Eq (14) and integrating over the surface of each fin, one has

$$F_z = \sigma\, q_\infty\int_a^{b_o}\int_{x_{\ell e}}^{x_{te}} C(x, r)\, S(r) \cdot \sum_{j=1}^{4} C_{N_j}(U_j/U_\infty)^2\cos\delta_j\cos\phi\, dx\, dr.$$

Transforming to fin coordinates (ξ,η) and nondimensionalizing by $q_\infty S_b$, one obtains the normal force coefficient due to the fins:

$$C_z = \frac{\sigma(b_o - a)}{\pi\, a^2}\int_0^1\int_0^1 \Omega(\eta)\, C(\xi)\, S(\eta) \cdot \sum_{j=1}^{4} C_{N_j}(U_j/U_\infty)^2\cos\delta_j\cos\phi\, d\xi\, d\eta \quad (48)$$

The pitch moment produced by the fins is composed of two types of terms: the first term is caused by the normal force just derived and the second by the sin δ_j component of the normal force on the fins (Figure 28). The second term produces a pure moment (i.e., a couple) on the missile body and is usually much smaller in magnitude than the first term. The differential pitch moment due to both terms from all four fins is

$$dm = -x\, dN_1\cos\delta_1\cos\phi_1 + r\, dN_1\sin(\Delta\delta_1)\sin\phi_1 + x\, dN_2\cos\delta_2\sin\phi_2 + r\, dN_2\sin(\Delta\delta_2)\cos\phi_2 + x\, dN_3\cos\delta_3\cos\phi_3 - r\, dN_3\sin(\Delta\delta_3)\sin\phi_3 - x\, dN_4\cos\delta_4\sin\phi_4 - r\, dN_4\sin(\Delta\delta_4)\cos\phi_4.$$

Writing the right side of this equation as a summation and substituting dN_j from Eq (13), one obtains

$$dm = -q_\infty\sum_{j=1}^{4} C_{n_j}(U_j/U_\infty)^2[x\cos\delta_j\cos\phi - r\sin(\Delta\delta_j)\sin\phi]dx\, dr.$$

Substituting in C_n from Eq (14) and integrating over the surface of each fin, one has

$$m = -\sigma\, q_\infty\int_a^{b_o}\int_{x_{\ell e}}^{x_{te}} C(x, r)\, S(r)\sum_{j=1}^{4} C_{N_j}(U_j/U_\infty)^2 \cdot [x\cos\delta_j\cos\phi - r\sin(\Delta\delta_j)\sin\phi]dx\, dr.$$

*Reference 10 accounted for rolling motion interference by way of $\vec{j}$ and $\vec{k}$ components of the velocity. That approach is not considered correct because it also changes the magnitude of the velocity. In fin - fin interference the magnitude of the approach velocity to the fin is not changed, but only the angle with which it approaches the fin.

**Note that the sign of dN_j is determined by its angular relationship to the surface normal vector; that is, positive dN_j is in the counterclockwise sense.

Transforming to fin coordinates (ξ,η) and nondimensionalizing by $q_\infty S_b d$, one obtains the pitch moment coefficient due to the fins:

$$C_m = \frac{-\sigma(b_o - a)}{2\pi a^3}\int_o^1\int_o^1 \Omega(\eta)\, C(\xi)\, S(\eta)\sum_{j=1}^{4} C_{N_j}(U_j/U_\infty)^2 \cdot$$

$$[\mathcal{X}(\xi,\eta)\cos\delta_j\cos\phi - \mathcal{R}(\eta)\sin(\Delta\delta_j)\sin\phi]\,d\xi\,d\eta \qquad (49a)$$

where

$$\mathcal{X}(\xi,\eta) = x_1 + c_r + (b_o - a)\tan\Lambda_{te}\,\eta - \Omega(\eta)\,\xi. \qquad (49b)$$

Side Force and Yaw Moment

The derivation of the side force and yaw moment is very similar to that of the normal force and pitch moment and, consequently, is not given. The side force coefficient and the yaw moment coefficient are given by:

$$C_y = \frac{-\sigma(b_o - a)}{\pi a^2}\int_o^1\int_o^1 \Omega(\eta)\, C(\xi)\, S(\eta)\cdot$$

$$\sum_{j=1}^{4} C_{N_j}(U_j/U_\infty)^2 \cos\delta_j \sin\phi\, d\xi\, d\eta \qquad (50)$$

and

$$C_n = \frac{-\sigma(b_o - a)}{2\pi a^3}\int_o^1\int_o^1 \Omega(\eta)\sum_{j=1}^{4} C_{N_j}(U_j/U_\infty)^2\,[\mathcal{X}(\xi,\eta)\cdot$$

$$\cos\delta_j \sin\phi + \mathcal{R}(\eta)\sin(\Delta\delta_j)\cos\phi]\,d\xi\,d\eta. \qquad (51)$$

Panel Loads

The panel loads on the fin surfaces are essentially the same forces and moments derived previously (Roll Moment, Normal Force and Pitch Moment, and Side Force and Yaw Moment) except that they are oriented in a fin coordinate system. Figure 29 shows the coordinate system and sign convention for the panel normal force (N), the panel hinge moment (H), and the panel root bending moment (B). The calculation of panel loads is useful for two reasons: first, they provide the most physically meaningful force and moments with which to compare theoretical predictions and experiment because they do not contain the geometry components of the roll angle and the fin-deflection angle. Second, they directly provide the loads needed by the structural designer and the actuator torques needed by the guidance and control designer.

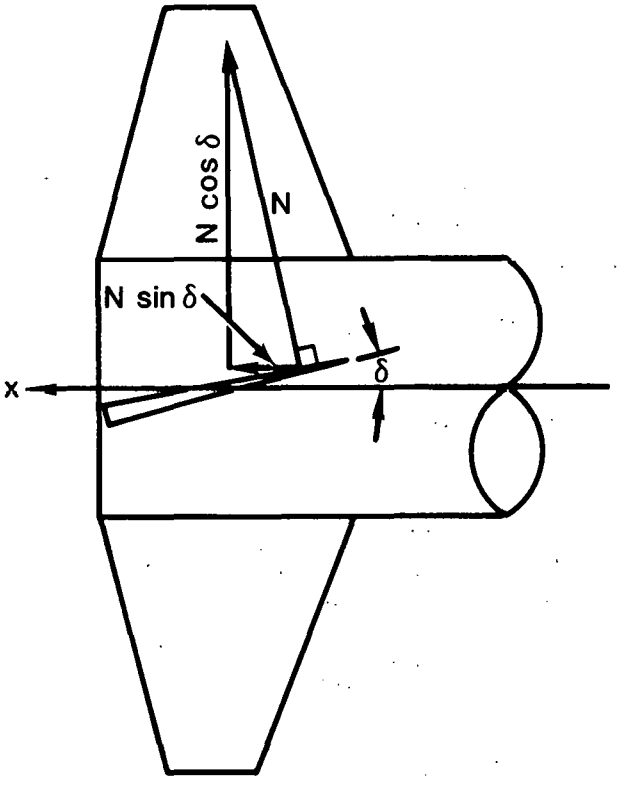

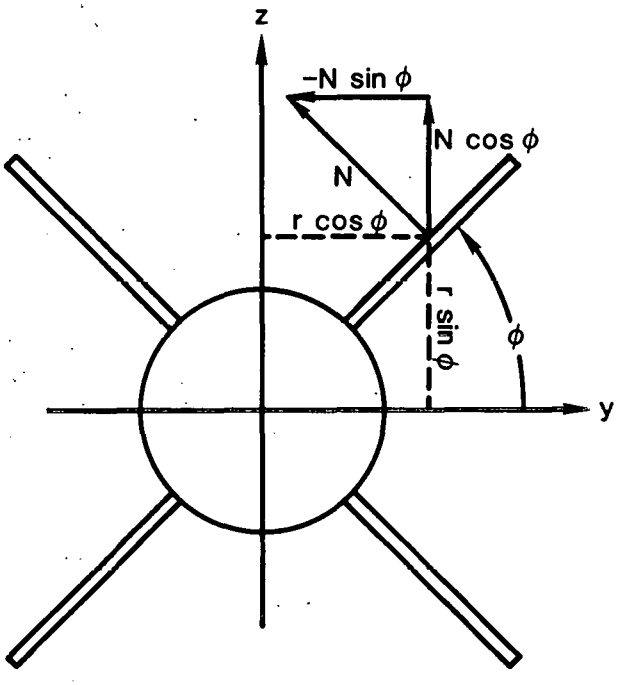

Figure 28. Components of the Fin Normal Force

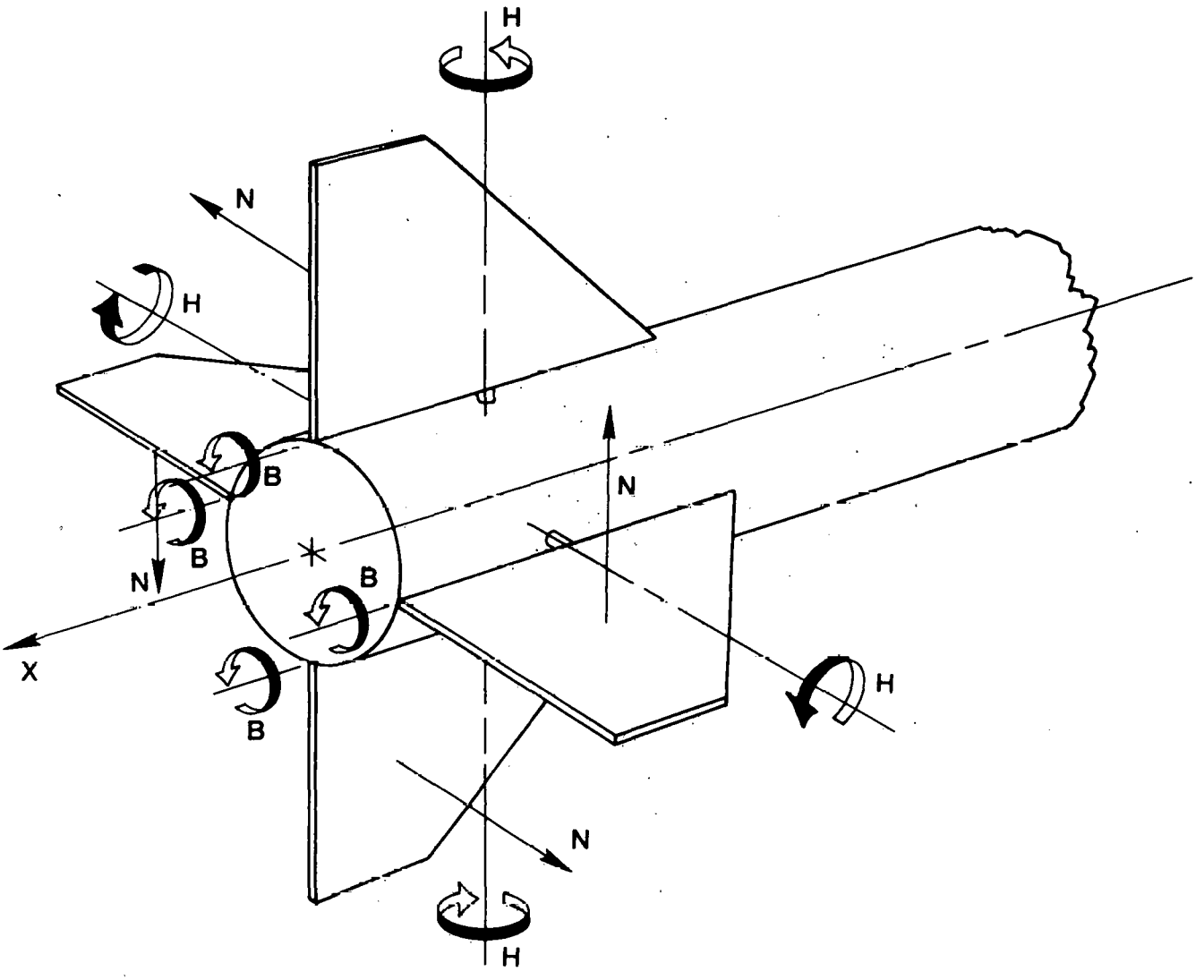

Figure 29. Sign Convention for Panel Normal Force, Hinge Moment, and Root Bending Moment

As the derivation of the panel loads is very similar to the previous derivations, it will only be sketched very briefly. Using Eq (13), the normal force on a fin panel caused by a differential surface element is

$$dN = q_\infty C_n (U/U_\infty)^2 dx\, dr .$$

Proceeding as before, one obtains the panel normal force coefficient, $N/q_\infty S_f$:

$$C_p = \frac{\sigma(b_o - a)}{S_f} \int_o^1 \int_o^1 \Omega(\eta)\, C(\xi)\, S(\eta)\, C_N (U/U_\infty)^2 d\xi\, d\eta . \tag{52}$$

Recall that positive normal force points in the direction of the counterclockwise rotational sense.

The panel hinge moment due to a differential surface element is

$$dH = -q_\infty (x - x_h) C_n (U/U_\infty)^2\, dx\, dr$$

where x_h is the axial location of the reference line for the hinge moment. Proceeding as before, one obtains the panel hinge moment coefficient, $H/q_\infty c_r S_f$:

$$C_h = \frac{-\sigma(b_o - a)}{c_r S_f} \int_o^1 \int_o^1 [\bar{x}(\xi, \eta) - x_h] \cdot \Omega(\eta)\, C(\xi)\, S(\eta)\, C_N (U/U_\infty)^2 d\xi\, d\eta . \tag{53}$$

The panel root bending moment due to a differential surface element is

$$dB = q_\infty (r-a) C_n (U/U_\infty)^2 dx\, dr .$$

Proceeding as before, one obtains the panel root bending moment coefficient, $B/q_\infty(b_o - a)S_f$:

$$C_b = \frac{\sigma(b_o - a)}{S_f} \int_o^1 \int_o^1 \eta\, \Omega(\eta)\, C(\xi)\, S(\eta) \cdot C_N (U/U_\infty)^2 d\xi\, d\eta . \quad (54)$$

Results and Discussion

The results computed and presented in this investigation were dictated solely by the requirement to validate and determine the bounds of the present theory. Consequently, no results are given without experimental measurements. The theory is evaluated by comparing predictions and measurements for six different fin planforms. The detailed geometry and reference from which the data were taken is given in Table 1. The planforms are shown in Figure 30. It can be seen that the aspect ratios range from 1.0 to 2.0 and the leading edge sweep angles range from 0° to 67.4°.

The results and comparison with experiment are discussed in three sections: panel loads, roll moments, and control forces and moments. The panel loads presented are panel normal force, panel bending moment, and panel hinge moment. Normal force, pitch moment, side force, and yaw moment predictions could have been compared with experimental measurements, but it is felt that the individual panel loads permit more physical insight into the aerodynamic generation of the forces and moments. Roll moment characteristics presented are the induced roll moment, roll damping moment, and steady-state roll rate. These roll characteristics are of great importance in the dynamic flight stability of finned missiles. Control deflection forces and moments presented are pitch (or yaw) control and roll control for various control deflections and roll angles.

Panel Loads

a. Panel Normal Force

The panel normal force on the windward fin (Fin 4) as a function of roll angle for $\alpha_b = 20°$ for Configuration A at $M_\infty = 0.8$ is shown in Figure 31.* Also shown in Figure 31 is the prediction of Nielsen, Hemsch, and Smith.[7] As Fin 4 sweeps from $\phi = 0$ to 90°, it moves on the windward side of the body from the angle of attack plane to the (x,y) plane. As can be seen by comparing the present result with experiment, the present method predicts very accurately the loadup of the fin. Above $\phi = 60°$, the present method predicts an increasing normal force, whereas experiment shows a slight drop in normal force. Examining the computer output for spanwise angle of attack and loading reveals that as ϕ increases from zero, the loading increases due to increase in local angle of attack across the span. At $\phi = 40°$, the body upwash near the fin root has increased to the extent that the root chord stalls. As the roll angle increases further, the stall location moves outboard, but the inboard sections begin to add lift as they progress further into poststall. Noting the experimental trend for $\phi > 40°$ and the rise in normal force near $\phi = 80°$ suggests the following explanation of the actual fin loading. The root chord stall is washed outboard due to the spanwise velocity component of the leading edge vortex. This, in turn, decreases the loading along the span such that the total loading decreases; however, as the roll angle increases further and the spanwise location of stall moves outboard, the portion of unstalled span that could be affected steadily decreases. At $\phi = 90°$ it is seen from the present computer results that stall occurs at the very tip of the fin; that is, the entire fin is in poststall. Once this occurs, the fin loading will begin to increase as the angle of attack increases. This hypothesis could be tested quantitatively by examining experimental spanwise pressure distributions on a fin. It could be tested qualitatively by comparing predictions of the present method with experimental data for unswept fins and noting that this phenomenon probably would not occur for unswept geometries.

The panel normal force on the windward fin vs roll angle for $\alpha_b = 20°$ at $M_\infty = 1.22$ is shown in Figure 32. Good agreement between the present method and experiment is demonstrated in the figure. The trend in panel normal force for $\phi < 50°$ is the same for supersonic flow as the the previous subsonic case. For $\phi > 50°$, however, the experimental data show that stall is delayed to a higher roll angle (i.e., angle of attack) as compared to $M_\infty = 0.8$. Figure 32 shows the experimental data still dropping at $\phi = 90°$ which implies, from the previous discussion, that the stall angle of attack has not reached the trip chord. As the present method does not include any dependence of stall angle of attack on Mach number (Eq (35)), this characteristic is not demonstrated by theory.

*All panel loads calculated and compared with experimental data are for missile Configuration A.
Configuration A ($M_\infty = 0.8$)

Table 1. Geometry of Missiles Used for Comparison of Theory and Experiment

Configuration	b_0/a	c_r/a	x_1/a	$\Lambda_{\ell e}$	Λ_{te}	x_h/a	A_e	Reference
A	2.4	2.8	17.2	45°	0°	18.4	1.33	27
B	2	1.2	18.1	0°,	0°	--	1.67	28
C	2	1.6	17.7	38.7°	0°	--	1.67	28
D	2	2.4	16.9	67.4°	0°	--	1.67	28
E	3	2	18.0	0°	0°	--	2.00	10,29
F	2	2.66	17.34	53.1°	0°	--	1.00	30

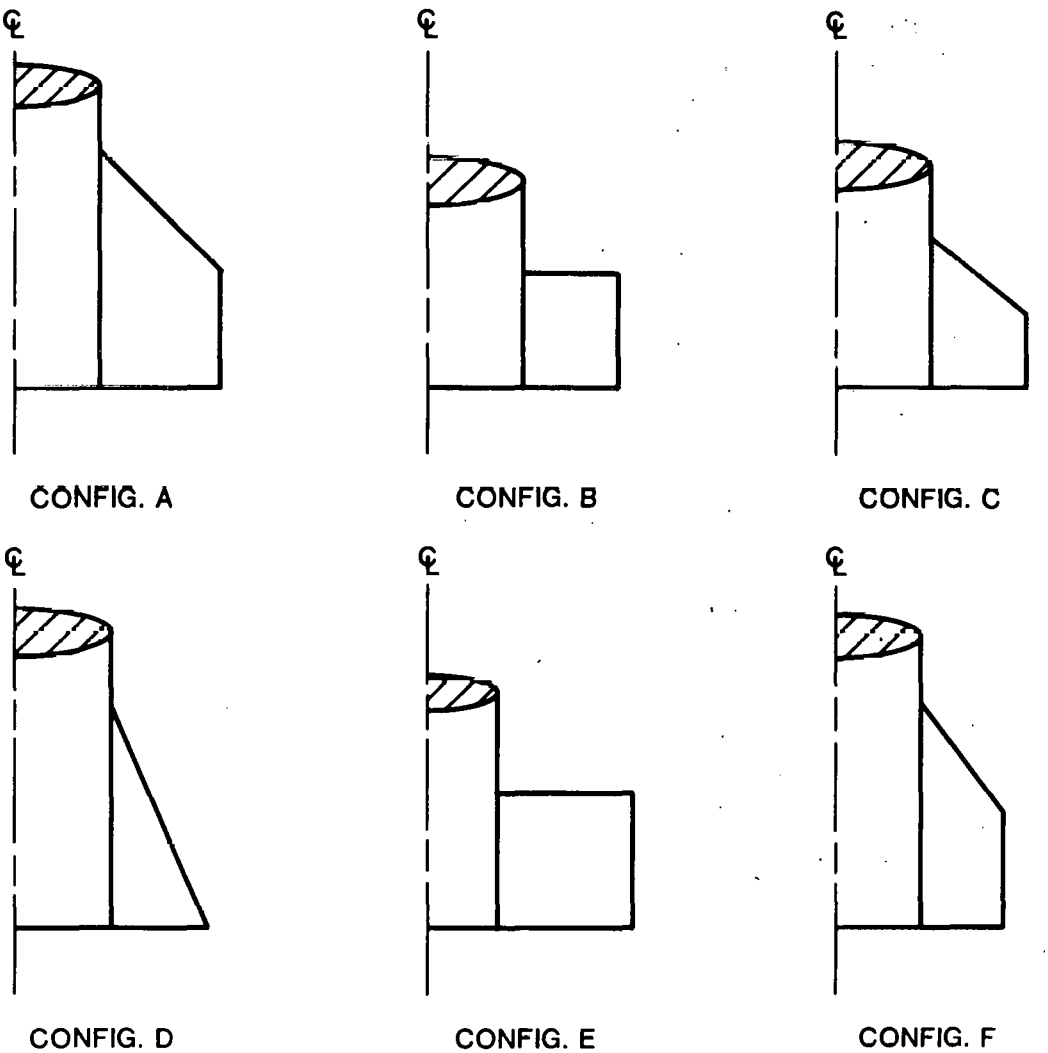

Figure 30. Fin Planforms Used for Comparison of Theory and Experiment

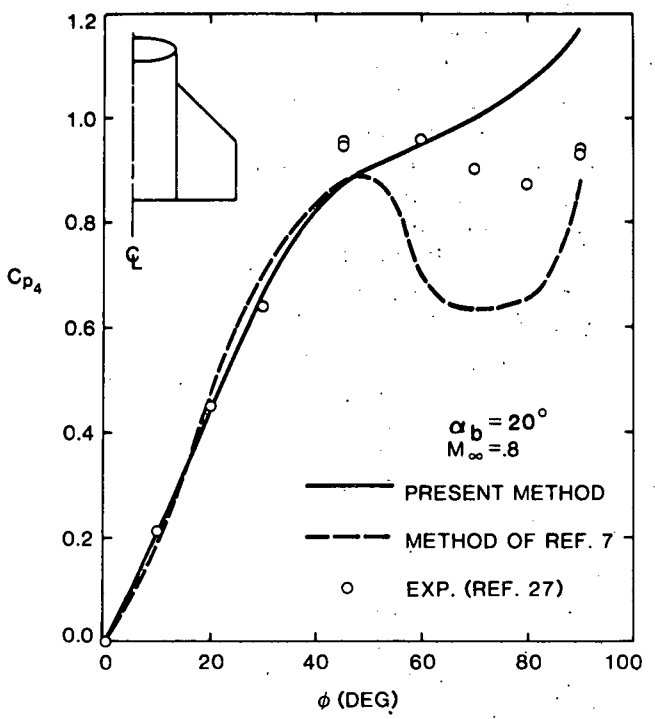

Figure 31. Windward Panel Normal Force vs Roll Angle for Configuration A (M_∞ = 0.8)

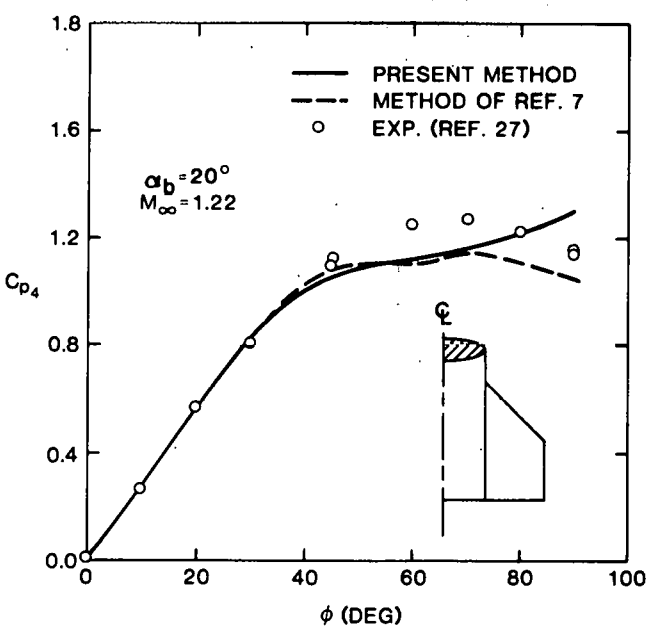

Figure 32. Windward Panel Normal Force vs Roll Angle for Configuration A (M_∞ = 1.22)

The panel normal force on the leeward fin vs roll angle for α_b at M_∞ = 0.8 is given in Figure 33. Very good agreement between theory and experiment is demonstrated except near $\phi = 0°$. As Fin 1 rolls from $\phi = 0°$, it begins to unload not only because of closer proximity to the angle of attack plane, but also immersion in the body vortex. The inboard portion of the fin unloads much more rapidly than the outboard portion because it is strongly influenced by the vortex feeding sheet. As the fin nears the center of the body vortex it produces essentially no net normal force. The portion inboard of the vortex produces negative force (i.e., in the negative roll moment direction) and the outboard portion produces an almost balancing positive force. This balance is highly dependent on the relation between the radial vortex location and the fin semispan. For example, if the fin had a smaller semispan, the zero load roll angle would be less than that shown in Figure 33.

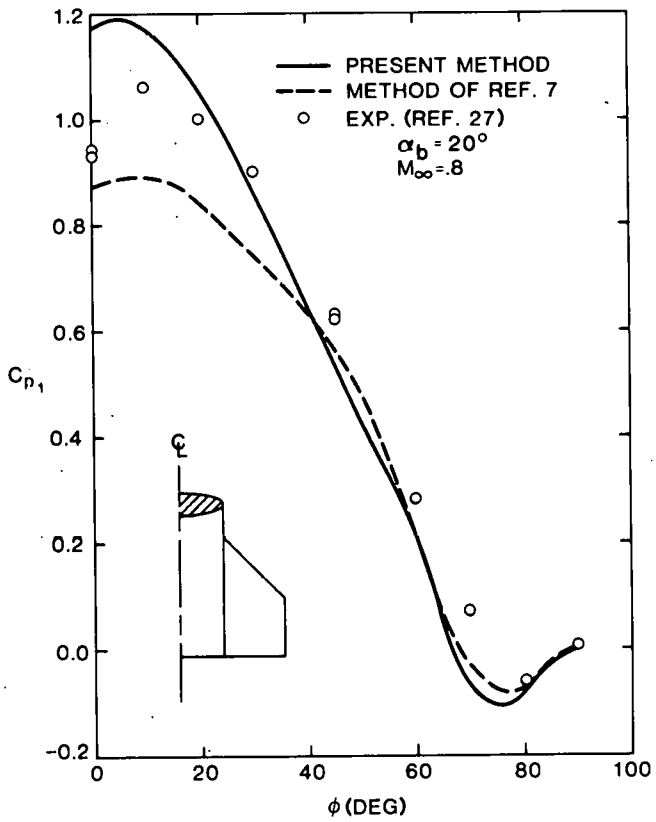

Figure 33. Leeward Panel Normal Force vs Roll Angle for Configuration A (M_∞ = 0.8)

Figure 34 shows the same type of comparison as Figure 33, except for $M_\infty = 1.22$. The agreement between theory and experiment is not as good as in the previous comparisons. Note that the experimental roll angle for zero cross-over loading decreased from $\phi = 75°$ for $M_\infty = 0.8$ to $\phi = 60°$ for $M_\infty = 1.22$. This could be caused by the body vortex becoming stronger or the radial location of the vortex increasing, or both. Recalling that the radial location of the vortex increases with Mach number (Eq (11)), one could infer that vortex strength increases significantly with Mach number. This has been suggested by Nielsen in Reference 26.

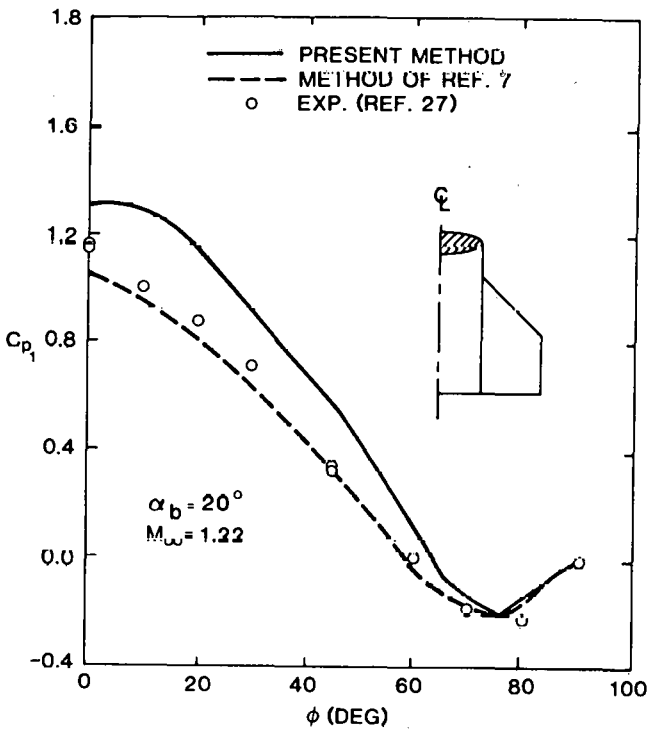

Figure 34. Leeward Panel Normal Force vs Roll Angle for Configuration A ($M_\infty = 1.22$)

b. Panel Bending Moment

Figures 35 and 36 show the panel bending moment for the windward fin vs roll angle for $\alpha_b = 20°$ at $M_\infty = 0.8$ and 1.22, respectively. Generally good agreement is demonstrated between theory and experiment. Good agreement between theory and experiment on the bending moment requires that both the magnitude of the total normal force, C_{p_4}, and spanwise pressure distribution are correct. Recall that the theory for panel normal force is in essentially perfect agreement with experiment (Figures 31 and 32) for $\phi < 40°$. Figures 35 and 36, however, show that the theory slightly underpredicts the bending moment for the same roll angle range. This implies that there is slightly more loading outboard and slightly less loading inboard than predicted by the present method. If bending moment data for other planforms indicated the same trend, the spanwise normal force distribution, $S(\eta)$, given by Eq (19b) could be modified slightly.

The root bending moment for the leeward fin vs roll angle for $\alpha_b = 20°$ at $M_\infty = 0.8$ and 1.22 is shown in Figures 37 and 38, respectively. Excellent agreement between theory and experiment is demonstrated for the subsonic case, and fair agreement is shown for the supersonic case. It is interesting that for $M_\infty = 0.8$ near $\phi = 80°$, the panel normal force is negative (Figure 33) while the bending moment remains near zero (Figure 37). The reason for this is that the reverse flow under the vortex is strong enough to generate a net negative panel force, but the bending moment produced by the outboard positive normal force overcomes the negative bending moment produced by the inboard sections.

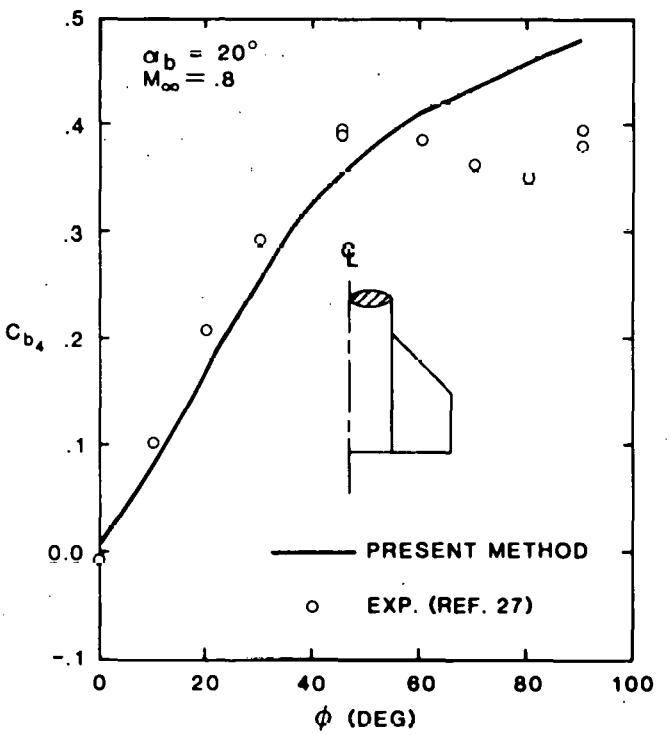

Figure 35. Windward Fin Root Bending Moment vs Roll Angle for Configuration A ($M_\infty = 0.8$)

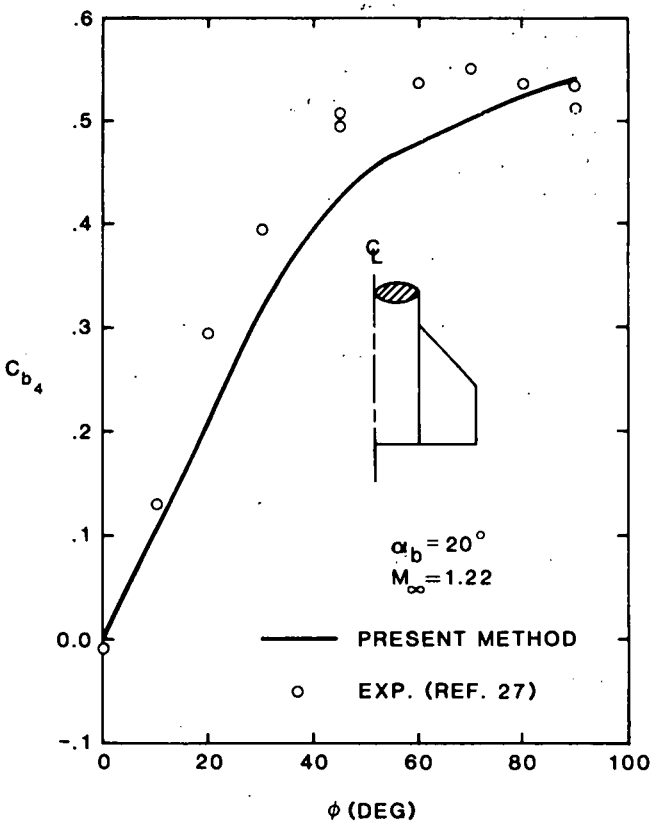

Figure 36. Windward Fin Root Bending Moment vs Roll Angle for Configuration A ($M_\infty = 1.22$)

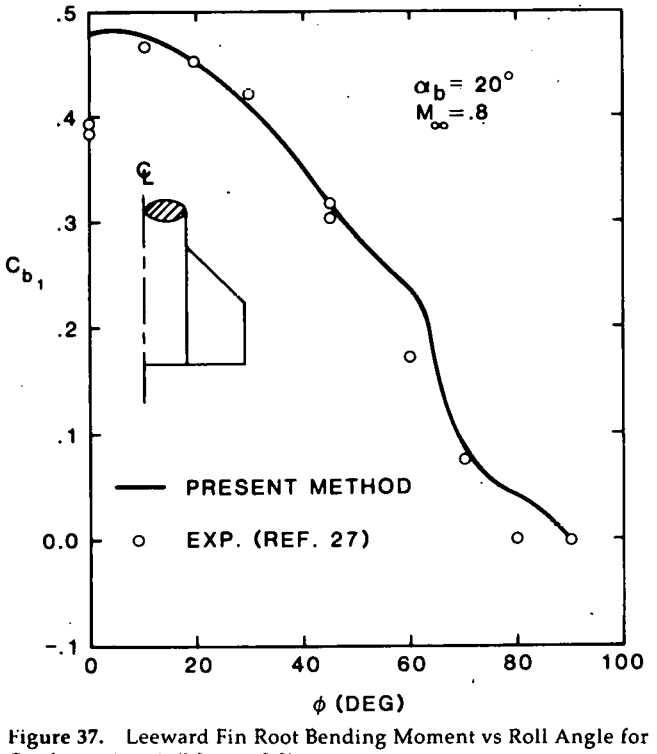

Figure 37. Leeward Fin Root Bending Moment vs Roll Angle for Configuration A ($M_\infty = 0.8$)

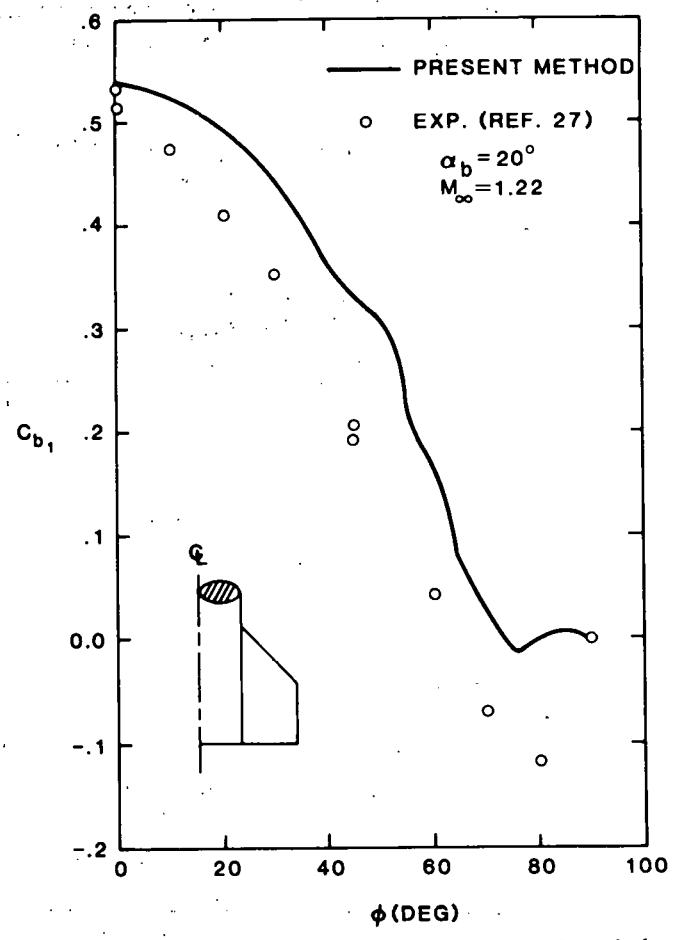

Figure 38. Leeward Fin Root Bending Moment vs Roll Angle for Configuration A ($M_\infty = 1.22$)

c. Panel Hinge Moment

The panel hinge moment for the windward fin vs roll angle for $\alpha_b = 20°$ at $M_\infty = 0.8$ and 1.22 is shown in Figures 39 and 40, respectively. The agreement between theory and experiment appears to be poor, particularly for $M_\infty = 1.22$. One must be aware, however, of the sensitivity of the hinge moment to the location of the hinge line. A better indication of the accuracy of the present method is obtained by a sample comparison of the theoretical and experimental axial location of the fin center of pressure. Using the hinge line, x_h, as the moment reference, one can write

$$x_{cp} C_p q_\infty S_f = H .$$

Solving for the location of the center of pressure, nondimensionalized by the root chord, one has

$$x_{cp}/c_r = C_h/C_p . \qquad (55)$$

Applying this equation to both the experimental and theoretical data at $\phi = 90°$ for Fin 4, one has

For $M_\infty = 0.8$

$$\left(\frac{x_{cp}}{c_r}\right)_{exp} = 0.113 \quad \text{and} \quad \left(\frac{x_{cp}}{c_r}\right)_{theory} = 0.023$$

For $M_\infty = 1.22$

$$\left(\frac{x_{cp}}{c_r}\right)_{exp} = 0.129 \quad \text{and} \quad \left(\frac{x_{cp}}{c_r}\right)_{theory} = 0.024$$

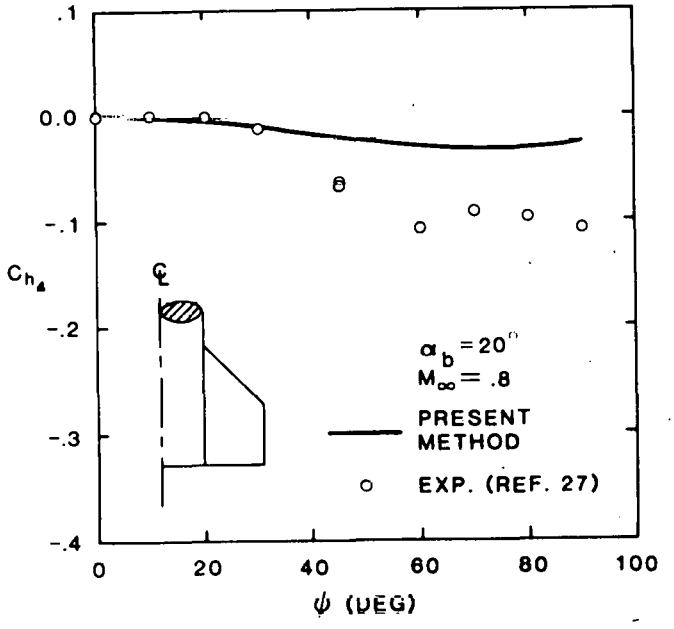

Figure 39. Windward Fin Hinge Moment vs Roll Angle for Configuration A ($M_\infty = 0.8$)

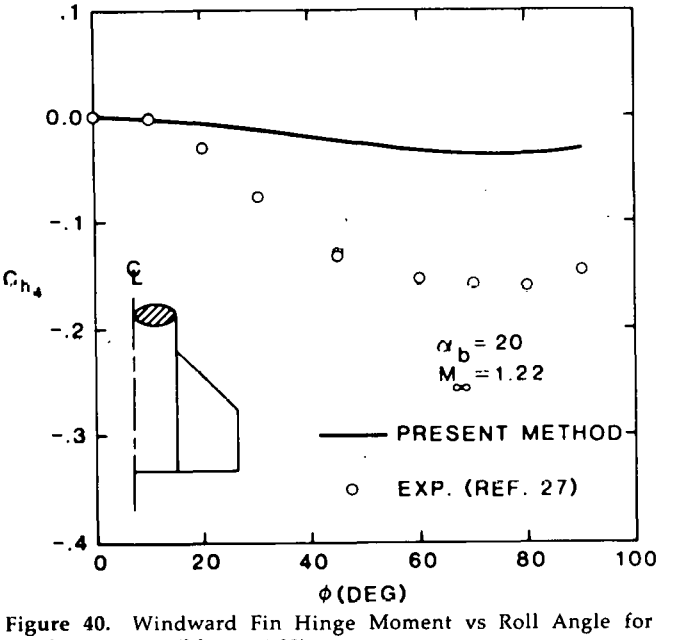

Figure 40. Windward Fin Hinge Moment vs Roll Angle for Configuration A ($M_\infty = 1.22$)

As can be seen by this calculation, the experimental center of pressure is slightly farther aft of the hinge line than predicted by theory. Taking the difference between each pair of ratios, the predicted axial center of pressure is in error only 9.0% and 10.5% of the root chord for $M_\infty = 0.8$ and 1.22, respectively, for the worst agreement between theory and experiment in Figures 39 and 40.

A second point should be made from the axial center of pressure calculation just presented. Note that the experimental data show that the center of pressure moves slightly rearward as the Mach number changes from subsonic to supersonic. This follows the usual trend of lifting surfaces in transonic flow. The predicted center of pressure, however, stays essentially constant with the Mach number; the reason is that the assumed normal force distribution for uniform approach flow (Eq (19)) does not depend upon the Mach number. A slight improvement to the present theory would be to insert Mach number dependence in the chordwise distribution function, $C(\xi)$.

Figures 41 and 42 give the hinge moment for the leeward fin vs roll angle for $\alpha_b = 20°$ at $M_\infty = 0.8$ and 1.22, respectively. Better agreement between theory and experiment is shown for the leeward fin than for the windward fin. This might be somewhat surprising because of the complexity of predicting fin loading for such a nonuniform approach flow. The reason is that for $\phi > 50°$ the panel normal force is small for the leeward fin; therefore, the hinge moment is also small.

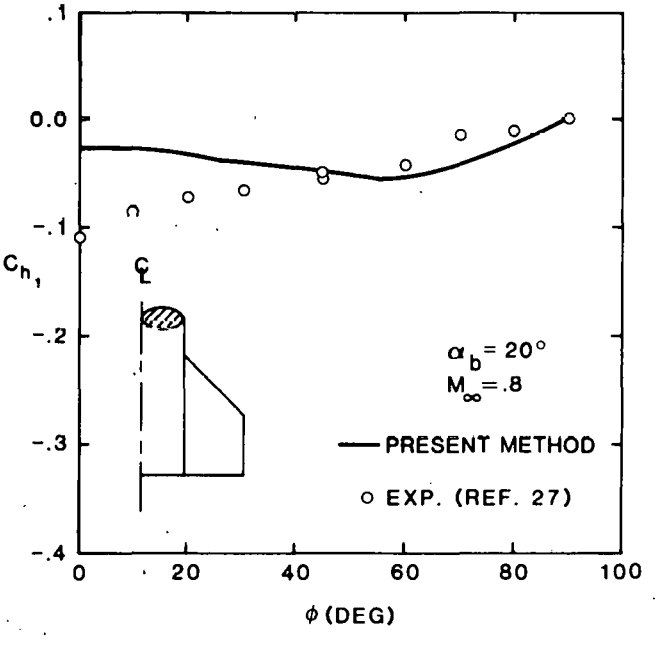

Figure 41. Leeward Fin Hinge Moment vs Roll Angle for Configuration A ($M_\infty = 0.8$)

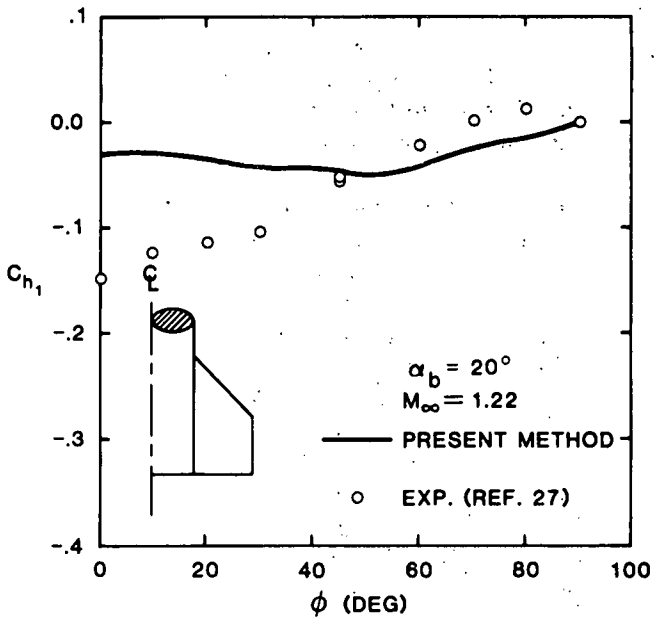

Figure 42. Leeward Fin Hinge Moment vs Roll Angle for Configuration A (M_∞ = 1.22)

Roll Moments

a. Induced Roll Moment

Figures 43 and 44 show the induced roll moment vs angle of attack of the body for missile Configuration A for ϕ = 20° at M_∞ = 0.8 and M_∞ = 1.22, respectively. Also shown in the figures is the prediction of Nielsen, Hemsch, and Smith.[7] Fairly good agreement is observed between the present method and experiment for M_∞ = 0.8, but for M_∞ = 1.22, the agreement is poor. Note that the induced roll moment is one of the most difficult nonlinear moments to predict because it is composed of the sum and difference of the first moment of four spanwise pressure distributions. The physical explanation of the slightly negative then rapidly increasing positive trend of the induced roll moment with angle of attack is very difficult to delineate because of the many complex aerodynamic phenomena embedded in the present theory. From numerical experiments with the theory, however, certain important elements can be identified: radial location of the body vortex, size of the vortex core, and local stall and poststall along the span of the fin.

To understand the trends plotted in Figures 43 and 44, one must examine the spanwise loading of all the fins. Figure 45 shows the spanwise loading for each fin for M_∞ = 0.8. The loading at a given spanwise location shown in Figure 45 is the integrated value over the local chord. The loading caused by the primary body vortex is clearly seen on Fin 2. The spanwise location of the stall angle of attack can be recognized as a slight drop in the normal force along Fin 3. The loading on Fins 1, 3, and 4 increases steadily as the root chord is approached because of body upwash and the increasing length of the chord. On Fin 1 the loading drops sharply near the root chord because it passes inside the vortex feeding sheet. The roll moment produced by each fin loading shown is: Fin 1, 0.794; Fin 2, -0.031; Fin 3, -0.751; and Fin 4, 0.313. It can be seen that the roll moments produced by Fin 1 and Fin 3 roughly balance. Fin 2 and Fin 4, however, do not balance because the reverse flow loading between the primary body vortex and the root chord on Fin 2 drop (in magnitude) the roll moment on Fin 2 to roughly zero. This results in a large net positive roll moment from Fin 4. By similar reasoning, the small negative induced roll moment for small angles of attack is due to the increased outboard loading on Fin 2 when the vortex is near the body surface.

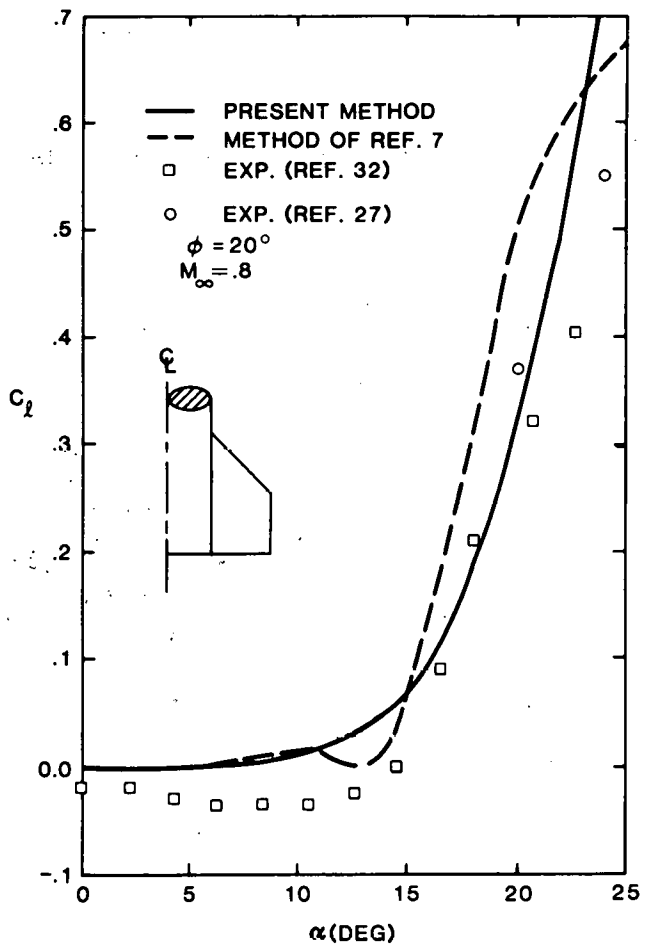

Figure 43. Induced Roll Moment vs α_b for Configuration A (M_∞ = 0.8)

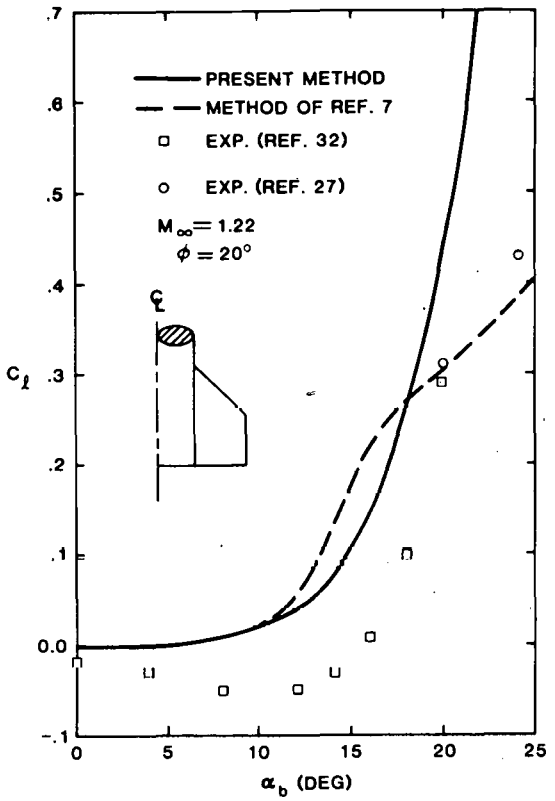

Figure 44. Induced Roll Moment vs α_b for Configuration A (M_∞ = 1.22)

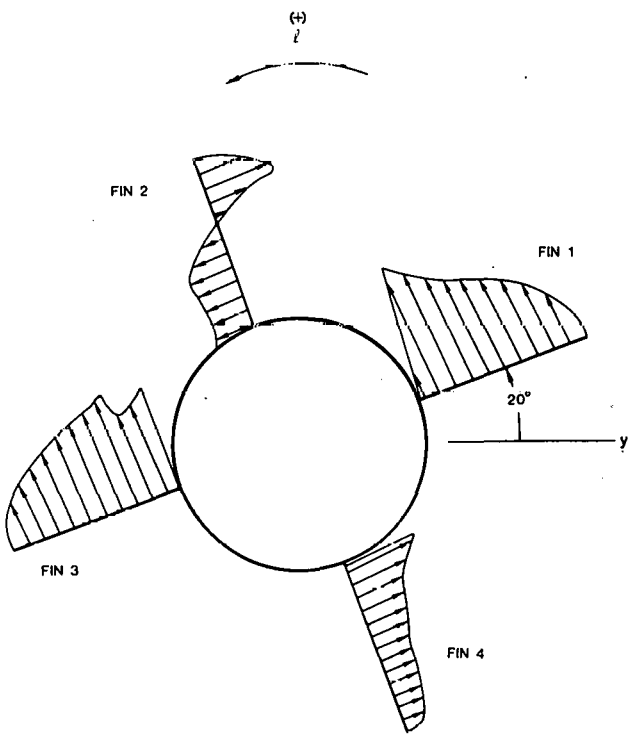

Figure 45. Spanwise Fin Loading for $\alpha_b = 20°$, $\phi = 20°$ Configuration A ($M_\infty = 0.8$)

Figure 46 gives the induced roll moment vs angle of attack for Configuration B for $\phi = 22.5°$ and $M_\infty = 0.7$. Theory and experiment are in very good agreement for the rectangular fin planform. Comparing the induced roll moment coefficient for the clipped delta and rectangular planform (Figures 43 and 46) for $\alpha_b = 20°$, it is seen that* $C_\ell = 0.325$ and 0.186, respectively. Recalling the previous explanation given concerning the origin of the large positive induced roll moment, one could ask why C_ℓ for the shorter span rectangular planform is not larger than that for the clipped delta. The reason for the question would be that the reverse flow loading on Fin 2 for the short span fin should produce a relatively larger positive roll moment than would the clipped delta. The reasoning is correct; the paradox, however, is created by the nondimensionalization used in the present analysis and in almost all other analyses. The roll moment coefficient is based on the body cross-sectional area, not on the fin planform area. If one converts the two previous coefficients to coefficients based on fin planform area, one has $[C_\ell]_{S_f} = 0.347$ and 0.487, respectively. Now it is clear that the short span rectangular planform is much more efficient at producing an induced roll moment than the longer span clipped delta.

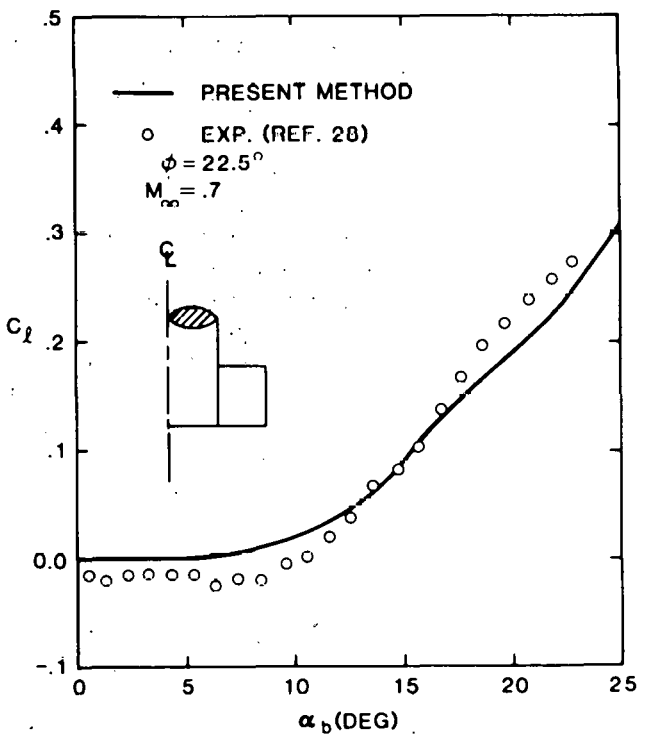

Figure 46. Induced Roll Moment vs α_b for Configuration B

*This comparison ignores the fact that the roll angle and Mach number are not exactly the same.

The induced roll moment vs angle of attack for Configuration D for $\phi = 22.5°$ and $M_\infty = 0.7$ and 1.2 is shown in Figure 47. The theory reproduces the experimental data fairly well, but the change in induced roll moment with Mach number is not predicted accurately for this planform geometry. The reason is probably the effect of Mach number on the spanwise and chordwise pressure distributions, $S(\eta)$ and $C(\xi)$, as mentioned earlier. Concerning the magnitude of the induced roll moment coefficient, a direct comparison can be made between the rectangular planform (Figure 46) and the delta planform (Figure 47) because they both have the same missile body and planform area. The delta planform produces a slightly smaller induced roll moment because of the greatly different spanwise loading and stall angle of attack (compare, for example, Figures 17 and 19).

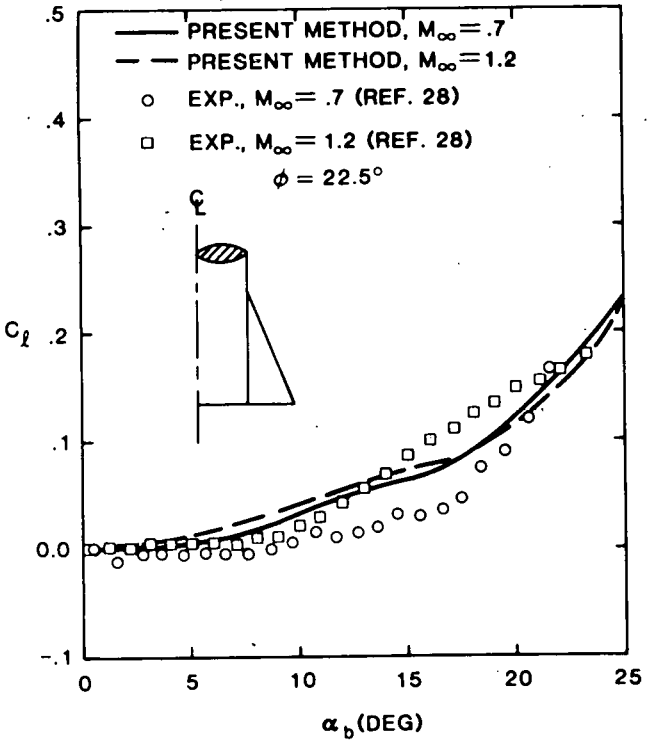

Figure 47. Induced Roll Moment vs α_b for Configuration D

b. Roll Damping Moment

Figure 48 shows the roll damping moment vs angle of attack for Configuration E for $M_\infty = 0.22$. There is excellent agreement between theory and experiment for angles of attack up to 12°, but above that the theory agrees well with one set of experimental data and not the other. The only comment that can be made is that the experimental techniques of the two investigators differ greatly. Clare[31] used a roll oscillation technique; Regan[29] used the standard rolling-speed decay method.

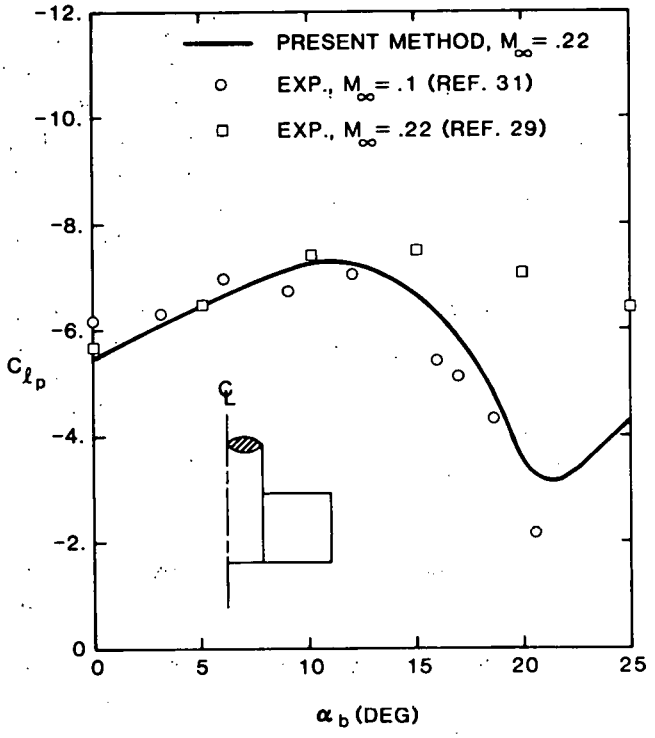

Figure 48. Roll Damping Moment vs α_b for Configuration E.

A comment should be made concerning the present numerical method of calculating dynamic derivatives, such as C_{ℓ_p}. As the missile fins rotate through a 90° roll cycle, the forces and moments continually change for nonzero angle of attack of the body. Therefore, one method of computing rolling motion derivatives is to numerically difference the average value of the force or moment coefficient over a roll cycle; that is,

$$C_{i_p} = \frac{2}{\pi}\left[\int_0^{\pi/2} C_i|_{p=\Delta p}\, d\phi - \int_0^{\pi/2} C_i|_{p=o}\, d\phi\right]/\Delta p \quad (56)$$

where C_i represents any force or moment coefficient. This computation of C_{i_p} is appropriate for large values of rolling speed. The method described by Eq (56) is one used in the present analysis. It should be mentioned, however, that another method could be used. This method computes the difference between two values of the coefficient at different rolling speeds, but at the same roll angle; that is

$$C_{i_p}|_{\phi=\phi_1} = \left[C_i\Big|_{\substack{\phi=\phi_1\\ p=\Delta p}} - C_i\Big|_{\substack{\phi=\phi_1\\ p=o}}\right]/\Delta p. \quad (57)$$

This method could be used for very low rolling speeds, such as roll oscillations about a roll trim angle; it would yield, for example, the roll angle variation of the roll damping moment while a missile is oscillating in roll lock-in.

Figure 49 gives the roll damping moment vs angle of attack for Configuration F for $M_\infty = 0.6$ and 1.3. Although the slight drop in C_{ℓ_p} near $\alpha_b = 17°$ is not predicted, the agreement between theory and experiment is generally good over the angle of attack range. Comparing Figures 48 and 49, it is seen that the trend of C_{ℓ_p} with α_b is very different between the two planforms. One might suspect, based on the earlier discussion of induced roll moment, that this different character would be due primarily to the difference in semispan between the two configurations. The roll damping moment for several fin planforms and semispans was computed in order to identify the dominant parameter causing the rapid decrease in C_{ℓ_p} for α_b near 20°; it was the stall angle of attack of the planform and not fin span. For example, consider the case of holding the planform and span constant (say a rectangular planform of a given span), and varying the aspect ratio so that the stall angle of attack varies. The aspect ratio decreases (and the stall angle of attack increases) as the drop in C_{ℓ_p} at large angle of attack disappears.

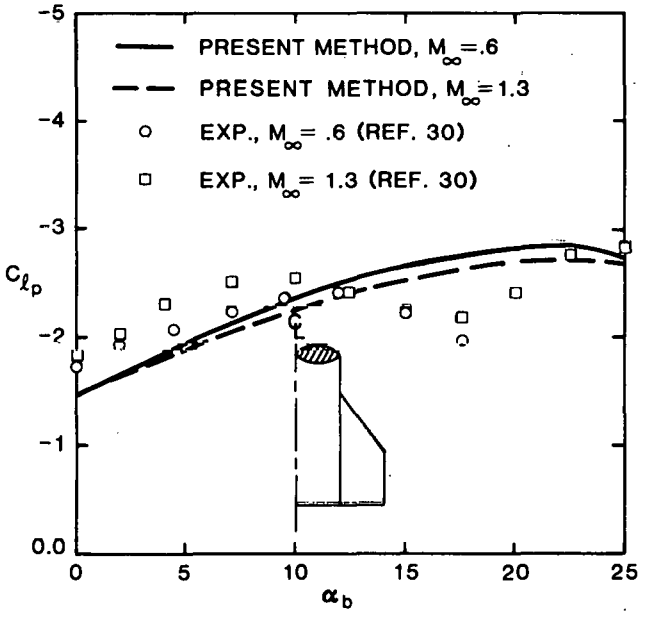

Figure 49. Roll Damping Moment vs α_b for Configuration F.

c. Steady-State Rolling Speed

The steady-state roll rate of a missile whose fins are canted is calculated in a manner similar to C_{ℓ_p}. The steady-state roll rate is defined as the rolling speed at which the roll driving moment balances with the roll damping moment. Therefore, the nondimensional steady-state roll rate, p_{ss} is the roll rate such that

$$\int_0^{\frac{\pi}{2}} [C_\ell]_{p=p_{ss}} d\phi = 0 .$$

Only one comparison of theory and experiment is made for steady-state rolling speed because of the lack of data for other planforms. Figure 50 shows the steady-state rolling speed vs angle of attack for Configuration E for a fin cant of 4° (differential fin deflection) and $M_\infty = 0.23$. The theory slightly overpredicts p_{ss} for angles of attack less than 12°, but for $\alpha_b > 12°$ the theory agrees perfectly with one set of data and underpredicts p_{ss} for the other set. The reason the theory predicts roll slowdown is rather difficult to determine. From numerical experiments with the present method it was found that roll slowdown was predicted for each of the planforms shown in Figure 30. One qualitative comment that can be made, however, is that even though the roll damping moment decreases at large angle of attack (Figure 48), the roll driving moment (i.e., fin cant) decreases at a faster rate on every planform investigated.

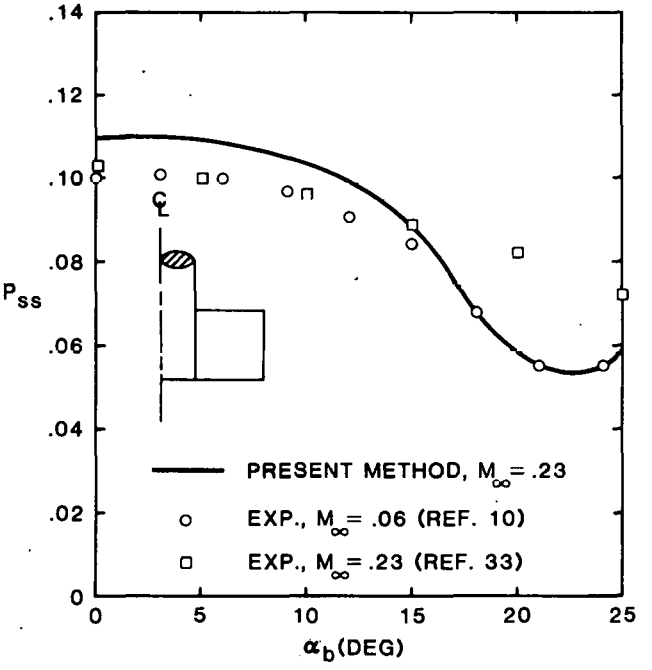

Figure 50. Steady-State Roll Rate vs α_b for Configuration E (4° fin cant)

Control Deflections

a. Pitch (or Yaw) Control

Pitch control force coefficient is defined as the normal force coefficient of the entire missile configuration (body plus fins) with the fins deflected minus the normal force coefficient of the entire missile without the fins deflected; that is,

$$\Delta C_z = [C_{z_{B+f}}]_{\delta_j \neq 0} - [C_{z_{B+f}}]_{\delta_j = 0}.$$

Using slender body theory notation, one can write

$$\Delta C_z = [C_{z_{B(f)}}]_{\delta_j \neq 0} + [C_{z_{f(B)}}]_{\delta_j \neq 0} - [C_{z_{B(f)}}]_{\delta_j = 0} - [C_{z_{f(B)}}]_{\delta_j = 0}. \quad (55)$$

The second and fourth terms are computed in the present analysis, but the first and third are not. The first term can be segregated into two terms:

$$[C_{z_{B(f)}}]_{\delta_j \neq 0} = [C_{z_{B(f)}}]_{\delta_j = 0} + C_{z_{B<\delta_j>}}, \quad (56)$$

where the second term on the right side of the equation is the normal force coefficient of the body due to control deflection of the fins. Substituting Eq (56) into Eq (55), one has

$$\Delta C_z = C_{z_{B<\delta_j>}} + [C_{z_{f(B)}}]_{\delta_j \neq 0} - [C_{z_{f(B)}}]_{\delta_j = 0}. \quad (57)$$

A simple result of slender body theory is used to estimate $C_{z_{B<\delta_j>}}$. Using the definition of the interference lift ratio, k_B (see Ref. 24, pp 213-218), one has

$$C_{z_{B<\delta_j>}} = k_B [C_{z_{f(B)}}]_{\delta_j \neq 0}.$$

Substituting this into Eq (57), one has

$$\Delta C_z = [1 + k_B] [C_{z_{f(B)}}]_{\delta_j \neq 0} - [C_{z_{f(B)}}]_{\delta_j = 0}. \quad (58)$$

The term k_B is calculated from slender body theory assuming that the angle of attack of the body is zero. One could use Eq (58) to calculate ΔC_z for any angle of attack and neglect the inconsistency between this and the derivation of k_B. The present analysis, however, chooses the approach of segregating the $\alpha_b = 0$ fin deflection interference and then using this constant value for nonzero α_b. Rewriting Eq (58) according to this approach, we have

$$\Delta C_z = [C_{z_{f(B)}}]_{\delta_j \neq 0} - [C_{z_{f(B)}}]_{\delta_j = 0} + k_B [C_{z_{f(B)}}]_{\substack{\delta_j \neq 0 \\ \alpha_b = 0}}. \quad (59)$$

Equation (59) was used in the present analysis for computing pitch control forces with fin-body interference. k_B is a simple function of a/b_o and is plotted in Figure 51.

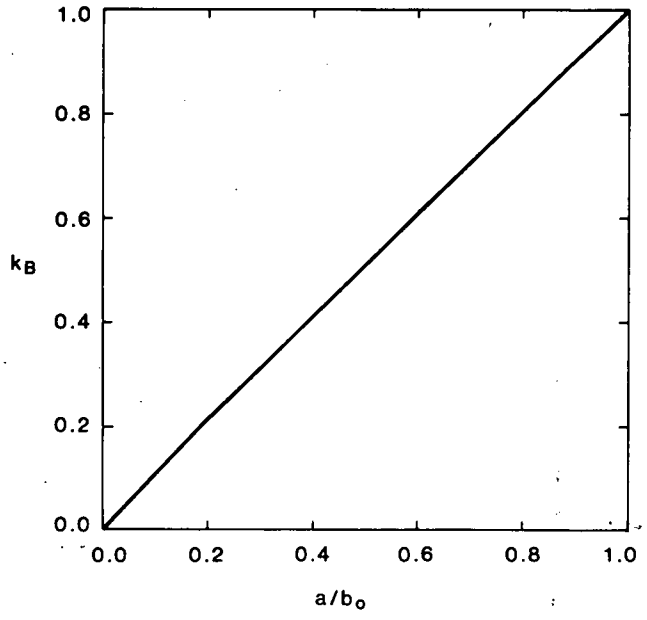

Figure 51. Interference Lift Ratio vs a/b_O (from Ref. 24)

Figures 52, 53, and 54 show the pitch control force versus angle of attack for $M_\infty = 0.7$ and 1.2 for fin configurations B, C, and D, respectively. The control force shown in these figures is for $\phi = 0°$ and the horizontal panels deflected 10°; that is, $\delta_1 = \delta_3 = 10°$ and $\delta_2 = \delta_4 = 0°$. The agreement between theory and experiment is generally fair for the three fin planforms and the angle of attack range. It can be seen from these three figures that the control force for $\alpha_b = 0°$ for the three planforms is almost identical. Although the leading edge sweep angles are 0°, 38.7°, and 67.4°, respectively, all three planforms have the same aspect ratio: 1.67. The trend with angle of attack is significantly different for the three planforms. For $\Lambda_{\ell e} = 0°$ (Figure 52), the control force drops off sharply with angle of attack to the extent that for $15° < \alpha_b < 20°$ a positive control input produces a negative control force. Note that this phenomenon is not caused by the body vortex wake, but by the interaction of the nonlinear normal force curve (i.e., fin stall and body upwash). For $\Lambda_{\ell e} = 38.7°$ (Figure 53), ΔC_z is nearly constant for low α_b and then drops off with angle of attack. The experimental data for $M_\infty = 0.7$ show a region of control force reversal

near $\alpha_b = 17°$. For $\Lambda_{\ell e} = 67.4°$ (Figure 54), ΔC_z is almost constant out to $\alpha_b = 14°$ and then shows a slight decrease with angle of attack. Also note the insensitivity of ΔC_z to Mach number. This is due to the low Mach number normal to the leading edge of the planform.

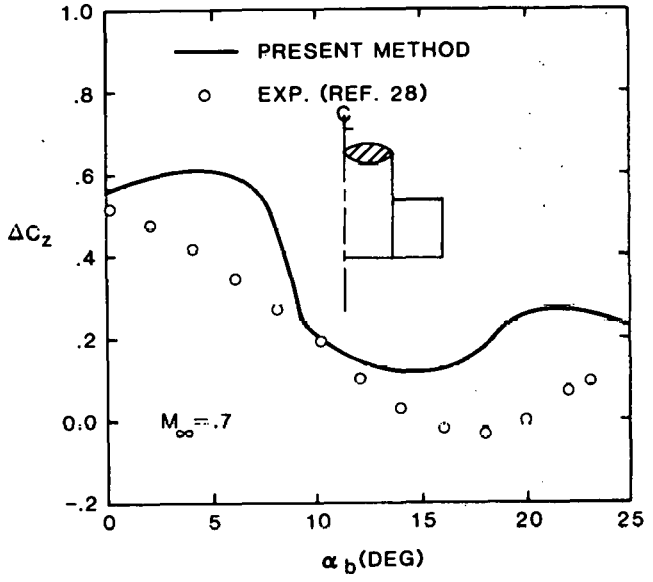

Figure 52. Pitch Control Force vs α_b for Configuration B ($\phi = 0°$, $\delta_1 = \delta_3 = 10°$, $\delta_2 = \delta_4 = 0°$)

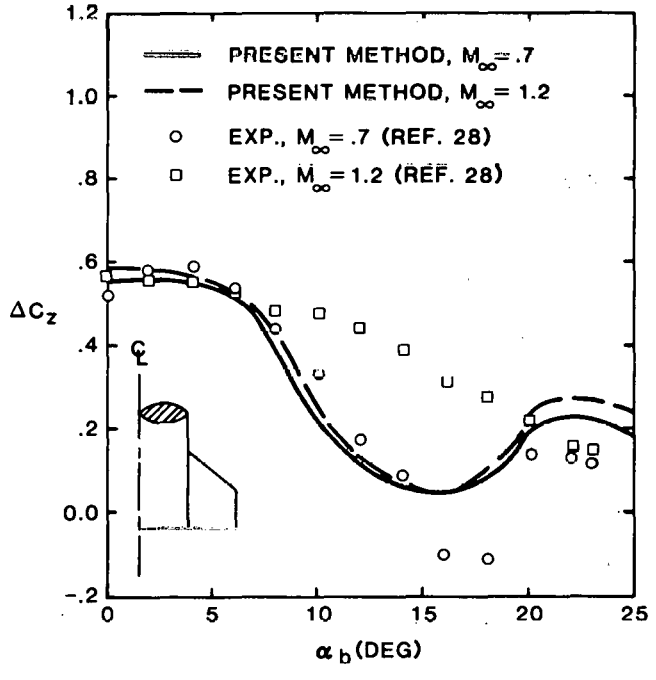

Figure 53. Pitch Control Force vs α_b for Configuration C ($\phi = 0°$, $\delta_1 = \delta_3 = 10°$, $\delta_2 = \delta_4 = 0°$)

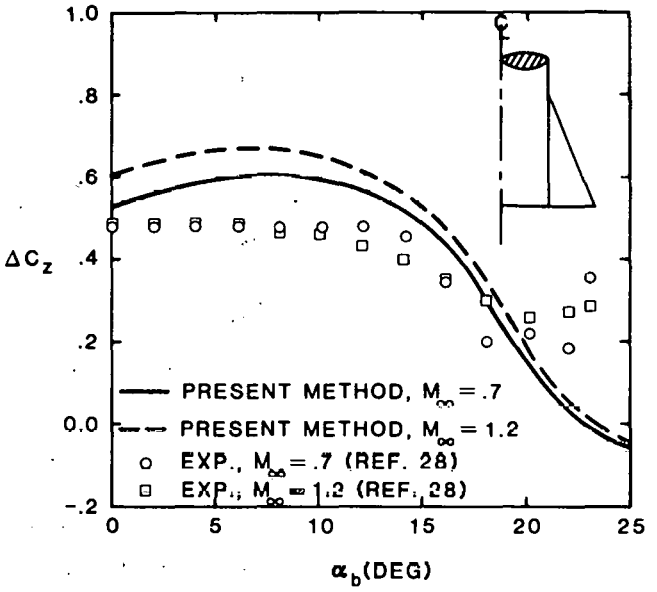

Figure 54. Pitch Control Force vs α_b for Configuration D ($\phi = 0°$, $\delta_1 = \delta_3 = 10°$, $\delta_2 = \delta_4 = 0°$)

Figures 55, 56, and 57 show the pitch control force vs angle of attack for all panels deflected 10° ($\phi = 45°$) for fin planforms B, C, and D, respectively. The agreement between theory and experiment is generally fair for the three planforms over the angle of attack range. Similar trends of ΔC_z vs angle of attack are seen in Figures 55, 56, and 57 as compared to Figures 52, 53, and 54, respectively. For $\phi = 45°$ and $\delta_j = 10°$, however, no control reversals are seen over the angle of attack range. Also, the delta planform (Figure 57) shows that the control effectiveness increases slightly with angle of attack up to $\alpha_b = 12°$ for both Mach numbers.

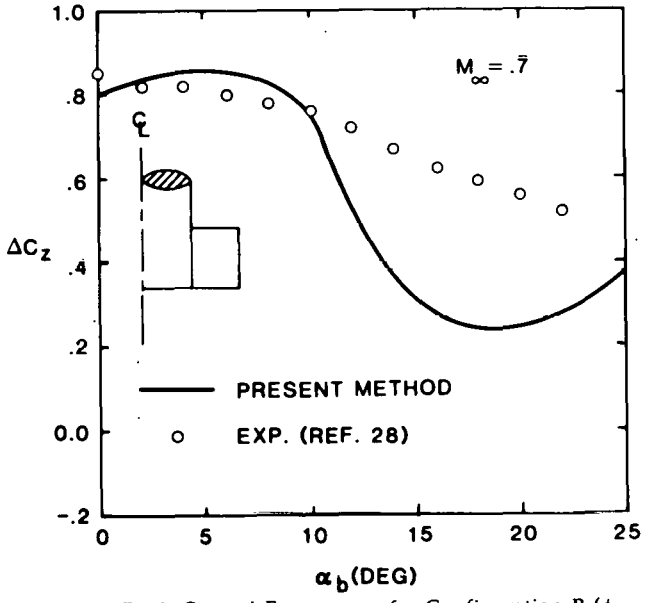

Figure 55. Pitch Control Force vs α_b for Configuration B ($\phi = 45°$, $\delta_1 = \delta_2 = \delta_3 = \delta_4 = 10°$)

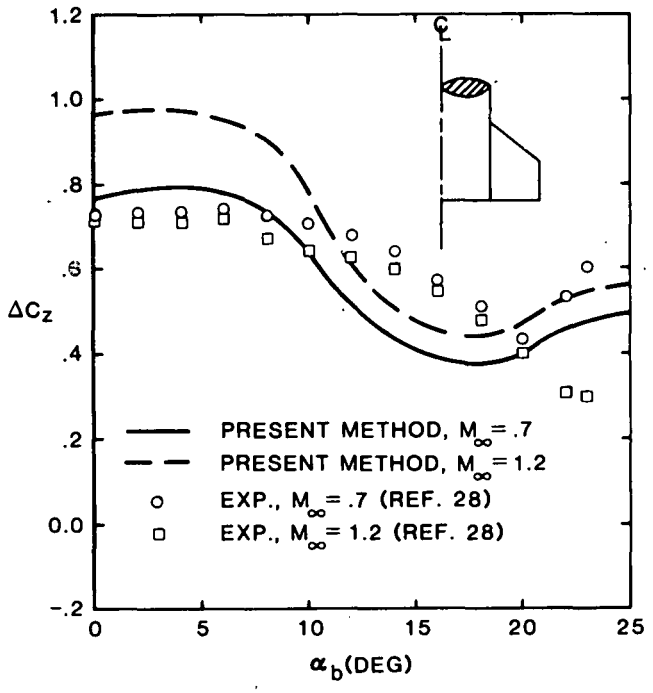

Figure 56. Pitch Control Force vs α_b for Configuration C (ϕ = 45°, $\delta_1 = \delta_2 = \delta_3 = \delta_4 = 10°$)

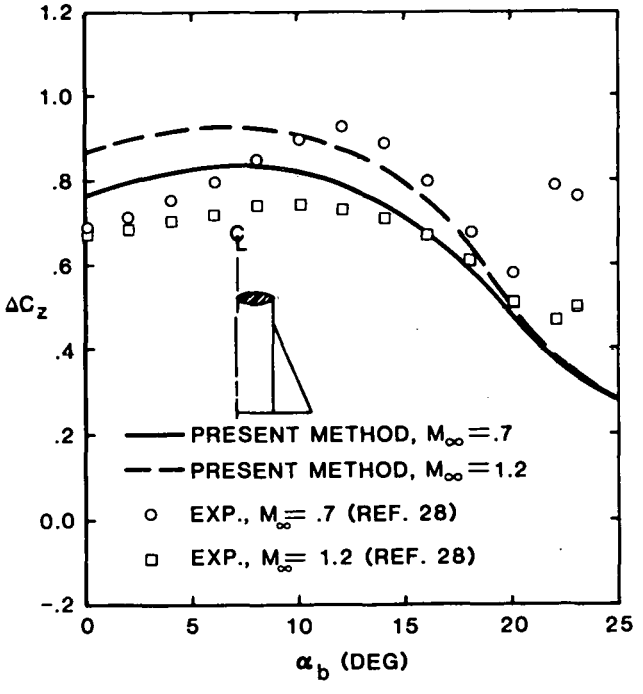

Figure 57. Pitch Control Force vs α_b for Configuration D (ϕ = 45°, $\delta_1 = \delta_2 = \delta_3 = \delta_4 = 10°$)

b. Roll Control

Figures 58, 59, and 60 show the roll control moment vs angle of attack for $M_\infty = 0.7$ and 1.2 for fin Configurations B, C, and D, respectively. These roll control moments are for $\phi = 0°$ and $\delta_1 = -\delta_3 = 10°$ and $\delta_2 = \delta_4 = 0°$. The theory generally predicts larger roll control moments than experiment, but the theoretical trends with angle of attack are valid. For the rectangular and clipped delta planform (Figure 58 and 59), a large region of roll control reversal occurs for $\alpha_b > 15°$. This region is fairly well predicted by the present analysis. For the delta planform (Figure 60), the theory substantially overpredicts the roll control moment up to $\alpha_b = 20°$ and then a control reversal is predicted. The overprediction near $\alpha_b = 0°$ could be due to an inaccurate spanwise loading or it could be due to a physical characteristic of control deflection not included in the present theory (for example, root chord gap). When a fin panel is deflected for control, a spanwise gap is created at the root chord of the fin. The gap size increases as the fin deflection and root chord length increases. For Configuration D the root chord length is 100% longer and 50% longer, respectively, than configurations B and C. This characteristic would decrease the predicted value of the roll control moment if it were included in the theory.

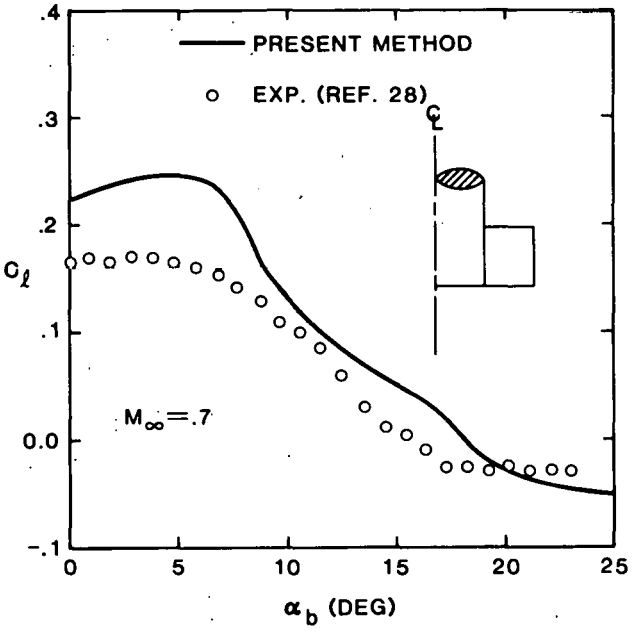

Figure 58. Roll Control Moment vs α_b for Configuration B (ϕ = 0°, $\delta_1 = -\delta_3 = 10°$, $\delta_2 = \delta_4 = 0°$)

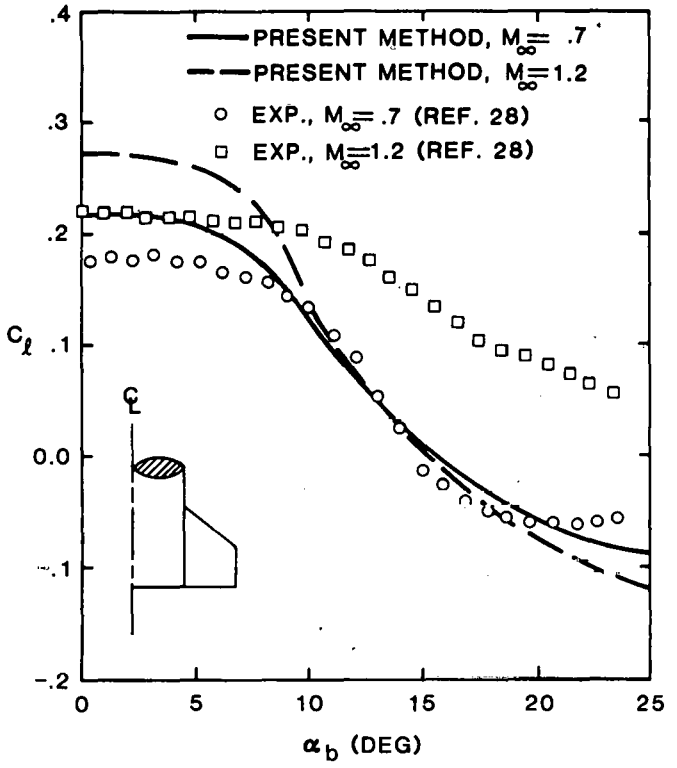

Figure 59. Roll Control Moment vs α_b for Configuration C (ϕ = 0°, $\delta_1 = -\delta_3 = 10°$, $\delta_2 = \delta_4 = 0°$)

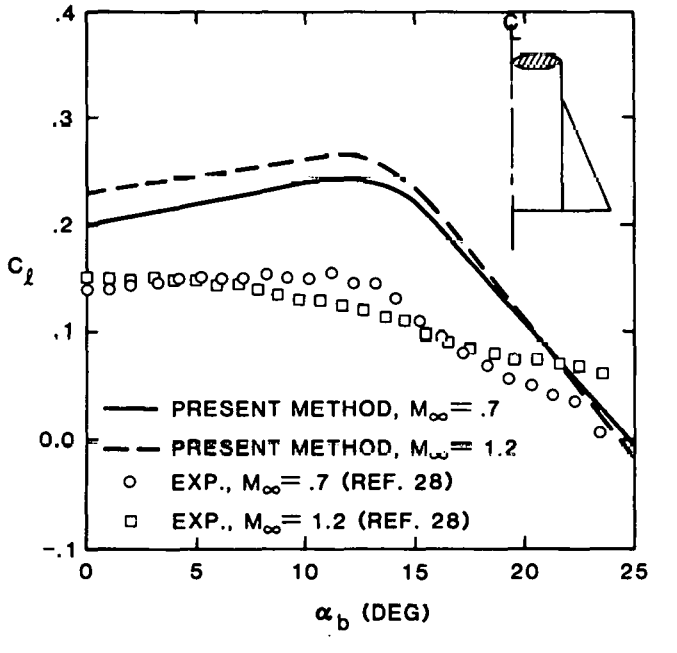

Figure 60. Roll Control Moment vs α_b for Configuration D (ϕ = 0°, $\delta_1 = -\delta_3 = 10°$, $\delta_2 = \delta_4 = 0°$)

Conclusions and Recommendations

The following conclusions and recommendations are drawn from the present investigation.

1. The spanwise and chordwise pressure distributions are of sufficient accuracy to be used as an aid in estimating root bending and hinge moment structural loads. The hinge moment predictions can also be used as a design aid in sizing control deflection actuators.
2. Evidence was found to suggest that stall near the root chord on highly swept fins washes outboard and, consequently, decreases the outboard loading on the fin. Although this element is not included in the present theory, one might conceive of a method of approximating this phenomenon in the analysis.
3. Certain comparisons between theory and experiment suggest that the stall angle of attack increases with Mach number. If sufficient data could be gathered on this trend, it should be added to the analysis.
4. The results of the present method could be enhanced by improving the empirical data for the body flow field model or by using a more accurate body flow field model. An improved flow model should contain more compressibility effects.
5. In general, short span fins produce larger nonlinear forces and moments (such as induced side force and induced roll moment) than larger span fins. This typically occurs even though the exposed fin area is smaller.
6. The present method could be improved by requiring the basic chordwise and spanwise pressure distributions to be dependent on free stream Mach number. This should be done after sufficient pressure distribution data on wings alone planforms becomes available for various Mach numbers.
7. The nonlinear decrease in roll damping for large angles of attack was found to be due to the stall angle of attack of the fin. The stall angle is primarily determined by the aspect ratio and leading edge sweep.
8. The present method should be coupled to a body force and moment predictive method

so that complete vehicle force and moment predictions are available.

9. The rapid decrease in pitch control force at large angles of attack is predicted by the method.
10. Predicted roll control reversal at large angles of attack generally agrees with experimental data.
11. The present method should prove a valuable tool for flight vehicle designers because of its ability to address general fin planforms.

References

[1]J. F. Mello and K. R. Sivier, *Supersonic Induced Rolling-Moment Characteristics of Cruciform Wing Body Configuration at High Angles of Attack*, Aerospace Engineering, Vol 20, No. 7, July 1961, pp 20-21, 44-51.

[2]W. L. Oberkampf and J. D. Nicolaides, *Aerodynamics of Finned Missiles at High Angle of Attack*, AIAA Journal, Vol 9, No. 12, December 1971, pp 2378-2384.

[3]W. L. Oberkampf, *Prediction of Roll Moments on Finned Bodies in Supersonic Flow*, J of Spacecraft and Rockets, Vol 12, No. 1, January 1975, pp 17-21.

[4]M. F. E. Dillenius and J. N. Nielsen, *Prediction of Aerodynamics of Missiles at High Angles of Attack in Supersonic Flow*, NEAR TR 99 (Mt. View, CA: Nielsen Enginering and Research, October 1975).

[5]M. R. Mendenhall and J. N. Nielsen, *Effect of Symmetrical Vortex Shedding on the Longitudinal Aerodynamic Characteristics of Wing-Body-Tail Combinations*, NEAR TR 69, NASA-CR-2473, (Mt. View, CA: Nielsen Engineering and Research, July 1977).

[6]S. B. Spangler and M. R. Mendenhall, *Further Studis of Aerodynamic Loads at Spin Entry*, NEAR TR 141 (Mt. View, CA: Nielsen Engineering and Research, July 1977).

[7]J. N. Nielsen, M. J. Hemsch, and C. A. Smith, *A Preliminary Method for Calculating the Aerodynamic Charactristics of Cruciform Missiles to High Angles of Attack Including Effects of Roll Angle and Control Deflections*, NEAR TR 152 (Mt. View, CA: Nielsen Engineering and Research, November 1977).

[8]F. J. Marshall and F. D. Deffenbaugh, *Separated Flow Over a Body of Revolution*, J of Aircraft, Vol 12, No. 2, February 1975, pp 78-85

[9]F. D. Deffenbaugh and W. G. Koerner, *Asymmetric Vortex Wake Development on Missiles at High Angles of Attack*, J Spacecraft, Vol 12, No. 3, March 1977, pp 155-162.

[10]W. L. Oberkampf, *Aerodyanmics of Finned Missiles at High Angle of Attack*, Ph.D. dissertation, August 1970, Univ. of Notre Dame, IN.

[11]W. L. Oberkampf and T. J. Bartel, *Supersonic Flow Measurements in the Body Vortex Wake of an Ogive Nose Cylinder*, AFATL-TR-78-127 (Eglin AFB, FL: Air Force Armament Laboratory, November 1978).

[12]F. R. Grosche, *Wind Tunnel Investigation of the Vortex System Near an Inclined Body of Revolution With and Without Wings*, AGARD-CP-71-71, Aerodynamic Interference, January 1971.

[13]B. E. Tinling and C. Q. Allen, *An Investigation of the Normal Force and Vortex Wake Characteristics of an Ogive Nose Cylinder*, NASA-TN-D-1297, April 1962.

[14]J. E. Fidler, J. N. Nielsen, and R. G. Schwind, *An Investigation of Slender-Body Wake Vortices*, AIAA 15th Aerospace Sciences Meeting, Paper No. 77-7, January 1977.

[15]H. Winter, *Flow Phenomena on Plates and Airfoils of Short Span*, Verein Deutscher Ingenieure, Special Issue (Avaiation) 1936 (English translation, NACA-TM-798, July, 1936).

[16]G. E. Bartlett and R. J. Vidal, *Experimental Investigation of Influence of Edge Shape on the Aerodynamic Charactristics of Low Aspect Ratio Wings at Low Speeds*, J Aero Sci, Vol 22, No. 8, August 1955, pp 517-533.

[17]D. J. Marsden, R. W. Simpson, and W. J. Rainbird, *An Investigation Into the Flow Over Delta Wings at Low Speeds With Leading Edge Separation*, Rept No. 114, College of Aeronautics, Cranfield, England: February 1958.

[18]D. Hummel, *Zur Umstromung Scharfkantiger Schlander Deltaflugel bei Grossen Anstellwinkeln*, Z. Flugwiss, Vol 15, No. 10, 1967.

[19]R. H. Wickens, *The Vortex Wake and Aerodynamic Load Distribution of Slender Rectangular Wings*, Can Aeron and Sp J, Vol 13, June 1967, pp 247-260.

[20]R. Lecat and J. Rietschlin, *Goniometric Aerodynamics: A Different Perspective: Description-Application*, AIAA Atmospheric Flight Mechanics Conference, Paper No. 79-1650, August 1979.

[21]E. C. Polhamus, *A Concept of the Vortex Lift of Sharp-Edge Delta Wings Based on a Leading Edge Suction Analogy*, NASA TN-D-3767, December 1966.

[22]W. H. Wentz and D. L. Kohlman, *Wind Tunnel Investigations of Vortex Breakdown on Slender Sharp-Edged Wings*, NASA-CR-98737, 1968.

[23]J. L. Johnson, *Low-Speed Measurements of Static Stability, Damping in Yaw, and Damping in Roll of a Delta, a Swept, and an Unswept Wing for Angles of Attack from 0° to 90°*, NACA-RM-L56B01, April 1956.

[24]J. N. Nielsen, *Missile Aerodynamics* (New York, McGraw-Hill, 1960).

[25]G. J. Adams and D. W. Dugan, *Theoretical Damping in Roll and Rolling Moment Due to Differntial Wing Incidence for Slender Cruciform Wings and Wing-Body Combinations*, NACA Report 1088, September 1950.

[26]J. N. Nielsen, *Nonlinearities in Missile Aerodynamics*, AIAA 16th Aerospace Sciences Meeting, AIAA Paper No. 78-20, January 1978.

[27]C. Q. Allen, R. G. Schwind, and G. N. Malcolm, *Canard-Body-Tail Missile Test at Angles of Attack to 50° in the Ames 11-Foot Transonic Wind Tunnel*, NASA-TM-78441, September 1978.

[28]G. E. Frantz, *Control Surface Interaction Study: Wind Tunnel Test Data Analysis Report*, Rept No. NA66H-139, (Columbus, OH: North American Aviation, February 1966).

[29]F. J. Regan, *Roll Damping Moment Measurements for the Basic Finner at Subsonic and Supersonic Speeds*, Rept 6652 (White Oak, MD: Naval Ordnance Laboratory, March 1964).

[30]L. M. Jenke, *Experimental Roll-Damping Magnus, and Static-Stability Characteristics of Two Slender Missile Configurations at High Angles of Attack (0 to 90 deg) and Mach Number 0.2 Through 2.5*, AEDC-TR-58, July 1976.

[31]T. A. Clare, *Non-Linear Resonance Instability in the Flight Dynamics of Missiles*, Ph.D. Dissertation, Univ. of Notre Dame, Notre Dame, IN, June 1970.

[32]M. J. Hemsch and J. N. Nielsen, *Test Report for Canard Missile Tests in Ames 6- by 6-Foot Supersonic Wind Tunnel*, NEAR TR 72 (Mt. View, CA: Nielsen Engineering and Research, August 1974).

[33]D. E. Startzell and F. J. De Meritte, *Effect of Fin Cant and Nose Shapes on Free Spin of Basic Spinner*, NAVORD Rept 6025, 1958.

APPENDIX A

Structure and Listing of Computer Program

The computer program which implements the theoretical method is constructed in a modular fashion. This design was chosen so that a user could more easily identify any difficulties one might have with the program and make changes. A large number of COMMENT cards also are included in the program to aid the user. The main program and subprogram names, card image lengths, and computer memory lengths are shown in Table A-1.

The structure of the program is depicted in the overview flow chart (Figure A-1). The flow chart shows the main program and every subprogram along with the communication between each of them. However, the flow chart does not show any data transfer by way of COMMON statements. All input and essentially all output is accomplished from the main program.

A complete listing of the computer program is given in Table A-2.

A user could rather easily reduce the computer memory requirements needed to run the program. The majority of memory (88%) is used in two triply dimensioned arrays: VVEL (6, 73, 51) and WVEL (6, 73, 51). These arrays are used to story v and w velocity components calculated in FLOW and transferred to FINLOAD. These arrays store v and w in the cross-flow plane at the axial location of the fins for a given angle of attack of the body. The first subscript sets the maximum number of α_b's that can be calculated in a given computer run, the second subscript sets the number of roll angles used to calculate fin loads, and the third subscript sets the number of spanwise locations along the exposed semispan used to calculate fin loads. By changing the program such that only three α_b's are permitted in one run, a user can reduce computer memory by 22,338 words. The second and third subscripts should not be changed in the program for purposes of conserving memory.

Although the computer run time is discussed in Appendix B, a short discussion is given here concerning a simple modification of the code that, for certain cases, would significantly reduce the run time. The majority of computation time in the execution of the program is consumed in calculating the body flow field in subroutine FLOW. As discussed in the previous paragraph, the v and w velocity components are calculated in a polar grid pattern for an axial location at the fins and for a given α_b. If a user plans to make a number of computer runs for fin planforms with the same semispan and located at the same axial station along the body, the modification should be made. For this case the body flow field calculated in FLOW would be exactly the same for each computer run. Therefore, the flow field stored in arrays U (I), VVEL (I, J, K), and WVEL (I, J, K) should be stored on disc or tape and recalled for later computer runs. In this way the subroutine FLOW will not have to be called each time a computer run is made.

Table A-1. Description of Quantity of Computer Code

Program Element Type	Name	Card Length	Memory Length (Words)
Main Program	FINLOAD	562	48 349
Subroutine Subprogram	IDSUB	22	81
Subroutine Subprogram	IPSUB	37	182
Function Subprogram	CN	25	118
Subroutine Subprogram	CNPREP	53	302
Subroutine Subprogram	FLOW	134	903
Function Subprogram	TBLOOK	29	82
Subroutine Subprogram	SIM	26	82
Blank Common	--	--	16
Labelled Common	--	--	233
	Total	888	50 348 ($142\ 254_8$)

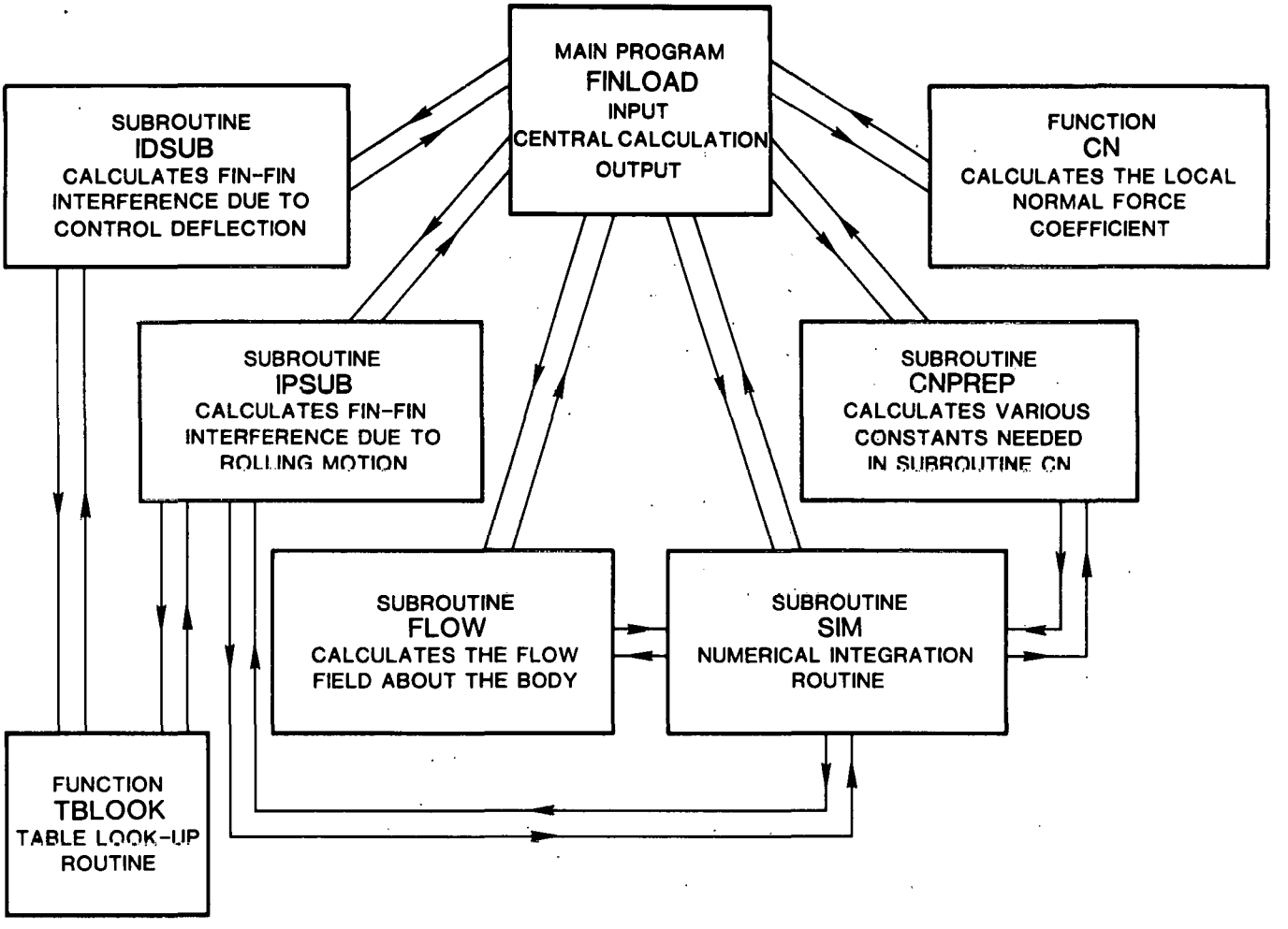

Figure A-1. Overview Flow Chart for Computer Program

Table A-2. Computer Program Listing

```
      PROGRAM FINLOAD(INPUT,OUTPUT,TAPE5=INPUT)                          FIN      2
C                                                                        FIN      3
C     THIS PROGRAM CALCULATES THE FORCES AND MOMENTS PRODUCED            FIN      4
C     BY CRUCIFORM FINS ATTACHED TO A MISSILE IN SUBSONIC AND            FIN      5
C     TRANSONIC FLOW.                                                    FIN      6
C     PROGRAMMED BY W. L. OBERKAMPF (NOV. 1979 - APRIL 1980)             FIN      7
C                                                                        FIN      8
      COMMON A,BJA,CR,AE,PI,DETA,COSLE,TANLE,TANTE,MACH,ALPHA            FIN      9
      COMMON /A/ BO,SF,SIGMA,CNA,INT1,INT2                               FIN     10
      COMMON /B/ RAD,XV,IALPHA                                           FIN     11
      COMMON /C/ UVEL,VSTO,WSTO,SINP,COSP,SINLE,IAB,SINTE,COSTE,         FIN     12
     CBETA,TANGM,GAMLE,GAMTE                                             FIN     13
      REAL MACH,IP,INT1,INT2,INT3,INT4,INT5,INT6,INT7,INT8,              FIN     14
     1INT9,INT10,INT11,INT12,INT13,INT14,INT15,INT16,INT17,INT18         FIN     15
      DIMENSION FCOTRL(4),ALPHA(6),ROLLR(6),INT1(51),INT2(51),ZETAS(51), FIN     16
     1ETAS(51),INT3(51),INT4(51),INT5(51),VVEL(6,73,51),WVEL(6,73,51),   FIN     17
     1VSTO(51),WSTO(51),INT6(51),INT7(51),INT8(51),INT9(51),INT10(51),   FIN     18
     1INT11(51),INT12(51),CSUBL(73),CSUBZ(73),CSUBM(73),CSUBY(73),CSUBN( FIN     19
     173),UVEL(6),INT13(51),INT14(51),INT15(51),INT16(51),INT17(51),     FIN     20
     1INT18(51),CSUBP(73),CSUBH(73),CSUBB(73),FCTRLE(4),CZAV(6),CMAV(6), FIN     21
     1CYAV(6),CNAV(6),CLAV(6),CZTOT(19),CMTOT(19),CYTOT(19),CNTOT(19),   FIN     22
     1CLTOT(19),TITLE(10)                                                FIN     23
```

Table A-2. Computer Program Listing (Cont)

```
C                                                                       FIN        24
C     BEGIN INPUT OF MISSILE AND FIN GEOMETRY (USE METRIC UNITS)        FIN        25
C     INPUT TITLE FOR MISSILE GEOMETRY (MAXIMUM OF 60 CHARACTERS)       FIN        26
C                                                                       FIN        27
      READ (5,120) (TITLE(I),I=1,10)                                    FIN        28
C                                                                       FIN        29
C     A=BODY RADIUS (METER)                                             FIN        30
C     B0=SEMI-SPAN (METER)                                              FIN        31
C     CR=ROOT CHORD (METER)                                             FIN        32
C     X1=X LOCATION OF LEADING EDGE ROOT CHORD (METER)                  FIN        33
C     GAMLE=LEADING EDGE SWEEP (DEG)                                    FIN        34
C     GAMTE=TRAILING EDGE SWEEP (DEG)                                   FIN        35
C     XH=X LOCATION OF PANEL HINGE MOMENT REFERENCE                     FIN        36
C                                                                       FIN        37
      READ (5,*) A,B0,CR,X1,GAMLE,GAMTE,XH                              FIN        38
C                                                                       FIN        39
C     END INPUT OF MISSILE AND FIN GEOMETRY                             FIN        40
C                                                                       FIN        41
C     BEGIN INPUT FOR DESIRED FORCES AND MOMENTS                        FIN        42
C     ENTER 1 IF QUANTITY DESIRED; ENTER ZERO IF NOT DESIRED            FIN        43
C     ICZCM=FIN NORMAL FORCE AND PITCH MOMENT                           FIN        44
C     ICYCN=FIN SIDE FORCE AND YAW MOMENT                               FIN        45
C     ICL=FIN ROLL MOMENT                                               FIN        46
C     IPANEL=PANEL NORMAL FORCE, HINGE MOMENT AND ROOT BENDING MOMENT   FIN        47
C                                                                       FIN        48
      READ (5,*) ICZCM,ICYCN,ICL,IPANEL                                 FIN        49
C                                                                       FIN        50
C     ENTER ANGULAR PARAMETERS OF FINS AND BODY                         FIN        51
C     FCOTRL(I)=CONTROL DEFLECTION OF EACH FIN (DEG); FOUR VALUES       FIN        52
C     IALPHA=NUMBER OF BODY ANGLES OF ATTACK (MAX. OF SIX)              FIN        53
C     ALPHA(I)=BODY ANGLES OF ATTACK (DEG)                              FIN        54
C     IROLLR=NUMBER OF BODY ROLL RATES (MAX. OF SIX)                    FIN        55
C     ROLLR(I)=BODY ROLL RATES (PHIDOT*B)/U, DIMENSIONLESS)             FIN        56
C                                                                       FIN        57
      READ (5,*) (FCOTRL(I),I=1,4)                                      FIN        58
      READ (5,*) IALPHA,(ALPHA(I),I=1,IALPHA)                           FIN        59
      READ (5,*) IROLLR,(ROLLR(I),I=1,IROLLR)                           FIN        60
C                                                                       FIN        61
C     ENTER FREESTREAM MACH NUMBER; FIN LEADING EDGE MUST BE SUBSONIC   FIN        62
C                                                                       FIN        63
      READ (5,*) MACH                                                   FIN        64
C                                                                       FIN        65
C     END INPUT FOR FORCES AND MOMENTS                                  FIN        66
C                                                                       FIN        67
C     BEGIN CALCULATION OF NEEDED CONSTANTS                             FIN        68
C                                                                       FIN        69
      PI=ACOS(-1.)                                                      FIN        70
      RAD=180./PI                                                       FIN        71
      DETA=1./5.                                                        FIN        72
      DZETA=DETA                                                        FIN        73
      AA=A*A                                                            FIN        74
      B0A=B0-A                                                          FIN        75
      GAMLE=GAMLE/RAD                                                   FIN        76
      GAMTE=GAMTE/RAD                                                   FIN        77
      SINLE=SIN(GAMLE)                                                  FIN        78
      COSLE=COS(GAMLE)                                                  FIN        79
      TANLE=TAN(GAMLE)                                                  FIN        80
      SINTE=SIN(GAMTE)                                                  FIN        81
      COSTE=COS(GAMTE)                                                  FIN        82
      TANTE=TAN(GAMTE)                                                  FIN        83
      SF=.5*B0A**2*(2.*CR/B0A-TANLE+TANTE)                              FIN        84
      AE=2.*B0A**2/SF                                                   FIN        85
      CT=CR-B0A*(TANLE-TANTE)                                           FIN        86
      XV=X1+.5*(.25*CR+.25*CT+B0A*TANLE)                                FIN        87
      GAMMAM=0.                                                         FIN        88
      IF(MACH.GT.1.) GAMMAM=ACOS(1./MACH)                               FIN        89
      TANGM=TAN(GAMMAM)                                                 FIN        90
      IF(GAMLE.GE.GAMMAM) GO TO 9                                       FIN        91
```

Table A-2. Computer Program Listing (Cont)

```
      PRINT 200                                                          FIN        92
      STOP                                                               FIN        93
    9 IF(MACH.LE.1.) BETA=SQRT(1.-MACH**2)                               FIN        94
      IF(MACH.GT.1.) BETA=SQRT(MACH**2-1.)                               FIN        95
      HCZCM=2HNO                                                         FIN        96
      HCYCN=2HNO                                                         FIN        97
      HCL=2HNO                                                           FIN        98
      HPANEL=2HNO                                                        FIN        99
      IF(ICZCM.EQ.1) HCZCM=3HYES                                         FIN       100
      IF(ICYCN.EQ.1) HCYCN=3HYES                                         FIN       101
      IF(ICL.EQ.1) HCL=3HYES                                             FIN       102
      IF(IPANEL.EQ.1) HPANEL=3HYES                                       FIN       103
C                                                                        FIN       104
C     END CALCULATION OF NEEDED CONSTANTS                                FIN       105
C                                                                        FIN       106
C     BEGIN CALCULATION OF SIGMA                                         FIN       107
C                                                                        FIN       108
      ETA=0.                                                             FIN       109
      DO 11 J=1,51                                                       FIN       110
      ZETA=0.                                                            FIN       111
      ETAF=(1.+ETA**(2.*AE))*SQRT(1.-ETA**2)                             FIN       112
      TEMP=CR-BOA*(TANLE-TANTE)*ETA                                      FIN       113
      DO 10 I=1,51                                                       FIN       114
      ZETAF=SQRT(ZETA)*EXP(ZETA**2/SQRT(COSLE))                          FIN       115
      INT1(I)=TEMP*ZETAF*ETAF                                            FIN       116
      ZETAS(I)=ZETA                                                      FIN       117
   10 ZETA=ZETA+DZETA                                                    FIN       118
      CALL SIM(INT1,DZETA,51,INT2(J))                                    FIN       119
      ETAS(J)=ETA                                                        FIN       120
   11 ETA=ETA+DETA                                                       FIN       121
      CALL SIM(INT2,DETA,51,SIGMA)                                       FIN       122
      SIGMA=SF/BOA/SIGMA                                                 FIN       123
C                                                                        FIN       124
C     END CALCULATION OF SIGMA                                           FIN       125
C                                                                        FIN       126
C     BEGIN CALCULATION OF CNA                                           FIN       127
C                                                                        FIN       128
      UVEL(1)=1.                                                         FIN       129
      DO 12 J=1,51                                                       FIN       130
      VSTO(J)=0.                                                         FIN       131
   12 WSTO(J)=0.                                                         FIN       132
      IAB=1                                                              FIN       133
      SINP=0.                                                            FIN       134
      COSP=1.                                                            FIN       135
      CALL CNPREP                                                        FIN       136
      CNA=CN(1./RAD)*RAD                                                 FIN       137
C                                                                        FIN       138
C     END CALCULATION OF CNA                                             FIN       139
C                                                                        FIN       140
C     CALL FIN-FIN INTERFERENCE SUBROUTINE                               FIN       141
C                                                                        FIN       142
      FCTRLE(1)=FCOTRL(1)                                                FIN       143
      FCTRLE(2)=FCOTRL(2)                                                FIN       144
      FCTRLE(3)=FCOTRL(3)                                                FIN       145
      FCTRLE(4)=FCOTRL(4)                                                FIN       146
      IF((FCOTRL(1).EQ.0.).AND.(FCOTRL(2).EQ.0.).AND.(FCOTRL(3).EQ.0.)   FIN       147
     C.AND.(FCOTRL(4).EQ.0.)) GO TO 14                                   FIN       148
      CALL IDSUB(FCOTRL,FCTRLE)                                          FIN       149
C                                                                        FIN       150
C     CALL ROLL DAMPING INTERFERENCE SUBROUTINE                          FIN       151
C                                                                        FIN       152
   14 IP=0.                                                              FIN       153
      DO 15 I=1,IROLLR                                                   FIN       154
   15 IF(ROLLR(I).NE.0.) GO TO 16                                        FIN       155
      GO TO 17                                                           FIN       156
   16 CALL IPSUB(IP)                                                     FIN       157
   17 GAMLE=GAMLE*RAD                                                    FIN       158
```

Table A-2. Computer Program Listing (Cont)

```
      GAMTE=GAMTE*RAD                                                    FIN      159
      CNA=CNA/RAD                                                        FIN      160
      PRINT 101,(TITLE(I),I=1,10),A,B),CR,X1,GAMLE,GAMTE,XH,SF,AE,CT,    FIN      161
     1SIGMA,CNA,IP,HCZCM,HCYCN,HCL,HPANEL,(I,FCOTRL(I),I=1,4)            FIN      162
      PRINT 102,(ALPHA(I),I=1,IALPHA)                                    FIN      163
      DO 18 I=1,IALPHA                                                   FIN      164
   18 ALPHA(I)=ALPHA(I)/RAD                                              FIN      165
      PRINT 103                                                          FIN      166
      PRINT 104,(ROLLR(I),I=1,IROLLR)                                    FIN      167
      PRINT 112,MACH                                                     FIN      168
      GAMLE=GAMLE/RAD                                                    FIN      169
      GAMTE=GAMTE/RAD                                                    FIN      170
      DO 19 I=1,4                                                        FIN      171
      FCOTRL(I)=FCOTRL(I)/RAD                                            FIN      172
   19 FCTRLE(I)=FCTRLE(I)/RAD                                            FIN      173
C                                                                        FIN      174
C     CALL FLOW FIELD CALCULATION SUBROUTINE                             FIN      175
C                                                                        FIN      176
      CALL FLOW(UVEL,VVEL,WVEL)                                          FIN      177
      IAB=1                                                              FIN      178
C                                                                        FIN      179
C     BEGIN ANGLE OF ATTACK LOOP                                         FIN      180
C                                                                        FIN      181
   30 AB=ALPHA(IAB)                                                      FIN      182
      COSAB=COS(AB)                                                      FIN      183
C                                                                        FIN      184
C     BEGIN ROLL RATE LOOP                                               FIN      185
C                                                                        FIN      186
      IRR=1                                                              FIN      187
   35 PHID=ROLLR(IRR)/80                                                 FIN      188
      PHI=0.                                                             FIN      189
      IPHI=1                                                             FIN      190
      DPHI=5./RAD                                                        FIN      191
      DIPHI=1                                                            FIN      192
      ISWTCH=1                                                           FIN      193
      ISAV=0                                                             FIN      194
C                                                                        FIN      195
C     BEGIN ROLL ANGLE LOOP                                              FIN      196
C                                                                        FIN      197
   40 SINP=SIN(PHI)                                                      FIN      198
      COSP=COS(PHI)                                                      FIN      199
      ITEMP=1                                                            FIN      200
      IF((IPHI.GE.20).AND.(IPHI.LE.37)) ITEMP=2                          FIN      201
      IF((IPHI.GE.38).AND.(IPHI.LE.55)) ITEMP=3                          FIN      202
      IF(IPHI.GE.56) ITEMP=4                                             FIN      203
      IF(ITEMP+ISAV.EQ.5) ISAV=0                                         FIN      204
      TEMP2=FCTRLE(ITEMP+ISAV)*SIGN(1.,COS(PHI-ISWTCH*(1.E-5)))          FIN      205
      SINDE=SIN(TEMP2)                                                   FIN      206
      COSDE=COS(TEMP2)                                                   FIN      207
      TEMP=FCOTRL(ITEMP+ISAV)*SIGN(1.,COS(PHI-ISWTCH*(1.E-5)))           FIN      208
      SIND=SIN(TEMP)                                                     FIN      209
      COSD=COS(TEMP)                                                     FIN      210
      DO 45 I=1,51                                                       FIN      211
      VSTO(I)=VVEL(IAB,IPHI,I)                                           FIN      212
   45 WSTO(I)=WVEL(IAB,IPHI,I)                                           FIN      213
C                                                                        FIN      214
C     CALL SUBROUTINE WHICH PREPARES CONSTANTS NEEDED IN SUBPROGRAM CN   FIN      215
C                                                                        FIN      216
      CALL CNPREP                                                        FIN      217
      ETA=0.                                                             FIN      218
C                                                                        FIN      219
C     BEGIN ETA(R) LOOP                                                  FIN      220
C                                                                        FIN      221
      DO 69 J=1,51                                                       FIN      222
      ZETA=0.                                                            FIN      223
      RTEMP=A+B1A*ETA                                                    FIN      224
      XTEMP=CR-B0A*(TANLE-TANTE)*ETA                                     FIN      225
      XTE=X1+CR+B0A*TANTE*ETA                                            FIN      226
```

Table A-2. Computer Program Listing (Cont)

```
      ETAF=(1.+ETA**(2.*AE))*SQRT(1.-ETA**2)                                FIN      227
      PHIDR=PHID*RTEMP                                                      FIN      228
      UL=SQRT(UVEL(IAB)**2+(VSTO(J)+PHIDR*SINP)**2+(WSTO(J)-                FIN      229
     1PHIDR*COSP)**2)                                                       FIN      230
      TEMP1=COSAB*(SINDE+IP*PHIDR)                                          FIN      231
      TEMP2=(VSTO(J)+PHIDR*SINP)*COSDE*SINP                                 FIN      232
      TEMP3=(WSTO(J)-PHIDR*COSP)*COSDE*COSP                                 FIN      233
      VECN=1.+2.*SINDE*IP*PHIDR+(IP*PHIDR)**2                               FIN      234
      AL=ASIN((TEMP1-TEMP2+TEMP3)/VECN/UL)                                  FIN      235
      CNN=CN(AL)                                                            FIN      236
C                                                                           FIN      237
C     BEGIN ZETA(X) LOOP                                                    FIN      238
C                                                                           FIN      239
      DO 59 I=1,51                                                          FIN      240
      ZETAF=SQRT(ZETA)*EXP(ZETA**2/SQRT(COSLE))                             FIN      241
      TEMP=XTEMP*ZETAF*ETAF*CNN*UL**2                                       FIN      242
      IF(ICL.EQ.0) GO TO 55                                                 FIN      243
      INT3(I)=RTEMP*TEMP                                                    FIN      244
   55 IF(ICZCM.EQ.0) GO TO 57                                               FIN      245
      INT4(I)=TEMP*COSD*COSP                                                FIN      246
      INT5(I)=TEMP*((XTE-XTEMP*ZETA)*COSD*COSP-RTEMP*SIND*SINP)             FIN      247
   57 IF(ICYCN.EQ.0) GO TO 58                                               FIN      248
      INT6(I)=TEMP*COSD*SINP                                                FIN      249
      INT7(I)=TEMP*((XTE-XTEMP*ZETA)*COSD*SINP+RTEMP*SIND*COSP)             FIN      250
   58 IF(IPANEL.EQ.0) GO TO 59                                              FIN      251
      INT13(I)=TEMP                                                         FIN      252
      INT14(I)=TEMP*((XTE-XTEMP*ZETA)-XH)                                   FIN      253
      INT15(I)=ETA*TEMP                                                     FIN      254
   59 ZETA=ZETA+DZETA                                                       FIN      255
C                                                                           FIN      256
C     END ZETA(X) LOOP                                                      FIN      257
C                                                                           FIN      258
      IF(ICL.EQ.0) GO TO 65                                                 FIN      259
      CALL SIM(INT3,DZETA,51,INT8(J))                                       FIN      260
   65 IF(ICZCM.EQ.0) GO TO 67                                               FIN      261
      CALL SIM(INT4,DZETA,51,INT9(J))                                       FIN      262
      CALL SIM(INT5,DZETA,51,INT10(J))                                      FIN      263
   67 IF(ICYCN.EQ.0) GO TO 68                                               FIN      264
      CALL SIM(INT6,DZETA,51,INT11(J))                                      FIN      265
      CALL SIM(INT7,DZETA,51,INT12(J))                                      FIN      266
   68 IF(IPANEL.EQ.0) GO TO 69                                              FIN      267
      CALL SIM(INT13,DZETA,51,INT16(J))                                     FIN      268
      CALL SIM(INT14,DZETA,51,INT17(J))                                     FIN      269
      CALL SIM(INT15,DZETA,51,INT18(J))                                     FIN      270
   69 ETA=ETA+DETA                                                          FIN      271
C                                                                           FIN      272
C     END ETA(R) LOOP                                                       FIN      273
C                                                                           FIN      274
      IF(ICL.EQ.0) GO TO 70                                                 FIN      275
      CALL SIM(INT8,DETA,51,CSUBL(IPHI))                                    FIN      276
   70 IF(ICZCM.EQ.0) GO TO 72                                               FIN      277
      CALL SIM(INT9,DETA,51,CSUBZ(IPHI))                                    FIN      278
      CALL SIM(INT10,DETA,51,CSUBM(IPHI))                                   FIN      279
   72 IF(ICYCN.EQ.0) GO TO 73                                               FIN      280
      CALL SIM(INT11,DETA,51,CSUBY(IPHI))                                   FIN      281
      CALL SIM(INT12,DETA,51,CSUBN(IPHI))                                   FIN      282
   73 IF(IPANEL.EQ.0) GO TO 74                                              FIN      283
      CALL SIM(INT16,DETA,51,CSUBP(IPHI))                                   FIN      284
      CALL SIM(INT17,DETA,51,CSUBH(IPHI))                                   FIN      285
      CALL SIM(INT18,DETA,51,CSUBB(IPHI))                                   FIN      286
   74 PHI=PHI+DPHI                                                          FIN      287
      IPHI=IPHI+DIPHI                                                       FIN      288
      IF(IPHI.LE.73) GO TO 40                                               FIN      289
      IF(((FCOTRL(1).EQ.0.).AND.(FCOTRL(2).EQ.).).AN).(FCOTRL(3).EQ.0.)     FIN      290
     1.AND.(FCOTRL(4).EQ.0.)).OR.(ISWTCH.EQ.-1)) GO TO 79                   FIN      291
C                                                                           FIN      292
C     BEGIN PREPARATIONS FOR DOUBLE VALUED CONTROL FORCES AND MOMENTS       FIN      293
```

Table A-2. Computer Program Listing (Cont)

```
C                                                                       FIN      294
      PHI=PI/2.                                                         FIN      295
      IPHI=19                                                           FIN      296
      DPHI=PI/2.                                                        FIN      297
      DIPHI=18                                                          FIN      298
      ISWTCH=-1                                                         FIN      299
      ISAV=1                                                            FIN      300
      IF(ICL.EQ.0) GO TO 75                                             FIN      301
      SAVL19=CSUBL(19)                                                  FIN      302
      SAVL37=CSUBL(37)                                                  FIN      303
      SAVL55=CSUBL(55)                                                  FIN      304
   75 IF(ICZCM.EQ.0) GO TO 76                                           FIN      305
      SAVZ19=CSUBZ(19)                                                  FIN      306
      SAVM19=CSUBM(19)                                                  FIN      307
      SAVZ37=CSUBZ(37)                                                  FIN      308
      SAVM37=CSUBM(37)                                                  FIN      309
      SAVZ55=CSUBZ(55)                                                  FIN      310
      SAVM55=CSUBM(55)                                                  FIN      311
   76 IF(ICYCN.EQ.0) GO TO 77                                           FIN      312
      SAVY19=CSUBY(19)                                                  FIN      313
      SAVN19=CSUBN(19)                                                  FIN      314
      SAVY37=CSUBY(37)                                                  FIN      315
      SAVN37=CSUBN(37)                                                  FIN      316
      SAVY55=CSUBY(55)                                                  FIN      317
      SAVN55=CSUBN(55)                                                  FIN      318
   77 IF(IPANEL.EQ.3) GO TO 78                                          FIN      319
      SAVP19=CSUBP(19)                                                  FIN      320
      SAVH19=CSUBH(19)                                                  FIN      321
      SAVB19=CSUBB(19)                                                  FIN      322
      SAVP37=CSUBP(37)                                                  FIN      323
      SAVH37=CSUBH(37)                                                  FIN      324
      SAVB37=CSUBB(37)                                                  FIN      325
      SAVP55=CSUBP(55)                                                  FIN      326
      SAVH55=CSUBH(55)                                                  FIN      327
      SAVB55=CSUBB(55)                                                  FIN      328
   78 GO TO 40                                                          FIN      329

C                                                                       FIN      330
C     END PREPARATIONS FOR DOUBLE VALUED CONTROL FORCES AND MOMENTS     FIN      331
C                                                                       FIN      332
   79 CONTINUE                                                          FIN      333
                                                                        FIN      334
C                                                                       FIN      335
C     END OF ROLL ANGLE LOOP                                            FIN      336
C                                                                       FIN      337
C     BEGIN PRIMARY OUTPUT                                              FIN      338
C                                                                       FIN      339
      TEMPM=SIGMA*BOA/2./PI/A**3                                        FIN      340
      TEMPF=SIGMA*BOA/PI/AA                                             FIN      341
      TEMPP=SIGMA*BOA/SF                                                FIN      342
      ATEMP=ALPHA(IAB)*RAD                                              FIN      343
      IF(ICZCM.EQ.0) GO TO 82                                           FIN      344
C                                                                       FIN      345
C     BEGIN OUTPUT FOR CZ AND CM                                        FIN      346
C                                                                       FIN      347
      PRINT 105,ROLLR(IRR),ATEMP                                        FIN      348
      PRINT 106                                                         FIN      349
      DO 80 I=1,19                                                      FIN      350
      PHI=5.*(I-1)                                                      FIN      351
      TEMP1=TEMPF*CSUBZ(I)                                              FIN      352
      TEMP2=TEMPF*CSUBZ(I+18)                                           FIN      353
      TEMP3=TEMPF*CSUBZ(I+36)                                           FIN      354
      TEMP4=TEMPF*CSUBZ(I+54)                                           FIN      355
      IF((I.NE.19).OR.(ISWTCH.EQ.1)) GO TO 795                          FIN      356
      TEMP1= TEMPF*SAVZ19                                               FIN      357
      TEMP2= TEMPF*SAVZ37                                               FIN      358
      TEMP3= TEMPF*SAVZ55                                               FIN      359
  795 CZTOT(I)=TEMP1+TEMP2+TEMP3+TEMP4                                  FIN      360
   80 PRINT 107,PHI,CZTOT(I),TEMP1,TEMP2,TEMP3,TEMP4
```

Table A-2. Computer Program Listing (Cont)

```
      PRINT 108                                                    FIN      361
      DO 81 I=1,19                                                 FIN      362
      PHI=5.*(I-1)                                                 FIN      363
      TEMP1=-TEMPM*CSUBM(I)                                        FIN      364
      TEMP2=-TEMPM*CSUBM(I+18)                                     FIN      365
      TEMP3=-TEMPM*CSUBM(I+36)                                     FIN      366
      TEMP4=-TEMPM*CSUBM(I+54)                                     FIN      367
      IF((I.NE.19).OR.(ISWTCH.EQ.1)) GO TO 805                     FIN      368
      TEMP1=-TEMPM*SAVM19                                          FIN      369
      TEMP2=-TEMPM*SAVM37                                          FIN      370
      TEMP3=-TEMPM*SAVM55                                          FIN      371
  805 CMTOT(I)=TEMP1+TEMP2+TEMP3+TEMP4                             FIN      372
   81 PRINT 107,PHI,CMTOT(I),TEMP1,TEMP2,TEMP3,TEMP4               FIN      373
C                                                                  FIN      374
C     END OUTPUT FOR CZ AND CM                                     FIN      375
C                                                                  FIN      376
   82 IF(ICYCN.EQ.0) GO TO 85                                      FIN      377
C                                                                  FIN      378
C     BEGIN OUTPUT FOR CY AND CN                                   FIN      379
C                                                                  FIN      380
      PRINT 105,ROLLR(IRR),ATEMP                                   FIN      381
      PRINT 109                                                    FIN      382
      DO 83 I=1,19                                                 FIN      383
      PHI=5.*(I-1)                                                 FIN      384
      TEMP1=-TEMPF*CSUBY(I)                                        FIN      385
      TEMP2=-TEMPF*CSUBY(I+18)                                     FIN      386
      TEMP3=-TEMPF*CSUBY(I+36)                                     FIN      387
      TEMP4=-TEMPF*CSUBY(I+54)                                     FIN      388
      IF((I.NE.19).OR.(ISWTCH.EQ.1)) GO TO 825                     FIN      389
      TEMP1=-TEMPF*SAVY19                                          FIN      390
      TEMP2=-TEMPF*SAVY37                                          FIN      391
      TEMP3=-TEMPF*SAVY55                                          FIN      392
  825 CYTOT(I)=TEMP1+TEMP2+TEMP3+TEMP4                             FIN      393
   83 PRINT 107,PHI,CYTOT(I),TEMP1,TEMP2,TEMP3,TEMP4               FIN      394
      PRINT 110                                                    FIN      395
      DO 84 I=1,19                                                 FIN      396
      PHI=5.*(I-1)                                                 FIN      397
      TEMP1=-TEMPM*CSUBN(I)                                        FIN      398
      TEMP2=-TEMPM*CSUBN(I+18)                                     FIN      399
      TEMP3=-TEMPM*CSUBN(I+36)                                     FIN      400
      TEMP4=-TEMPM*CSUBN(I+54)                                     FIN      401
      IF((I.NE.19).OR.(ISWTCH.EQ.1)) GO TO 835                     FIN      402
      TEMP1=-TEMPM*SAVN19                                          FIN      403
      TEMP2=-TEMPM*SAVN37                                          FIN      404
      TEMP3=-TEMPM*SAVN55                                          FIN      405
  835 CNTOT(I)=TEMP1+TEMP2+TEMP3+TEMP4                             FIN      406
   84 PRINT 107,PHI,CNTOT(I),TEMP1,TEMP2,TEMP3,TEMP4               FIN      407
C                                                                  FIN      408
C     END OUTPUT FOR CY AND CN                                     FIN      409
C                                                                  FIN      410
   85 IF(ICL.EQ.0) GO TO 87                                        FIN      411
C                                                                  FIN      412
C     BEGIN OUTPUT FOR CL                                          FIN      413
C                                                                  FIN      414
      PRINT 105,ROLLR(IRR),ATEMP                                   FIN      415
      PRINT 111                                                    FIN      416
      DO 86 I=1,19                                                 FIN      417
      PHI=5.*(I-1)                                                 FIN      418
      TEMP1=TEMPM*CSUBL(I)                                         FIN      419
      TEMP2=TEMPM*CSUBL(I+18)                                      FIN      420
      TEMP3=TEMPM*CSUBL(I+36)                                      FIN      421
      TEMP4=TEMPM*CSUBL(I+54)                                      FIN      422
      IF((I.NE.19).OR.(ISWTCH.EQ.1)) GO TO 855                     FIN      423
      TEMP1= TEMPM*SAVL19                                          FIN      424
      TEMP2= TEMPM*SAVL37                                          FIN      425
      TEMP3= TEMPM*SAVL55                                          FIN      426
  855 CLTOT(I)=TEMP1+TEMP2+TEMP3+TEMP4                             FIN      427
   86 PRINT 107,PHI,CLTOT(I),TEMP1,TEMP2,TEMP3,TEMP4               FIN      428
```

Table A-2. Computer Program Listing (Cont)

```
C                                                                       FIN      429
C     END OUTPUT FOR CL                                                 FIN      430
C                                                                       FIN      431
   87 IF(IPANEL.EQ.0) GO TO 89                                          FIN      432
C                                                                       FIN      433
C     BEGIN OUTPUT FOR PANEL LOADS                                      FIN      434
C                                                                       FIN      435
      IF(ICL.EQ.0) PRINT 105,ROLLR(IRR),ATEMP                           FIN      436
      PRINT 113                                                         FIN      437
      DO 88 I=1,19                                                      FIN      438
      PHI=5.*(I-1)                                                      FIN      439
      TEMP1=TEMPP*CSUBP(I)                                              FIN      440
      TEMP2=TEMPP*CSUBP(I+18)                                           FIN      441
      TEMP3=TEMPP*CSUBP(I+36)                                           FIN      442
      TEMP4=TEMPP*CSUBP(I+54)                                           FIN      443
      TEMP5=-TEMPP*CSUBH(I)/CR                                          FIN      444
      TEMP6=-TEMPP*CSUBH(I+18)/CR                                       FIN      445
      TEMP7=-TEMPP*CSUBH(I+36)/CR                                       FIN      446
      TEMP8=-TEMPP*CSUBH(I+54)/CR                                       FIN      447
      TEMP9=TEMPP*CSUBB(I)                                              FIN      448
      TEMP10=TEMPP*CSUBB(I+18)                                          FIN      449
      TEMP11=TEMPP*CSUBB(I+36)                                          FIN      450
      TEMP12=TEMPP*CSUBB(I+54)                                          FIN      451
      IF((I.NE.19).OR.(ISWTCH.EQ.1)) GO TO 88                           FIN      452
      TEMP1=TEMPP*SAVP19                                                FIN      453
      TEMP2=TEMPP*SAVP37                                                FIN      454
      TEMP3=TEMPP*SAVP55                                                FIN      455
      TEMP5=-TEMPP*SAVH19/CR                                            FIN      456
      TEMP6=-TEMPP*SAVH37/CR                                            FIN      457
      TEMP7=-TEMPP*SAVH55/CR                                            FIN      458
      TEMP9=TEMPP*SAVB19                                                FIN      459
      TEMP10=TEMPP*SAVB37                                               FIN      460
      TEMP11=TEMPP*SAVB55                                               FIN      461
   88 PRINT 114,PHI,TEMP1,TEMP2,TEMP3,TEMP4,TEMP5,TEMP6,TEMP7,TEMP8,    FIN      462
     CTEMP9,TEMP10,TEMP11,TEMP12                                        FIN      463
C                                                                       FIN      464
C     END OUTPUT FOR PANEL LOADS                                        FIN      465
C                                                                       FIN      466
   89 DPHI=5./RAD                                                       FIN      467
      IF(ICZCM.EQ.0) GO TO 90                                           FIN      468
      CALL SIM(CZTOT,DPHI,19,CZAV(IRR))                                 FIN      469
      CALL SIM(CMTOT,DPHI,19,CMAV(IRR))                                 FIN      470
      CZAV(IRR)=CZAV(IRR)*2./PI                                         FIN      471
      CMAV(IRR)=CMAV(IRR)*2./PI                                         FIN      472
   90 IF(ICYCN.EQ.0) GO TO 91                                           FIN      473
      CALL SIM(CYTOT,DPHI,19,CYAV(IRR))                                 FIN      474
      CALL SIM(CNTOT,DPHI,19,CNAV(IRR))                                 FIN      475
      CYAV(IRR)=CYAV(IRR)*2./PI                                         FIN      476
      CNAV(IRR)=CNAV(IRR)*2./PI                                         FIN      477
   91 IF(ICL.EQ.0) GO TO 92                                             FIN      478
      CALL SIM(CLTOT,DPHI,19,CLAV(IRR))                                 FIN      479
      CLAV(IRR)=CLAV(IRR)*2./PI                                         FIN      480
   92 IRR=IRR+1                                                         FIN      481
      IF(IRR.LE.IROLLR) GO TO 35                                        FIN      482
C                                                                       FIN      483
C     END ROLL RATE LOOP                                                FIN      484
C                                                                       FIN      485
      IF((ROLLR(1).EQ.0.).AND.(IROLLR.EQ.1)) GO TO 99                   FIN      486
      IF((ICZCM.EQ.0).AND.(ICYCN.EQ.0).AND.(ICL.EQ.0)) GO TO 99         FIN      487
C                                                                       FIN      488
C     BEGIN OUTPUT FOR AVERAGE FORCES AND MOMENTS OVER A CYCLE OF ROLL  FIN      489
C                                                                       FIN      490
      PRINT 115,ATEMP                                                   FIN      491
      IF(ICZCM.EQ.0) GO TO 94                                           FIN      492
      PRINT 116                                                         FIN      493
      DO 93 I=1,IROLLR                                                  FIN      494
   93 PRINT 117,ROLLR(I),CZAV(I),CMAV(I)                                FIN      495
   94 IF(ICYCN.EQ.0) GO TO 96                                           FIN      496
```

Table A-2. Computer Program Listing (Cont)

```
      PRINT 118                                                          FIN      497
      DO 95 I=1,IROLLR                                                   FIN      498
   95 PRINT 117,ROLLR(I),CYAV(I),CNAV(I)                                 FIN      499
   96 IF(ICL.EQ.0) GO TO 99                                              FIN      500
      PRINT 119                                                          FIN      501
      DO 97 I=1,IROLLR                                                   FIN      502
   97 PRINT 117,ROLLR(I),CLAV(I)                                         FIN      503
C                                                                        FIN      504
C     END OUTPUT FOR AVERAGE FORCES AND MOMENTS OVER A CYCLE OF ROLL     FIN      505
C                                                                        FIN      506
C     END PRIMARY OUTPUT                                                 FIN      507
C                                                                        FIN      508
   99 IAB=IAB+1                                                          FIN      509
      IF(IAB.LE.IALPHA) GO TO 30                                         FIN      510
C                                                                        FIN      511
C     END ANGLE OF ATTACK LOOP                                           FIN      512
C                                                                        FIN      513
  100 FORMAT(1H1)                                                        FIN      514
  101 FORMAT (1H1,//,60X,*F I N L O A D*,//,42X,*PREDICTION OF FORCES AN FIN      515
     1D MOMENTS PRODUCED BY FINS*,//,5X,13A6,//5X,*BODY RADIUS =*,       FIN      516
     1F6.3,* M*,//5X,*FIN SEMI-SPAN =*,F6.3,* M*,//5X,*ROOT CHORD =*,   FIN      517
     1F6.3,* M*,//5X,*AXIAL LOCATION OF FIN LEADING EDGE AT THE BODY =*, FIN      518
     1F7.3,* M*,//5X,*LEADING EDGE SWEEP =*,F6.2,* DEG*,//5X,           FIN      519
     1*TRAILING EDGE SWEEP =*,F6.2,* DEG*,//5X,                         FIN      520
     1*AXIAL LOCATION OF HINGE LINE =*,F7.3,* M*,//5X,                   FIN      521
     1*EXPOSED SURFACE AREA OF A FIN =*,F7.3,* SQ. M*,//5X,              FIN      522
     1*EXPOSED ASPECT RATIO =*,F6.3,//5X,*TIP CHORD =*,F6.3,* M*,//5X,   FIN      523
     1*NORMAL FORCE SCALING COEFFICIENT =*,F6.3,//5X,*NORMAL FORCE COEFF FIN      524
     1ICIENT SLOPE (FIN ALONE, N/Q SFIN) =*,F6.4,* (1/DEG)*,//5X,        FIN      525
     1                                *ROLL DAMPING INTERFERENCE CO      FIN      526
     1EFFICIENT =*,F5.3,//5X,*CZ AND CM DESIRED, *A1),//5X,             FIN      527
     1*CY AND CN DESIRED, *A10,//5X,*CL DESIRED, *A1),//5X,             FIN      528
     1*CP, CH AND CB DESIRED, *,A10,4(//5X,*CONTROL DEFLECTION FIN*,I2,  FIN      529
     1* =*,F6.2,* DEG*),//5X,*ANGLES OF ATTACK DESIRED (DEG)*)          FIN      530
  102 FORMAT (10X,6F7.1)                                                 FIN      531
  103 FORMAT (/5X,*ROLL RATES DESIRED (DIMENSIONLESS)*)                  FIN      532
  104 FORMAT (10X,6F7.3)                                                 FIN      533
  105 FORMAT(1H1,//5X,*ROLL RATE =*,F6.3,* (DIMENSIONLESS)*,5X,          FIN      534
     1*ANGLE OF ATTACK =*,F5.1,* DEG*)                                   FIN      535
  106 FORMAT(////5X,*PHI*,10X,*CZ FINS*,10X,*CZ FIN1*,10X,*CZ FIN2*,     FIN      536
     110X,*CZ FIN3*,10X*CZ FIN4*,/)                                      FIN      537
  107 FORMAT(F8.1,F16.3,4F17.3)                                          FIN      538
  108 FORMAT(////5X,*PHI*,10X,*CM FINS*,10X,*CM FIN1*,10X,*CM FIN2*,     FIN      539
     110X,*CM FIN3*,10X,*CM FIN4*,/)                                     FIN      540
  109 FORMAT(////5X,*PHI*,10X,*CY FINS*,10X,*CY FIN1*,10X,*CY FIN2*,     FIN      541
     110X,*CY FIN3*,10X,*CY FIN4*,/)                                     FIN      542
  110 FORMAT(////5X,*PHI*,10X,*CN FINS*,10X,*CN FIN1*,10X,*CN FIN2*,     FIN      543
     110X,*CN FIN3*,10X,*CN FIN4*,/)                                     FIN      544
  111 FORMAT(////5X,*PHI*,10X,*CL FINS*,10X,*CL FIN1*,10X,*CL FIN2*,     FIN      545
     110X,*CL FIN3*,10X,*CL FIN4*,/)                                     FIN      546
  112 FORMAT (/5X,*MACH NUMBER =*,F5.2)                                  FIN      547
  113 FORMAT (////5X,*PHI*,3X,*CP FIN1*,3X,*CP FIN2*,3X,*CP FIN3*,3X,    FIN      548
     1*CP FIN4*,3X,*CH FIN1*,3X,*CH FIN2*,3X,*CH FIN3*,3X,*CH FIN4*,3X,  FIN      549
     1*CB FIN1*,3X,*CB FIN2*,3X,*CB FIN3*,3X,*CB FIN4*/)                 FIN      550
  114 FORMAT (F8.1,F9.3,11F10.3)                                         FIN      551
  115 FORMAT (1H1,//5X,*AVERAGE VALUE OF FORCES AND MOMENTS OVER ONE ROL FIN      552
     1L CYCLE*,//5X,*ANGLE OF ATTACK =*,F5.1,* DEG*)                     FIN      553
  116 FORMAT (////5X,*ROLL RATE*,10X,*CZ AVERAGE*,10X,*CM AVERAGE*/)     FIN      554
  117 FORMAT (F12.3,F20.4,F20.3)                                         FIN      555
  118 FORMAT (////5X,*ROLL RATE*,10X,*CY AVERAGE*,10X,*CN AVERAGE*/)     FIN      556
  119 FORMAT (////5X,*ROLL RATE*,10X,*CL AVERAGE*/)                      FIN      557
  120 FORMAT (10A6)                                                      FIN      558
  200 FORMAT (1H1,10(/),10X,                                             FIN      559
     1*$$$$$$$$$$$$$$$$$$$$$$$$$$$$$$$$$$$$$$$$$$$$$$$$$$$$$$$$$$$$*//10X FIN      560
     1*MACH NUMBER TOO LARGE. SUPERSONIC LEADING EDGE WILL RESULT.*//10X FIN      561
     1*$$$$$$$$$$$$$$$$$$$$$$$$$$$$$$$$$$$$$$$$$$$$$$$$$$$$$$$$$$$$*)  FIN      562
      END                                                                FIN      563
      SUBROUTINE IDSUB(F,FE)                                             FIN      564
```

Table A-2. Computer Program Listing (Cont)

```
C                                                                       FIN       555
C     THIS SUBROUTINE CALCULATES FIN-FIN INTERFERENCE DUE TO CONTROL     FIN       566
C     DEFLECTION                                                        FIN       567
C                                                                       FIN       568
      COMMON A,BOA,CR,AE,PI,DETA,COSLE,TANLE,TANTE,MACH,ALPHA           FIN       569
      REAL IDT,MACH,ID                                                  FIN       570
      DIMENSION F(4),IDT(11),DOBT(11),ALPHA(6),FE(4)                    FIN       571
      DATA (IDT(I),I=1,11)/.275,.249,.214,.171,.128,.090,.057,.028,     FIN       572
     C.000,.000,.000/                                                   FIN       573
      DOB=A/(BOA+A)                                                     FIN       574
      X=0.                                                              FIN       575
      DO 5 I=1,11                                                       FIN       576
      DOBT(I)=X                                                         FIN       577
    5 X=X+.1                                                            FIN       578
      ID=TBLOOK(DOB,DOBT,IDT,11)                                        FIN       579
      FE(1)=F(1)+ID*(F(2)-F(4))                                         FIN       580
      FE(2)=F(2)+ID*(F(1)-F(3))                                         FIN       581
      FE(3)=F(3)+ID*(F(4)-F(2))                                         FIN       582
      FE(4)=F(4)+ID*(F(3)-F(1))                                         FIN       583
      RETURN                                                            FIN       584
      END                                                               FIN       585
      SUBROUTINE IPSUB(IP)                                              FIN       586
C                                                                       FIN       587
C     THIS SUBROUTINE CALCULATES THE ROLL DAMPING MOMENT INTERFERENCE    FIN       588
C     COEFFICIENT                                                       FIN       589
C                                                                       FIN       590
      COMMON A,BOA,CR,AE,PI,DETA,COSLE,TANLE,TANTE,MACH,ALPHA           FIN       591
      COMMON /A/ BO,SF,SIGMA,CNA,INT1,INT2                              FIN       592
      REAL IP,INT1,INT2,MACH                                            FIN       593
      DIMENSION DOBT(11),CLPT(11),INT1(51),INT2(51),ALPHA(6)            FIN       594
      DATA (CLPT(I),I=1,11)/-.159,-.159,-.161,-.163,-.160,-.146,-.121,  FIN       595
     1-.086,-.043,-.013,.000/                                           FIN       596
      SFP=2.*SF+A*(2.*CR+A*(TANLE-TANTE))                               FIN       597
      AP=(2.*BO)**2/SFP                                                 FIN       598
      TEMP=SFP*2.*BO/(PI*A*A*2.*A)                                      FIN       599
      DOB=A/BO                                                          FIN       600
      X=0.                                                              FIN       601
      DO 5 I=1,11                                                       FIN       602
      DOBT(I)=X                                                         FIN       603
    5 X=X+.1                                                            FIN       604
      CLP=TBLOOK(DOB,DOBT,CLPT,11)*TEMP*AP                              FIN       605
      DZETA=1./50.                                                      FIN       606
      DETA=DZETA                                                        FIN       607
      ETA=0.                                                            FIN       608
      DO 11 J=1,51                                                      FIN       609
      ZETA=0.                                                           FIN       610
      DO 10 I=1,51                                                      FIN       611
      ZETAF=SQRT(ZETA)*EXP(ZETA**2/SQRT(COSLE))                         FIN       612
      ETAF=(1.+ETA**(2.*AE))*SQRT(1.-ETA**2)                            FIN       613
      INT1(I)=(A+BOA*ETA)**2*(CR-BOA*(TANLE-TANTE)*ETA)*ZETAF*ETAF      FIN       614
   10 ZETA=ZETA+DZETA                                                   FIN       615
      CALL SIM(INT1,DZETA,51,INT2(J))                                   FIN       616
   11 ETA=ETA+DETA                                                      FIN       617
      CALL SIM(INT2,DETA,51,TEMP)                                       FIN       618
      IP=1.+CLP/(2./PI*SIGMA*BOA/BO/A**3*CNA*TEMP)                      FIN       619
      IF(IP.LT.0.) IP=0.                                                FIN       620
      RETURN                                                            FIN       621
      END                                                               FIN       622
      FUNCTION CN(A)                                                    FIN       623
C                                                                       FIN       624
C     THIS SUBPROGRAM CALCULATES THE LOCAL NORMAL FORCE COEFFICIENT     FIN       625
C     GIVEN THE LOCAL ANGLE OF ATTACK                                   FIN       626
C                                                                       FIN       627
      COMMON /D/ KP,KV,AS,SAV1,SAV2,SAV3                                FIN       628
      REAL KP,KV                                                        FIN       629
      CN=0.                                                             FIN       630
      IF(A.EQ.0.) RETURN                                                FIN       631
      ASAVE=A                                                           FIN       632
```

Table A-2. Computer Program Listing (Cont)

```
      SIGN=A/ABS(A)                                                          FIN       633
      A=ABS(A)                                                               FIN       634
      IF(A.GT.AS) GO TO 1                                                    FIN       635
      CN=(KP*SIN(A)*COS(A)+KV*SIN(A)**2)*(1.-SAV1*A**3)                      FIN       636
      GO TO 3                                                                FIN       637
    1 CNAS=(KP*SIN(AS)*COS(AS)+KV*SIN(AS)**2)*(1.-SAV1*AS**3)                FIN       638
      IF(A.GT.2.*AS) GO TO 2                                                 FIN       639
      CNAMAS=(KP*SIN(A-AS)*COS(A-AS)+KV*SIN(A-AS)**2)*(1-SAV1*(A-AS)**3)     FIN       640
      CN=SAV2*CNAS+SAV3*CNAMAS                                               FIN       641
      GO TO 3                                                                FIN       642
    2 CN=(SAV2+SAV3)*CNAS                                                    FIN       643
    3 CN=SIGN*CN                                                             FIN       644
      A=ASAVE                                                                FIN       645
      RETURN                                                                 FIN       646
      END                                                                    FIN       647
      SUBROUTINE CNPREP                                                      FIN       648
C                                                                            FIN       649
C     THIS SUBPROGRAM CALCULATES VARIOUS CONSTANTS NEEDED IN THE             FIN       650
C     SUBPROGRAM CN                                                          FIN       651
C                                                                            FIN       652
      COMMON A,B0A,CR,AE,PI,DETA,COSLE,TANLE,TANTE,MACH,ALPHA                FIN       653
      COMMON /C/ UVEL,VSTO,WSTO,SINP,COSP,SINLE,IAB,SINTE,COSTE,             FIN       654
     CBETA,TANGM,GAMLE,GAMTE                                                 FIN       655
      COMMON /D/ KP,KV,ASTL,SAV1,SAV2,SAV3                                   FIN       656
      REAL MACH,MU,KP,KV                                                     FIN       657
      DIMENSION VSTO(51),WSTO(51),UVEL(6),ALPHA(6)                           FIN       658
      UAV=UVEL(IAB)                                                          FIN       659
      CALL SIM(VSTO,DETA,51,VAV)                                             FIN       660
      CALL SIM(WSTO,DETA,51,WAV)                                             FIN       661
      VRAV=VAV*COSP+WAV*SINP                                                 FIN       662
      GAMLEE=GAMLE+ASIN(VRAV/SQRT(UAV**2+VRAV**2))                           FIN       663
      GAMTEE=GAMTE+ASIN(VRAV/SQRT(UAV**2+VRAV**2))                           FIN       664
      IF(ABS(GAMLEE).GT.1.57) GAMLEE=SIGN(1.57,GAMLEE)                       FIN       665
      IF(GAMLEE.LT.0.) GAMLEE=0.                                             FIN       666
      IF(ABS(GAMTEE).GT.1.57) GAMTEE=SIGN(1.57,GAMTEE)                       FIN       667
      COSLEE=COS(GAMLEE)                                                     FIN       668
      SINLEE=SIN(GAMLEE)                                                     FIN       669
      TANTEE=TAN(GAMTEE)                                                     FIN       670
      CRE=CR*COSTE/COS(GAMTE-BAMLE+BAMLEE)                                   FIN       671
      B0AE=B0A*COSLEE/COSLE                                                  FIN       672
      AEE=4./(2.*CR*COSTE*COSLE/(B0A*COSLEE*COS(GAMTE-GAMLE+GAMLEE))+       FIN       673
     1TANTEE-TAN(GAMLEE))                                                    FIN       674
      CRS=CRE+B0AE*TANTEE                                                    FIN       675
      GAMMA=ATAN(CRS/B0AE)                                                   FIN       676
      TANG=TAN(GAMMA)                                                        FIN       677
      PS=2./AEE/TANG                                                         FIN       678
      IF(MACH.GT.1.) PS=PS/(1.-TANGM/2./TANG)                                FIN       679
      PSI=ATAN(2.*PS*TANG)                                                   FIN       680
      IF(MACH.GT.1.) PSI=ATAN(2.*PS*(TANG-TANGM))                            FIN       681
      TANPSI=TAN(PSI)                                                        FIN       682
      SINPSI=SIN(PSI)                                                        FIN       683
      KP=4.*PI/(TANPSI+SQRT(TANPSI**2+SINPSI**2/PS**2+4.*BETA**2))           FIN       684
      KV=(KP-KP**2*TANPSI/4./PI)*SQRT(1.+TANPSI**2)                          FIN       685
      AETEMP=AEE                                                             FIN       686
      IF(AETEMP.LT.1.) AETEMP=1.                                             FIN       687
      IF(AETEMP.GT.4.) AETEMP=4.                                             FIN       688
      ASTL=.6632*(1.+.02*(AETEMP-2.)**4)*(1.+1.1*(AETEMP-1.)**2.5*           FIN       689
     CCOSLEE**2)*(1.+6.*(AETEMP-1.)**2*SINLEE**4/EXP(AETEMP))/(COSLEE+1)     FIN       690
     C**(2.*(AETEMP-1.))                                                     FIN       691
      MU=.9-.2*SQRT(AETEMP)*SIN(2.*GAMLEE)                                   FIN       692
      SAV1=(1.-MU)/ASTL**3                                                   FIN       693
      SINLEE=ABS(SINLEE)                                                     FIN       694
      SAV2=1.-.35*(1.+EXP(AETEMP)/8.*SINLEE**(1./AETEMP)*SIN((AETEMP-2.1     FIN       695
     C)*GAMLEE))/(1.+.5*(AETEMP-1.)**3)                                      FIN       696
      IF(SAV2.LT..65) SAV2=.65                                               FIN       697
      SAV3=COSLEE**2*AEE/10.                                                 FIN       698
      RETURN                                                                 FIN       699
      END                                                                    FIN       700
```

Table A-2. Computer Program Listing (Cont)

```
      SUBROUTINE FLOW (U,VVEL,WVEL)                                    FIN       731
C                                                                      FIN       732
C     THIS SUBROUTINE CALCULATES THE FLOW FIELD ABOUT THE BODY         FIN       733
C     FOR UP TO SIX ANGLES OF ATTACK, EVERY FIVE DEGREES IN ROLL       FIN       734
C     ANGLE, AND AT 51 EQUALLY SPACED RADIAL LOCATIONS ALONG THE       FIN       735
C     FIN SEMI-SPAN. A DIFFERENT BODY FLOW FIELD CALCULATION           FIN       736
C     TECHNIQUE CAN BE USED IF THE RESULT IS PROPERLY STORED IN        FIN       737
C     U, VVEL, AND WVEL.                                               FIN       738
C                                                                      FIN       739
      COMMON A,BODA,CR,AE,PI,DETA,COSLE,TANLE,TANTE,MACH,ALPHA         FIN       740
      COMMON /B/ RAD,X1,IALPHA                                         FIN       741
      REAL LS,LSHEET,MACH                                              FIN       742
      DIMENSION YV(44),ZV(44),PHIV(44),RV(44),LS(102),PHISS(102),      FIN       743
     1VVEL(6,73,51),WVEL(6,73,51),ALPHA(5),U(6)                        FIN       744
      NV=44                                                            FIN       745
      BR=BODA/A*DETA                                                   FIN       746
      XV=X1/A                                                          FIN       747
      IAB=1                                                            FIN       748
   10 AB=ALPHA(IAB)                                                    FIN       749
      U(IAB)=COS(AB)                                                   FIN       750
      SINAB=SIN(AB)                                                    FIN       751
C                                                                      FIN       752
C     BEGIN CONCENTRATED VORTEX CALCULATION                            FIN       753
C                                                                      FIN       754
      PHIV(1)=74./RAD                                                  FIN       755
      RV(1)=.70+.060*SQRT(MACH+1.)*(XV+6.)*SQRT(AB)                    FIN       756
      GT=.35*PI*(XV-6.)*AB**2                                          FIN       757
      GCOGT=1.-.15*AB*XV+.008*(AB*XV)**2                               FIN       758
      GC=GCOGT*GT                                                      FIN       759
      GS=GT-GC                                                         FIN       760
      RC=.030*XV*SQRT(AB)                                              FIN       761
      IF(RC.LT.1.E-10) RC=1.E-10                                       FIN       762
      YV(1)=RV(1)*COS(PHIV(1))                                         FIN       763
      ZV(1)=RV(1)*SIN(PHIV(1))                                         FIN       764
C                                                                      FIN       765
C     END CONCENTRATED VORTEX CALCULATION                              FIN       766
C                                                                      FIN       767
C     BEGIN VORTEX SHEET CALCULATION                                   FIN       768
C                                                                      FIN       769
      PHISS(1)=3.                                                      FIN       770
      DPHIV=PHIV(1)/100.                                               FIN       771
      DO 21  N=1,101                                                   FIN       772
      COSDUM=COS(PI*PHISS(N)/(2.*PHIV(1)))                             FIN       773
      SINDUM=SIN(PI*PHISS(N)/(2.*PHIV(1)))                             FIN       774
      BLANK=1.+(RV(1)+RC)*(PHIV(1)-PHISS(N))                           FIN       775
      RSHEET=COSDUM+(RV(1)+RC)*SINDUM**2/BLANK                         FIN       776
      DRSDPH=-PI/(2.*PHIV(1))*SINDUM+((RV(1)+RC)*PI*SINDUM*COSDUM*     FIN       777
     1BLANK/PHIV(1)+(RV(1)+RC)**2*SINDUM**2)/BLANK**2                  FIN       778
      LS(N)=SQRT(RSHEET**2+DRSDPH**2)                                  FIN       779
      IF(RSHEET.LT.1.01  ) GO TO 20                                    FIN       780
      GO TO 21                                                         FIN       781
   20 LS(N)=0.                                                         FIN       782
      PHIV(5)=PHISS(N)                                                 FIN       783
   21 PHISS(N+1)=PHISS(N)+DPHIV                                        FIN       784
      CALL SIM(LS,DPHIV,101,LSHEET)                                    FIN       785
      YV(5)=1.01  *COS(PHIV(5))                                        FIN       786
      ZV(5)=1.01  *SIN(PHIV(5))                                        FIN       787
      NDUM=NV-3                                                        FIN       788
      N=1                                                              FIN       789
      DO 23  NN=9,NDUM,4                                               FIN       790
      BLANK2=(NN-5)*LSHEET/(NV-4)                                      FIN       791
   22 N=N+1                                                            FIN       792
      CALL SIM(LS,DPHIV,N,BLANK1)                                      FIN       793
      IF(BLANK2.GT.BLANK1) GO TO 22                                    FIN       794
      PHIV(NN)=(PHISS(N)+PHISS(N-1))/2.                                FIN       795
      COSDUM=COS(PI*PHIV(NN)/(2.*PHIV(1)))                             FIN       796
      SINDUM=SIN(PI*PHIV(NN)/(2.*PHIV(1)))                             FIN       797
      BLANK=1.+(RV(1)+RC)*(PHIV(1)-PHIV(NN))                           FIN       798
```

Table A-2. Computer Program Listing (Cont)

```
      RV(NN)=COSDUM*(RV(1)*RC)*SINDUM**2/BLANK                          FIN       769
      YV(NN)=RV(NN)*COS(PHIV(NN))                                       FIN       770
   23 ZV(NN)=RV(NN)*SIN(PHIV(NN))                                       FIN       771
      NDUM=NV-2                                                         FIN       772
      DO 24  N=2,NDUM,4                                                 FIN       773
      YV(N)=   YV(N-1)/(YV(N-1)**2+ZV(N-1)**2)                          FIN       774
      ZV(N)=   ZV(N-1)/(YV(N-1)**2+ZV(N-1)**2)                          FIN       775
      YV(N+1)=-YV(N)                                                    FIN       776
      ZV(N+1)=ZV(N)                                                     FIN       777
      YV(N+2)=-YV(N-1)                                                  FIN       778
   24 ZV(N+2)=ZV(N-1)                                                   FIN       779
C                                                                       FIN       780
C     END VORTEX SHEET CALCULATION                                      FIN       781
C                                                                       FIN       782
C     BEGIN VELOCITY COMPONENT CALCULATION                              FIN       783
C                                                                       FIN       784
      PHI=0.                                                            FIN       785
      IPHI=1                                                            FIN       786
   30 PHI=PHI/RAD                                                       FIN       787
      COSP=COS(PHI)                                                     FIN       788
      SINP=SIN(PHI)                                                     FIN       789
      R=1.                                                              FIN       790
      IR=1                                                              FIN       791
   31 Y=R*COSP                                                          FIN       792
      Z=R*SINP                                                          FIN       793
      IF(ABS(Y-YV(1)).LT.ABS(Y-YV(4))) GO TO 32                         FIN       794
      Y14=YV(4)                                                         FIN       795
      Z14=ZV(4)                                                         FIN       796
      GO TO 33                                                          FIN       797
   32 Y14=YV(1)                                                         FIN       798
      Z14=ZV(1)                                                         FIN       799
   33 C=1.254*((Y-Y14)**2+(Z-Z14)**2)/RC**2                             FIN       800
      V=0.                                                              FIN       801
      W=0.                                                              FIN       802
      DO 34 J=1,4                                                       FIN       803
      CON1=(Y-YV(J))**2+(Z-ZV(J))**2                                    FIN       804
      V=V+(-1)**J*(Z-ZV(J))/CON1                                        FIN       805
   34 W=W+(-1)**J*(Y-YV(J))/CON1                                        FIN       806
      VS=0.                                                             FIN       807
      WS=0.                                                             FIN       808
      DO 35  N=5,NV                                                     FIN       809
      CON1=(Y-YV(N))**2+(Z-ZV(N))**2                                    FIN       810
      VS=VS+(-1)**N*(Z-ZV(N))/CON1                                      FIN       811
   35 WS=WS+(-1)**N*(Y-YV(N))/CON1                                      FIN       812
      V=            (-2.   *Y*Z*SINAB/(Y**2+Z**2)**2+GC*W/(2.*PI)+    FIN       813
     12.*GS/(PI*(NV-4))*VS)*(1.-EXP(-C))                                FIN       814
      W=             (SINAB*(1.+   (Y**2-Z**2)/(Y**2+Z**2)**2)-        FIN       815
     1GC*W/(2.*PI)-2.*GS*WS/(PI*(NV-4)))*(1.-EXP(-C))                   FIN       816
      IF(ABS(V).GT.2.) V=2.*V/ABS(V)                                    FIN       817
      IF(ABS(W).GT.2.) W=2.*W/ABS(W)                                    FIN       818
      VVEL(IAB,IPHI,IR)=V                                               FIN       819
      WVEL(IAB,IPHI,IR)=W                                               FIN       820
      R=R+DR                                                            FIN       821
      IR=IR+1                                                           FIN       822
      IF(IR.LE.51) GO TO 31                                             FIN       823
      PHI=PHI*RAD                                                       FIN       824
      PHI=PHI+5.                                                        FIN       825
      IPHI=IPHI+1                                                       FIN       826
      IF(IPHI.LE.73) GO TO 30                                           FIN       827
      IAB=IAB+1                                                         FIN       828
      IF(IAB.LE.IALPHA) GO TO 10                                        FIN       829
C                                                                       FIN       830
C     END VELOCITY COMPONENT CALCULATION                                FIN       831
C                                                                       FIN       832
      RETURN                                                            FIN       833
      END                                                               FIN       834
      FUNCTION TBLOOK(X,AB,ORD,N)                                       FIN       835
C                                                                       FIN       836
```

Table A-2. Computer Program Listing (Cont)

```
C     LINEAR INTERPOLATION SUBPROGRAM. ABSCISSA MUST BE IN                FIN      837
C     INCREASING VALUES.  LETS YOU KNOW IF VALUE IS OUT OF THE            FIN      838
C     RANGE OF THE TABLE, AND THEN CONTINUES ASSUMING SINTER=1.           FIN      839
C     N IS THE NUMBER OF ENTRIES IN THE TABLE.                            FIN      840
C                                                                         FIN      841
      DIMENSION AB(1),ORD(1)                                              FIN      842
      IF(X.LT.AB(1).OR.X.GT.AB(N)) GO TO 5                                FIN      843
      NN=N/2                                                              FIN      844
      IF(X.LT.AB(NN)) GO TO 3                                             FIN      845
      I=NN                                                                FIN      846
      NN=NN+NN/2                                                          FIN      847
      IF(X.GT.AB(NN)) I=NN                                                FIN      848
      GO TO 4                                                             FIN      849
    3 I=1                                                                 FIN      850
      NN=NN/2                                                             FIN      851
      IF(X.GT.AB(NN)) I=NN                                                FIN      852
    4 I=I+1                                                               FIN      853
      IF(X.GT.AB(I)) GO TO 4                                              FIN      854
      TBLOOK=ORD(I-1)+(X-AB(I-1))/(AB(I)-AB(I-1))*(ORD(I)-ORD(I-1))       FIN      855
      RETURN                                                              FIN      856
    5 PRINT 1,X                                                           FIN      857
      TBLOOK=1.                                                           FIN      858
    1 FORMAT(  //30X,                                                     FIN      859
     152HABSCISSA WAS NOT IN THE RANGE OF THE TABLE,ABSCISSA=              FIN      860
     1F10.5,//  )                                                         FIN      861
      RETURN                                                              FIN      862
      END                                                                 FIN      863
      SUBROUTINE SIM(Y,H,NN,ANS)                                          FIN      864
C                                                                         FIN      865
C     SIMPSON RULE INTEGRATION. INTEGRAND MUST BE EVENLY SPACED.          FIN      866
C     NN IS THE NUMBER OF INTEGRAND POINTS.                               FIN      867
C                                                                         FIN      868
      DIMENSION Y(1)                                                      FIN      869
      ANS=0.                                                              FIN      870
      IF(NN-2) 2,3,5                                                      FIN      871
    2 RETURN                                                              FIN      872
    3 ANS=.5*H*(Y(1)+Y(2))                                                FIN      873
      RETURN                                                              FIN      874
    5 II=NN/2                                                             FIN      875
      II=II*2                                                             FIN      876
      IF(NN-II)6,8,6                                                      FIN      877
    6 II=NN-2                                                             FIN      878
      DO 7 J=1,II,2                                                       FIN      879
    7 ANS=ANS+     (Y(J)+4.*Y(J+1)+Y(J+2))                                FIN      880
      ANS=ANS*H/3.                                                        FIN      881
      RETURN                                                              FIN      882
    8 II=NN-3                                                             FIN      883
      DO 9 J=1,II,2                                                       FIN      884
    9 ANS=ANS+     (Y(J)+4.*Y(J+1)+Y(J+2))                                FIN      885
      ANS=ANS*H/3.                                                        FIN      886
      ANS=ANS+.5*H*(Y(II+2)+Y(II+3))                                      FIN      887
      RETURN                                                              FIN      888
      END                                                                 FIN      889
```

APPENDIX B

Use of the Computer Program

The input for the program is very simple. Seven data cards are needed to execute the program.

Card 1: Input the title of the missile and fin geometry. The title can be any combination of letters and numbers and must be located in columns 1 through 60. Sample card:

```
AMRAAM CONFIGURATION
0000000000000  00  0000000000000000000000000000000000000000000000000
1 2 3 4 5 6 7 8 9 10 11 12 13 14 15 16 17 18 19 20 21 22 23 24 25 26 27 28 29 30 31 32 33 34 35 36 37 38 39 40 41 42 43 44 45 46 47 48 49 50 51 52 53 54 55 56 57 58 59 60
 11   1111111111  1111111111111111111111111111111111111111111111111111
```

Card 2: Input missile and fin geometry. The order of input variables is: body radius (meter), fin semispan (meter), fin root chord (meter), axial location of where the fin leading edge intersects the body (meter), fin leading edge sweep (degree), fin trailing edge sweep (degree), and axial location of panel hinge moment reference (meter). All data (cards 2 through 7) are input in free format; that is, any format you like. Sample card:

```
.165,.375,.325,3.8,30,-20.,3.955
0000 0000 0000 000 0  00 0 0000000000000000000000000000000000
1 2 3 4 5 6 7 8 9 10 11 12 13 14 15 16 17 18 19 20 21 22 23 24 25 26 27 28 29 30 31 32 33 34 35 36 37 38 39 40 41 42 43 44 45 46 47 48 49 50 51 52 53 54 55 56 57 58 59 60
1 11111111111111111111111111111111111111111111111111111111111111111111
```

Card 3: Input the forces and moments that the user desires. Enter 1 if quantity is desired and enter 0 if quantity is not desired. The order of input variables is: fin normal force and pitch moment, fin side force and yaw moment, fin roll moment, panel normal force, hinge moment, and root bending moment. Sample card:

```
1,1,0,1
0 0    0000000000000000000000000000000000000000000000000000000000
1 2 3 4 5 6 7 8 9 10 11 12 13 14 15 16 17 18 19 20 21 22 23 24 25 26 27 28 29 30 31 32 33 34 35 36 37 38 39 40 41 42 43 44 45 46 47 48 49 50 51 52 53 54 55 56 57 58 59 60
 1 111 1111111111111111111111111111111111111111111111111111111111111111
```

Card 4: Input the control deflection angle of each fin. The order of input variables is: control deflection Fin 1 (degree), control deflection Fin 2 (degree), control deflection Fin 3 (degree), and control deflection Fin 4 (degree). Use the sign convention shown in Figure 10 of this document. Sample card.

```
5.,-8.,-5.,-8.
00 000 000 0000000000000000000000000000000000000000000000000000000000
1 2 3 4 5 6 7 8 9 10 11 12 13 14 15 16 17 18 19 20 21 22 23 24 25 26 27 28 29 30 31 32 33 34 35 36 37 38 39 40 41 42 43 44 45 46 47 48 49 50 51 52 53 54 55 56 57 58 59 60
1111111111111111111111111111111111111111111111111111111111111111111111
```

Card 5: Input the number of angles of attack desired and the angles of attack of the body desired. The maximum number of angles of attack allowed is six. The order of input variables is: number of body angles of attack desired, first angle of attack of the body desired (degree), second angle of attack of the body desired (degree), third angle of attack of the body desired (degree), fourth angle of attack of the body desired (degree), fifth angle of attack of the body desired (degree), and sixth angle of attack of the body desired (degree). Sample card:

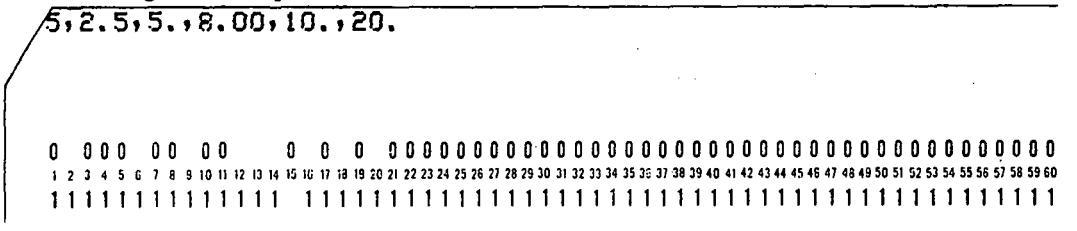

Card 6: Input the number of roll rates desired and the specific roll rates desired. The maximum number of roll rates allowed is six. The input roll rate must be nondimensionlized as $\phi\ b_o/U_\infty$. The order of input variables is: number of roll rates desired, first roll rate desired, second roll rate desired, third roll rate desired, fourth roll rate desired, fifth roll rate desired, and sixth roll rate desired. Sample card:

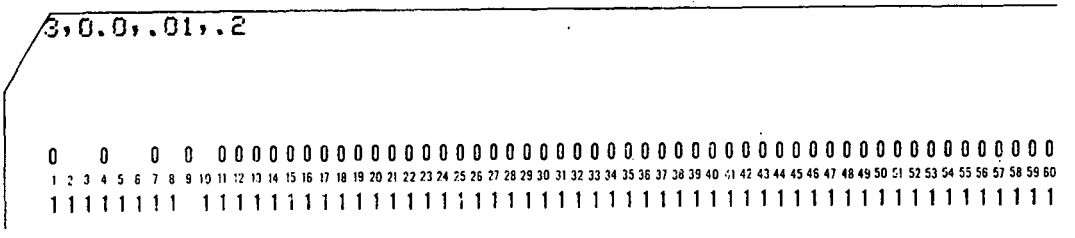

Card 7: Input the free stream Mach number. Sample card:

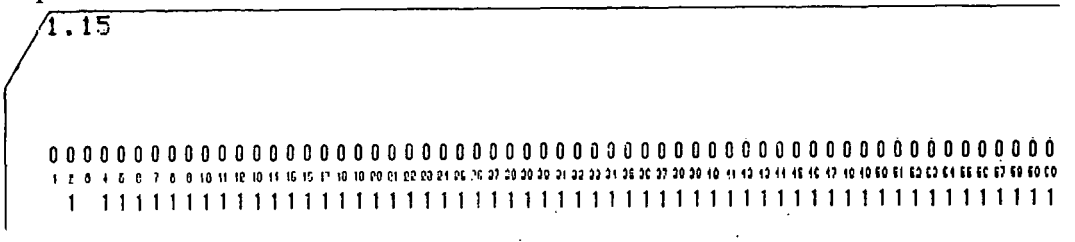

The output from the program is divided into six parts. The first part contains a description and listing of all input data and several other values related to the fin geometry. Part two contains the normal force coefficient and pitch moment coefficient of each fin and the fins summed together; if these forces and moments are not requested, this part is eliminated. Part three contains the side force coefficient and yaw moment coeficient of each fin and the fins summed together; if these force and moments are not requested, this part is eliminated. Part four contains the roll moment coefficient of each fin and the fins summed together; if this moment is not requested, this part is eliminated. Part five contains the panel normal force coefficient, hinge moment coefficient, and root bending moment coefficient of each fin; if these forces and moments are not requested, this part is eliminated. Part six contains the normal force coefficient, pitch moment coefficient, side force coefficient, yaw moment coefficient, and roll moment coefficient averaged over one 90° roll cycle; if the roll rate is specified as zero, this part is eliminated.

Parts two through five list the forces and moments as a function of roll angle for each angle of attack of the body and each roll rate. Part six lists the forces and moments as a function of roll rate for each angle of attack of the body. The output in part six is used to calculated quantities such as C_{ℓ_p} and steady-state roll raise rate.

The computer run time depends on certain options chosen in the input variables. Two examples of run time on a CDC 7600 are as follows: Example 1, calculate all forces and moments (3 forces and 5 moments), six angles of attack of the body, and one roll rate: 39 s. Example 2, calculate all forces and moments, six angles of attack of the body, and six roll rates: 184 s.

DISTRIBUTION:

0400 C. Winter
1252 G. W. Stone
4300 R. L. Peurifoy, Jr.
Attn: E. E. Ives, 4330
H. W. Schmitt, 4340
J. A. Hood, 4360
4310 C. C. Burks
Attn: D. L. McCoy, 4311
5000 J. K. Galt
Attn: F. L. Vook, 5100
R. S. Claassen, 5800
5500 O. E. Jones
Attn: T. B. Lane, 5520
T. G. Priddy, 5522
5600 D. B. Shuster
Attn: A. A. Lieber, 5610
G. J. Simmons, 5640
5620 M. M. Newsom
Attn: C. E. Dalton, 5621
R. D. Andreas, 5622
5630 R. C. Maydew
5631 H. R. Vaughn (10)
5631 D. W. Barnette
5631 G. R. Eisler
5631 R. W. Greene
5631 A. E. Hodapp
5631 W. L. Oberkampf (20)
5632 C. W. Peterson
5633 S. McAlees
5634 D. D. McBride
Attn: E. L. Clark
5635 W. R. Barton
Attn: W. E. Williamson
5636 J. K. Cole
5636 H. R. Spahr
5650 D. J. Rigali
8100 W. J. Spencer
Attn: J. Barham, 8110
W. E. Alzheimer, 8120
R. D. Cozine, 8160
8150 J. L. Wirth
Attn: G. N. Beeler, 8152
8214 M. A. Pound
3141 L. J. Erickson (5)
3151 W. L. Garner (3)
For: DOE/TIC (Unlimited Release)
DOE/TIC (25)
(J. Hernandez, 3154-4)

Org.	Bldg.	Name	Rec'd by *	Org.	Bldg.	Name	Rec'd by *